The Abdus Salam
International Centre for Theoretical Physics

United Nations
Educational, Scientific
and Cultural Organization

International Atomic
Energy Agency

SMR/1758-16

"Workshop on Ion Beam Studies of Nanomaterials:
Synthesis, Modification and Characterization"

26 June - 1 July 2006

Structural Modifications Induces in Various Types of Materials under Energetic Clusters Bombardment

A. Dunlop
Ecole Polytechnique
Laboratoire des Solides Irradies,
Palaiseau, France

This study has been made possible because of the energetic clusters that are now available at the tandem accelerator at the IPN Orsay where, for example, charged fullerene ions with energies ranging from 8 to 30 MeV have been accelerated [14]. Negative molecular C_{60}^- ions are accelerated in the first section of the tandem accelerator. At the positive high voltage terminal in the center of the accelerator (4 to 15 MV), the negative C_{60}^- ions collide with N_2 molecules in a stripper cell and become positively charged. Multiply charged C_{60}^{n+} (with $n \leq 4$) are formed, and it has been argued theoretically [15] that multiple ionization can occur only in plural binary collisions with nitrogen atoms passing through the fullerene. Time-of-flight (TOF) measurements combined with a magnetic deflection at a small angle (1.5°) allow us to identify unambiguously the beam of C_{60}^{1+} that has been used in this experiment. Figure 1 presents a TOF spectrum of C_{60}^{1+} measured at this deflecting angle of 1.5°. The beam intensity on the target varies between 10^5 and 10^6 projectiles per second on an area of 10 mm^2.

Pure titanium and zirconium targets [16], suitable for transmission electron microscopy observations (i.e., thickness ~100 nm), have been irradiated at 300 K with C_{60} under normal incidence up to a fluence of 10^{10} cm^{-2}. Figure 2 shows the corresponding electron micrographs of titanium irradiated by 18 MeV C_{60} molecules and, for comparison, electron micrographs of titanium irradiated by 845 MeV Pb ions. It must be noticed that in this case (GeV ion irradiations) the experimental procedure was slightly different [10]. The samples (~15 μm thick) are electrochemically thinned after irradiation in order to observe slices located at about 7 μm from the surfaces. This procedure ensures that the energy deposited in the observed part of the sample corresponds totally to the energy loss of the projectile. In both cases, observations under normal and tilted incidences are presented in order

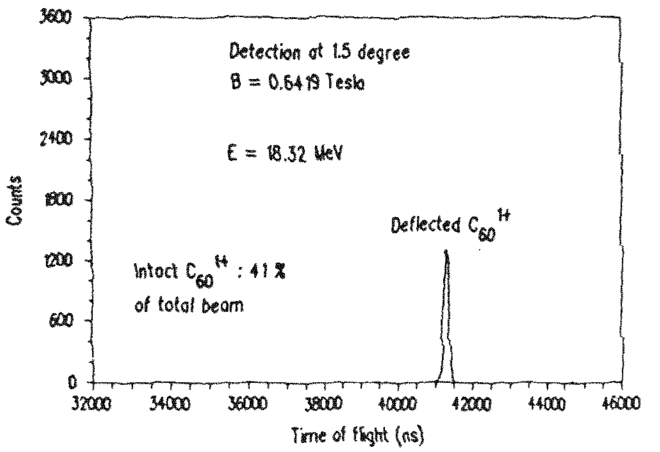

Fig. 1. Time-of-flight spectrum of a high energy fullerene beam obtained after magnetic deflection at 1.5°. The terminal voltage of the tandem accelerator is 9 MV and the C_{60}^- ion beam is pulsed before the entrance of the accelerator. There are intact only C_{60}^+ at 18.32 MeV at the target site.

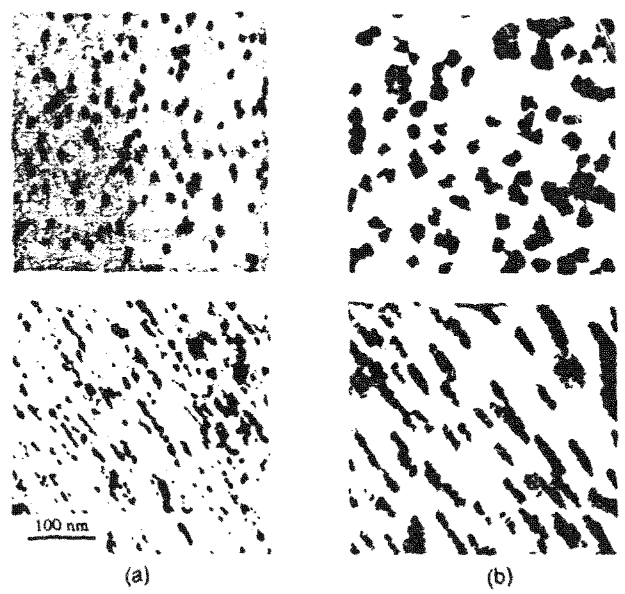

Fig. 2. Bright field images of titanium irradiated at 300 K: (a) with 845 MeV lead ions up to a fluence of 10^{11} cm^{-2} and (b) with 18 MeV C_{60} up to a fluence of 6×10^{10} cm^{-2}. In the upper part the electron beam direction is parallel to the ion beam. (a) Kinematic condition. (b) Two beam condition with $g = \{101\}$. In the lower part, the sample is tilted in the microscope. (a) Tilt angle 26°; two beam condition with $g = \{101\}$) and (b) tilt angle 30°; kinematic condition with $k_0 \parallel [354]$).

to illustrate that the damage takes place in a cylindrical region around the projectile path. After irradiation with monatomic Pb beams, the contrast in the microscope consists of small dots of average diameter 5 nm, the characteristic distance between these dots being close to 30 nm. The analysis of the images shows that the contrast is associated to dislocation loops located in the prismatic planes of the hexagonal structure [17]. After irradiation with C_{60} beams, the observed damaged zones entirely go through the sample thickness with an almost constant diameter of 20 nm. The analysis of the images shows that the contrast cannot be associated to microcrystallized matter nor to amorphous phase, but corresponds to a dense dislocation loop network. The detailed study of these contrasts is not yet completed and will be published elsewhere.

It is worth noticing that there is a one to one correspondence between the numbers of impinging projectiles and observed "tracks." The radial extension and the longitudinal distribution of the damage demonstrate the very large efficiency of the C_{60} beam to create tracks.

Figure 3 shows electron micrographs of zirconium irradiated by 18 MeV C_{60} molecules. In this case micrographs corresponding to samples irradiated by swift heavy ions (prepared as mentioned above for titanium targets [10]) are not presented because they do not exhibit any contrast ascribable to damaged zones greater than the electron microscope resolution. This enforces the greater

Tracks in Metals by MeV Fullerenes

H. Dammak, A. Dunlop, and D. Lesueur
Laboratoire des Solides Irradiés, Commissariat à l'Energie Atomique/Ecole Polytechnique, 91128 Palaiseau, France

A. Brunelle, S. Della-Negra, and Y. Le Beyec
Institut de Physique Nucléaire, CNRS-IN2P3, 91406 Orsay, France
(Received 22 July 1994)

It is shown that new specific effects take place during irradiation of metals with high energy fullerene beams. The observed quasicontinuous damage is confined inside ~20 nm diam cylinders around the projectile paths and is compared to the damage resulting from GeV heavy ion irradiation. The large extension of the highly damaged zones after cluster irradiations might be due to the strong localization of the deposited energy during the slowing-down process.

PACS numbers: 61.80.Lj, 61.80.Jh

It is now well accepted that electronic excitation and ionization arising from the slowing down of swift heavy ions can lead to structural modifications in bulk metallic targets as it has been known for a long time in insulators [1] and in thin [2] or discontinuous [3,4] metallic films. These modifications resulting from the high rates of energy deposition, which can reach values as high as 10 keV/nm, were unexpected in metallic materials where numerous and very mobile charge carriers allow a fast spreading of the deposited energy and an efficient screening of the space charge created in the projectile wake [5]. The main difference between insulators and conductors lies in the threshold above which the linear rate of energy deposition can lead to structural modifications.

So it has been shown that irradiation of bulk metallic targets with swift heavy ions can induce effects as varied as the so-called growth phenomenon of amorphous alloys [6,7], the amorphization of metal-metalloid alloys [8] or metal-metal alloys [9], a phase transformation in pure titanium [10], and defect creation in pure iron and zirconium [11]. The question of the transformation of the energy deposited by the projectile during the slowing-down process into energy stored in the target as lattice defects is still to be answered. Two mechanisms have been proposed: (i) The thermal spike model [12] in which the kinetic energy of the ejected electrons is transmitted to the lattice by electron-phonon interaction in a way efficient enough to increase the local lattice temperature above the melting point. This temperature increase is then followed by a rapid quenching. (ii) The Coulomb explosion model [13] in which the electrostatic energy of the space charge created just after the ion passage is converted into coherent radial atomic movements leading to a cylindrical shock wave.

Both mechanisms are sensitive to the rate of energy loss (dE/dx) as well as to the deposited energy density. The volume in which the energy is deposited scales with the range of the δ electrons—emitted during the ionization process—which depends only on the projectile velocity v. In monatomic ion irradiation it is not possible to vary significantly one of these parameters, say, v, keeping the second one unchanged, say, dE/dx, whereas it is easier using cluster ions. The aim of this paper is to compare damage induced in metallic targets (Ti, Zr) by MeV cluster ions with that previously observed [10,11] after irradiation with GeV heavy ions. The linear energy loss of MeV clusters (evaluated below) is comparable to that of GeV heavy ions, whereas their velocity is 1 order of magnitude lower (see Table I).

TABLE I. Characteristics of the experiments presented in this Letter. E_m is the maximum energy of the δ electrons (see text).

Target	Projectile	Incident energy (MeV)	$(dE/dx)_n$ (keV/nm)	$(dE/dx)_e$ (keV/nm)	E_m (eV)	Observations
Ti	Pb	845	0.08	36	8800	Dotted tracks Diameter ~5 nm
	C_{60}	18	1.8	43	50	Quasicontinuous tracks Diameter ~15 to 25 nm
Zr	U	5550	0.03	41	49 000	No observable damage
	C_{60}	18	1.8	44	50	Dotted tracks Diameter ~10 to 20 nm

Fig. 3. Two beam condition bright field images of zirconium irradiated at 300 K with 18 MeV C_{60} molecules up to a fluence of 3.1×10^{10} cm^{-2}. In the upper part the electron beam direction is parallel to the ion beam (g = {101}), whereas in the lower one, the sample is tilted by 36° in the microscope (g = {100}).

efficiency of aggregate beams in producing damage in metallic targets.

The determination of the rate of energy deposition for clusters is still, to our knowledge, an open question from experimental and theoretical points of view. It is admitted that an aggregate entering a solid breaks into several fragments. However, the cylindrical shape of the damaged regions shows that these different fragments keep a close spatial correlation during the slowing-down process at least up to the sample thickness (100 to 200 nm). In order to estimate the energy deposited in both electronic excitation and nuclear collisions, it has been assumed that the energy loss of the initial C_{60} molecule is the sum of the energy losses of 60 individual carbon atoms.

As far as elastic collisions are concerned, the rate of energy deposition $(dE/dx)_n$ (see Table I) and the number of displaced atoms have been evaluated. Each C_{60} molecule would lead in such an approach to eight displacements every interatomic distance [19]. This number is certainly much too low to account for the huge observed damaged zones. Moreover, a complementary irradiation of a thin titanium foil was performed on the ARAMIS facility [20] at Orsay with 2.4 MeV Au_3 clusters. In this experiment, although each cluster induces about 30 atomic displacements every interatomic distance, no damage has ever been observed in the electron microscope after irradiations at fluences of 2×10^{10} or even 9×10^{12} clusters/cm^2. So, as in the case of GeV heavy ions [11], the damage induced by MeV C_{60} projectiles cannot result from the sole elastic collisions.

As far as inelastic collisions are concerned, the use of the above sum rule to calculate the rate of energy deposition $(dE/dx)_e$ (reported in Table I) implies that the equilibrium charge state reached by each individual carbon atom is not affected by the close vicinity of the other fragments. This hypothesis is based on the following remark: *The main contribution to the slowing* down comes from close collisions in which the impact parameter is smaller than the interatomic distance in the C_{60} molecule. As a matter of fact, the sole experimental results available in this field concerns measurements of the energy loss of C_{60} projectiles in thin (30 to 50 nm thick) amorphous carbon foils [18]. They show that the energy loss *per carbon* is, within the experimental uncertainty (about 5%), that of an individual carbon projectile of the same velocity.

The resulting stopping powers calculated with these assumptions are reported in Table I. As $(dE/dx)_e$ is always much larger than $(dE/dx)_n$, the range of the projectiles is *governed by electronic energy losses*. The ranges of 18 MeV C_{60} molecules (~490 nm in Ti and ~420 nm in Zr) are thus given by that of monatomic carbon of the same velocity. The thicknesses of the targets are much smaller than this range, so that the stopping region is avoided and that the electronic stopping power is almost constant throughout the sample thickness.

It appears that, although the rates of energy deposition in electronic excitation are close using monatomic GeV and aggregate MeV projectiles, both the radial and longitudinal characteristics of the damage differ strongly: Going from monatomic to aggregate beams, the radial extension increases markedly, whereas the longitudinal distribution evolves from a clearly dotted structure to a quasicontinuous one. The explanation for such different behaviors might originate from the great difference in the velocities of swift heavy ions and C_{60} projectiles. The transport of energy away is governed by δ electrons, which have an angular and a kinetic energy distribution related to the projectile velocity. Maximum kinetic energy values of δ electrons $E_m = 2mv^2$ (ejected in the forward direction) are given in Table I. For similar rates of energy deposition in electronic excitation, as the volume in which the energy is deposited is related to the radial range of secondary electrons, the lower the projectile velocity, the higher the energy deposition and, space charge densities. Using GeV Pb or U ions the radial range of the δ electrons is of some 1000 nm, whereas using a C_{60} beam, this radial range falls to a few interatomic distances. In this latter case, a crude estimate of the density of deposited energy by C_{60} ions leads to huge values as high as 10 eV/Å^3 (or 100 eV/atom). The relaxation of such a high energy density induces the spectacular structural modifications observed in this work. The damage is located inside a cylinder which has a radius at least 1 order of magnitude greater than the radius of the cylinder in which the primary energy is deposited.

Other new effects are expected to result from irradiation of solids with large MeV clusters as, for example, intense secondary emission.

[1] R.L. Fleischer, P.B. Price, and R.M. Walker, J. Appl. Phys. **36**, 3645 (1965).

[2] T.S. Noggle and J.O. Stiegler, J. Appl. Phys. **33**, 1726 (1962).

[3] K.L. Merkle, Phys. Rev. Lett. **9**, 150 (1962).

[4] H.H. Andersen, H. Knudsen, and P. Moller Petersen, J. Appl. Phys. **49**, 5638 (1978).

[5] This obviously does not apply to very thin metallic films or small size metallic clusters in which the spreading of the deposited energy is strongly limited by the close vicinity of the boundaries.

[6] S. Klaumünzer and G. Schumacher, Phys. Rev. Lett. **51**, 1987 (1983).

[7] A. Audouard, E. Balanzat, G. Fuchs, J.C. Jousset, D. Lesueur, and L. Thomé, Europhys. Lett. **3**, 327 (1987).

[8] A. Audouard, E. Balanzat, J.C. Jousset, A. Chamberod, A. Dunlop, D. Lesueur, G. Fuchs, R. Spohr, J. Vetter, and L. Thomé, Phys. Rev. Lett. **65**, 875 (1990).

[9] A. Barbu, A. Dunlop, D. Lesueur, and R.S. Averback, Europhys. Lett. **15**, 37 (1991).

[10] H. Dammak, A. Barbu, A. Dunlop, D. Lesueur, and N. Lorenzelli, Philos. Mag. Lett. **67**, 253 (1993).

[11] A. Dunlop and D. Lesueur, Radiat. Eff. Defects Solids **126**, 123 (1993).

[12] M. Toulemonde, C. Dufour, and E. Paumier, Phys. Rev B **46**, 14362 (1992).

[13] D. Lesueur and A. Dunlop, Radiat. Eff. Defects Solids **126**, 163 (1993).

[14] S. Della-Negra, A. Brunelle, Y. Le Beyec, J.M Curaudeau, J.P. Mouffron, B. Waast, P. Hakansson B.U.R. Sundquist, and E.S. Parilis, Nucl. Instrum Methods Phys. Res., Sect. B **74**, 453 (1993).

[15] E.S. Parilis, Nucl. Instrum. Methods Phys. Res., Sect. B **88**, 21 (1994).

[16] The dominant impurity is oxygen with an atomic concentration lower than 100 ppm.

[17] J. Henry, A. Barbu, B. Leridon, D. Lesueur, and A. Dunlop, Nucl. Instrum. Methods Phys. Res., Sect. B **67**, 390 (1992).

[18] K. Baudin, A. Brunelle, M. Chabot, S. Della-Negra J. Depauw, D. Gardes, P. Hakansson, Y. Le Beyec A. Billebaud, M. Fallavier, J. Remilleux, J.C. Poizat and J.P. Thomas, Nucl. Instrum. Methods Phys. Res. Sect. B **94**, 341 (1994).

[19] J.P. Biersack, in *Ion Beam Modifications of Insulators* edited by P. Mazzoldi and G.W. Arnold (Elsevier Amsterdam, 1987), p. 1.

[20] The authors wish to acknowledge the useful help of the ARAMIS facility team, especially Dr. J. Chaumont, for the gold cluster irradiations.

to the hexagonal ω phase (Dammak *et al.* 1993). A study of the structural modifications by TEM observations after irradiations performed under various conditions (Dammak *et al.* 1996) showed that the complete $\alpha \rightarrow \omega$ phase transformation is obtained, firstly, during irradiation at low temperatures (20–90 K), secondly, for LED levels higher than 33 keV nm^{-1} and, thirdly, for fluences higher than 10^{12} ions cm^{-2}. This latter condition was confirmed later by using *in situ* electrical resistance and length measurements during irradiation at 20 K by 2.4 GeV U ions (Dammak *et al.* 1999). These workers showed that, firstly, at low fluences (i.e. in each track) the damage creation is identified by TEM observations as the formation of dislocation loops and, secondly, the incubation fluence above which ω domains are formed in the α matrix is about 1.2×10^{12} ions cm^{-2}.

On the other hand during irradiations at 300 K under the same conditions (LED level about 35 keV nm^{-1}), the ω phase is not formed for fluences up to 10^{13}cm^{-2} (Dammak *et al.* 1996). In this case, TEM observations show a dense dislocation structure in the α matrix caused by the spatial overlap of tracks.

The mechanism proposed for the phase transformation during irradiation by gigaelectronvolt monomers (Dammak *et al.* 1999) is based on the propagation of localized displacement waves of the $[100]_\alpha$ close-packed rows. The creation of dislocation loops or stacking faults in a track is assumed to be due to a shearing of neighbouring $(010)_\alpha$ prismatic planes. The formation of ω domains at low temperatures (20–90 K) requires a spatial overlap of these tracks and is assumed to be the result of a local rearrangement. The deduction of the existence of stacking faults arising from a disorder in the transverse displacements in $(010)_\alpha$ prismatic planes takes into account the diffuse intensity lines observed in the electron diffraction pattern. At room temperature the spatial overlap of tracks leads to a partial recovery and so to a dense dislocation structure.

However, it has been recently established that, using 10–40 MeV C_{60} ions for which the LED levels are slightly higher than those obtained by using gigaelectronvolt monomers, the resulting structural modifications were extremely important in Ti (Dammak *et al.* 1995). In fact 18 MeV C_{60} ions create quasicontinuous tracks of about 20 nm diameter. The important resulting structural modification is thought to arise from the very strong localization of the deposited energy.

In the following we present the influence of the irradiation temperature on the structural modification in Ti during irradiation by megaelectronvolt C_{60} ions using TEM observations.

§ 2. Experimental details

High-purity polycrystalline Ti ribbons of 11 μm thickness were annealed in vacuum (3×10^{-4} Pa) for 17 h at 1090 K in a furnace containing Ti sponge; the ribbons were then slowly cooled to room temperature. From the ribbons, discs of 3 mm diameter were punched out and were ground and electrochemically thinned up to electron transparency by a double-jet technique using a perchloric acid electrolyte at 240 K and an applied voltage of 17.5 V.

The discs were irradiated with 30.2 MeV C_{60}^{2+} ions either at room temperature or in a liquid-N_2-cooled cryostat at the Orsay tandem accelerator; the fluences were chosen in order to avoid overlapping of the damaged regions, with values around 5×10^9 ions cm^{-2}. At such incident energies, when hitting the target surface, the C_{60} clusters will break up into single ions or small assemblies of ions. During the slowing-down of this flow of neighbouring projectile constituents, a spatial separation of the fragments occurs as a consequence of Coulomb repulsion between charged fragments and multiple scattering by elastic collision processes. A detailed description of these effects was given by Dunlop *et al.* (1997). The range of 30.2 MeV C_{60}^{2+} in Ti (about 700 nm) is much larger than the thickness (less than 100 nm) of the regions observed by TEM, so that in this work we deal only with the regions of correlated slowing-down of the fragments in which energy loss occurs mainly through electronic excitation and ionization.

The microstructure of the irradiated samples was examined using a Philips CM30 transmission electron microscope operated at 300 kV.

§ 3. Results

The analysis of the images obtained in the microscope shows that the observed damaged zones (tracks) go entirely through the sample thickness with an almost constant 'diameter'. The absence of haloes and thin rings in the electron diffraction patterns shows that the damage cannot be associated with an amorphous phase nor with microcrystallized matter. In the following we show that orientation relationships exist between the new phase and the hcp α-matrix.

3.1. *Irradiations at 300 K*

For the samples irradiated at room temperature, tilting around $\mathbf{g} = (010)_\alpha$ (i.e. prismatic planes of α-Ti remain parallel to the electron beam in the microscope) in the diffraction patterns, extra spots indexable as $(030)_\omega$ along the direction of the $(0h0)_\alpha$ (spots (figures 1 (*a*) and (*b*)) are associated with the tracks. The bright-field images (figure 1 (*c*)), taken in orientations such that a row of $(0h0)_\alpha$ reflections are excited, show that fringes parallel to the $(010)_\alpha$ planes with a spacing of about 3 nm are associated with the tracks. These fringes have been identified as parallel moiré fringes, that is a double-diffraction effect due to an overlapping of the structure of the tracks with the α matrix. The spacing of the fringes is very close to the value of $\delta = 3.2$ nm expected from the lattice spacing of $(030)_\omega$ and $(020)_\alpha$ $(1/\delta = 1/d^{\alpha}_{(020)} - 1/d^{\omega}_{(030)})$. Other diffraction effects related to the structure of the tracks were seldom found and it was not possible to establish unambiguously the crystallographic structure of the tracks. In fact the observed extra spot can also be indexed in the bcc β phase as $(111)_\beta$ with $\delta = 3.2$ nm, and in the hcp α phase as $(103)_\alpha$ with $\delta = 3.1$ nm.

3.2. *Irradiations at liquid-N_2 temperature*

In samples irradiated at liquid-N_2 temperature, the diffraction patterns (figures 2 and 3) show the coexistence of both α and ω phases with the orientation relationships $(002)_\alpha \| (2\bar{1}0)_\omega$ and $[100]_\alpha \| [001]_\omega$ previously found after irradiation with gigaelectronvolt monomers at high fluences (Dammak *et al.* 1993). Figure 2 shows the electron diffraction pattern corresponding to the superposition of the $[320]_\alpha$ zone axis with the $[\bar{1}\bar{2}3]_\alpha$ zone axis and $(002)_\alpha$ parallel to $(\bar{2}10)_\omega$. The evidence of the ω phase in this case is confirmed by the observation of the $(111)_\omega$ reflection (figure 2 (*b*)) for which there is no equivalence in the β or α phases.

The bright-field image given in figure 1 (*d*) taken with the same diffraction conditions as that in figure 1 (*a*), shows fringes spaced by 3 nm as found in the samples irradiated at room temperature. It is important to note that the parallelism of $(010)_\alpha$ to $(030)_\omega$, which is also observed after room-temperature irradiation, is coherent with the α–ω orientation relationship. The dark-field image (figure 3 (*a*)), made

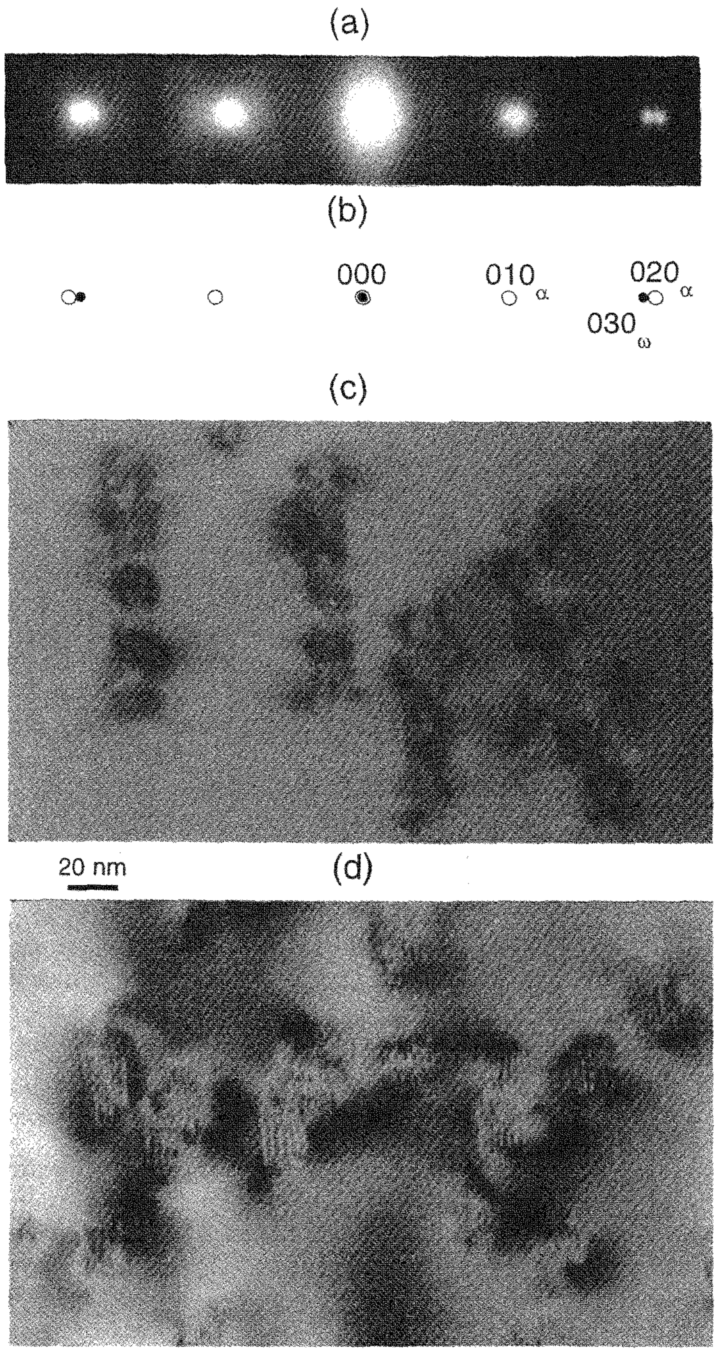

Figure 1. Ti irradiated at (*a*)–(*c*) 300 K and (*d*) 80 K with 30 MeV C_{60} ions. (*a*) Electron diffraction pattern showing the $(0h0)_\alpha$ row. (*b*) Index of the diffraction pattern showing the $(030)_\alpha$ extra spot. (*c*), (*d*) Bright-field images of tilted tracks, observed after irradiations at 300 and 80 K respectively, showing fringes perpendicular to the $(0h0)_\alpha$ row. The spacing of the fringes is very close to the value of $\delta = 3.2$ nm expected from the lattice spacing of $(030)_\omega$ and $(020)_\alpha (1/\delta = 1/d^{\alpha}_{(020)} - 1/d^{\omega}_{(030)})$. The tilt angles of the tracks are about 35° and 13° for (*c*) and (*d*) respectively.

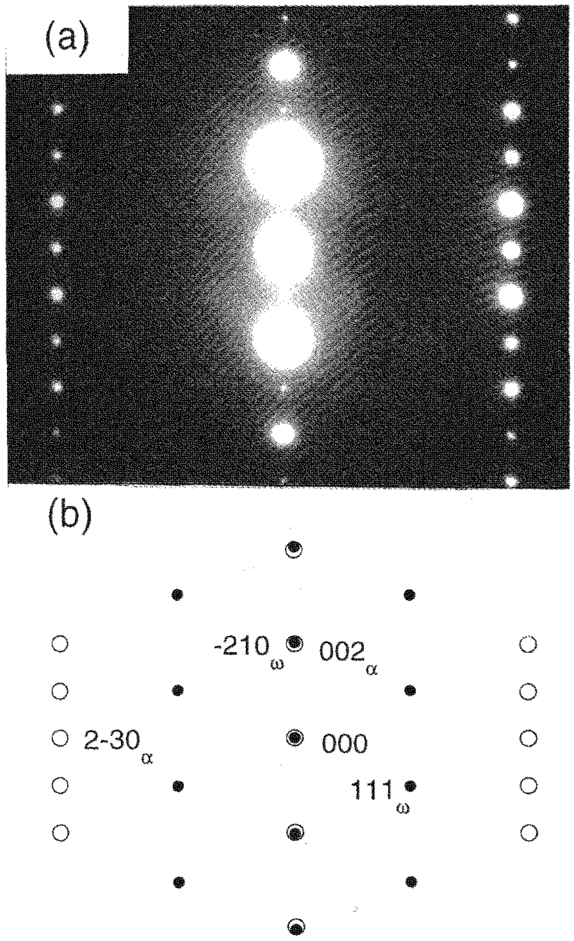

Figure 2. Ti irradiated at liquid-N_2 temperature with 30 MeV C_{60} ions. (*a*) Electron diffraction pattern showing the superposition of the $[320]_\alpha$ zone axis with the $[\bar{1}\bar{2}3]_\omega$ zone axis. (*b*) Index of (*a*) using the orientation relationship $(002)_\alpha \| (2\bar{1}0)_\omega$ and $[100]_\alpha \| [001]_\omega$.

with a beam diffracted by the structure associated with the tracks and corresponding to $(121)_\omega$, shows the ω phase in the 'cylindrical' region surrounding the ion path. It is interesting to note that, despite the fact that the moiré fringes extend continuously all over the tracks, the dark-field images show small transformed domains. The structure of the track seems to be continuous parallel to the $(010)_\alpha$ (i.e. parallel to $[120]_\alpha$) and defective normal to $(010)_\alpha$ (i.e. perpendicular to $[120]_\alpha$).

The average lateral size of tracks measured in figure 3 (*a*) is equal to 21 ± 2 nm. On the other hand, using figures 1 (*c*) and (*d*), the number of fringes is about six for both room-temperature and liquid-N_2 irradiations. The lateral size of tracks is then about $6\delta \approx 19$ nm. The images in figures 1 and 3 obtained by tilting tracks around two different directions give approximately the same measured lateral size of the track. The tracks have an approximately cylindrical morphology.

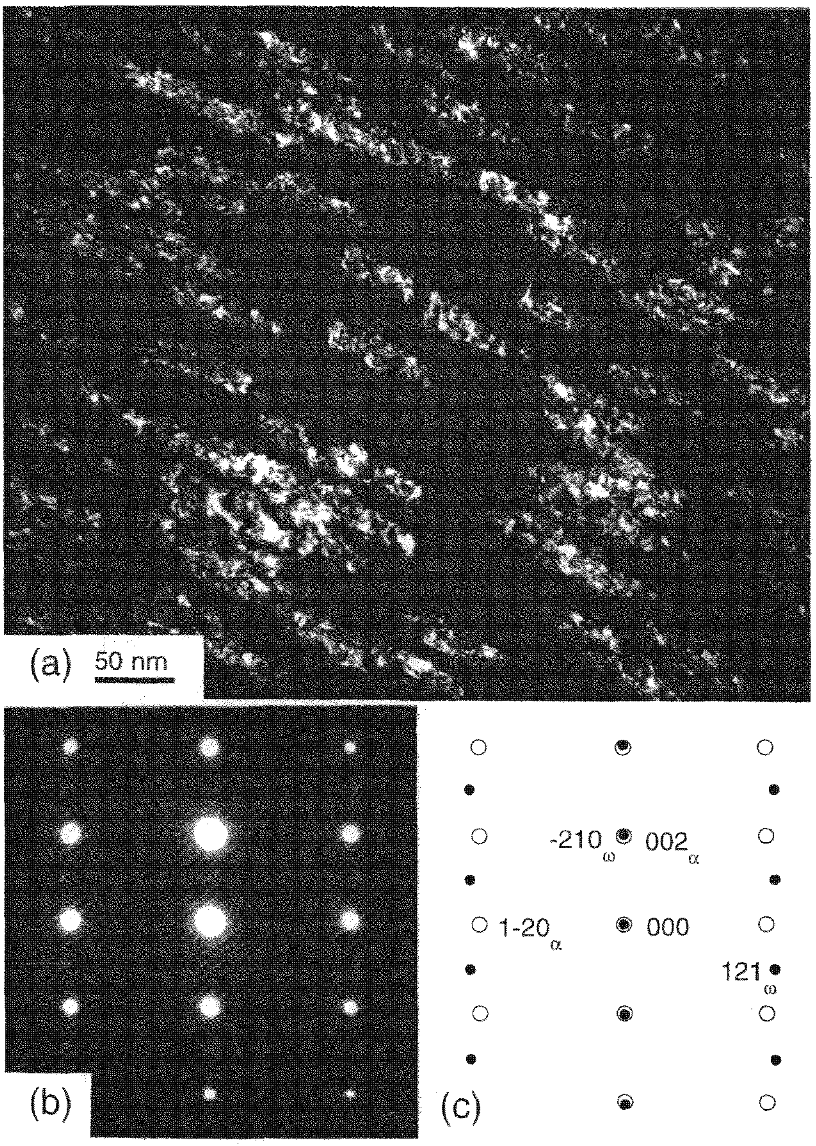

Figure 3. Ti irradiated at liquid-N_2 temperature with 30 MeV C_{60} ions up to a fluence of 5×10^9 ions cm^{-2}. (*a*) Dark-field image of tilted tracks. (*b*) Electron diffraction pattern showing the superposition of the $[210]_\alpha$ zone axis with the $[\bar{1}\bar{2}5]_\omega$ zone axis. (*c*) Index of (*b*) showing the spot $(121)_\omega$ selected to make the dark-field image (*a*). The double weak spots result from double reflection.

§ 4. Discussion and conclusions

On the basis of these observations it is possible to say that the end product of 30 MeV C_{60} irradiation is a highly defective ω phase along the ion paths. The absence or weakness of ω reflections other than $(030)_\omega$ in samples irradiated at room temperature could be due to the presence of many faults in the stacking of the $(030)_\omega$ planes. After irradiations at 300 K, we find the same orientation relationship of the $(030)_\omega$ planes as after low-temperature irradiation.

These results should be compared to those (see § 1) obtained under the same conditions by gigaelectronvolt monomers (table 1).

Comparing 10–40 MeV C_{60} ions and gigaelectronvolt monomer ions, for which the LED levels are similar, the resulting structural modifications in Ti are extremely different. The enhancement of the resulting damage after cluster ion irradiations is expected to be due to the very strong localization of the deposited energy (Dammak *et al.* 1995). The transport of the energy away from the ion path is governed by the ejected δ electrons, which have an angular and kinetic energy distribution related to the projectile velocity. The volume in which the energy is deposited is related to the radial range of secondary electrons. Using gigaelectronvolt Pb or U ions the radial range of δ electrons is some 1000 nm whereas, using a few 10 MeV C_{60} ions, this radial range falls to a few interatomic distances. In this latter case the deposited energy density can reach values as high as 100 eV atom^{-1}. The relaxation of such a high-energy density induces very strong structural modifications around the ion path.

Table 1 shows that, after irradiations with 30 MeV C_{60} ions, the volume of the regions in which structural modifications takes place is temperature independent; the cross-section diameters of the tracks are approximately the same for both room-temperature and liquid-N_2 irradiations, but the nature of structural modifications (i.e. the resulting latent damage) is temperature dependent (table 1). It seems that the deposited energy density threshold above which the ω phase is obtained in a track increases when the irradiation temperature increases.

This temperature effect is similar to that observed for the $\alpha \rightarrow \omega$ phase transformation induced by applied static or dynamic pressure. From the pressure–temperature phase diagram of Ti (Zil'Bershteyn *et al.* 1973, Sikka *et al.* 1982), the athermal martensitic start pressure $P_{M_s}^{\alpha\rightarrow\omega}$ (above which the $\alpha \rightarrow \omega$ transformation occurs) also increases when the temperature increases. Kustar and German (1979) show that no ω phase is formed in Ti samples shock-loaded at 290 K with pressures in the 12–50 GPa range. At 120 K, the ω phase is formed and the amount of this increases (from 6 to 54%) when the shock pressure amplitude increases from 12 to 50 GPa. This temperature effect is related by Kustar and German to an increase of the shock residual

Table 1. Structural modifications in Ti observed by TEM after irradiation at room and liquid-N_2 temperatures. A comparison between the previous results using gigaelectronvolt U ions (Dammak *et al.* 1995, 1996, 1999) and the present results using 30 MeV C_{60} ions.

Irradiation temperature (K)	Gigaelectronvolt U ions	Megaelectronvolt C_{60} ions
300	Discontinuous tracks with 3–5 nm cross-section diameter No ω phase, even after high irradiation fluences	Quasicontinuous tracks with approximately 20 nm cross-section diameter Only $(030)_\omega$ reflection is observed
80	Discontinuous tracks with 3–5 nm cross-section diameter ω phase observed only after high irradiation fluences	Continuous tracks with approximately 20 nm cross-section diameter ω phase is formed in individual tracks

temperature above the back transformation temperature $T^{\omega\to\alpha}$ (about 400 K at atmospheric pressure).

When the cluster fragments slow down in a material, the energy is deposited in a very short time in a highly non-equilibrium process, so that the resulting damage can be compared with the results of the shock experiments. In fact, the time taken by a 30 MeV C_{60} ion to travel a distance of 10 nm in the material is of the order of 10^{-14} s, which is much shorter than the characteristic time for the lattice motion (10^{-13}–10^{-12} s). However, for the phase transition under shock conditions, Duvall and Graham (1977) showed that the brief duration (less than 1 μs) for which the pressure pulse is applied rules out the possibility of any diffusion-assisted growth. Recently Lavrentiev *et al.* (1999) show that the ω phase is formed during surface irradiation of Ti by 800 keV electron beam with a pulse duration of 10 ns. The explanation for this result by these workers is based on the stress waves that arise in such exposures.

Hence it can be expected that, in the vicinity of the C_{60} ion path, the transformation has to proceed rapidly and directly because the brief duration of the excited state cannot allow the formation of nucleation centres through creation and motion of defects. A collective and coherent movement of atoms is necessary to obtain the observed structural modification in the tracks; the $\alpha \to \omega$ phase change may be realized by a transformation of the martensitic type. The phase transition may proceed as described by the direct mechanism proposed by Rabinkin *et al.* (1981) which is based on the shearing of the prismatic planes and developed recently in a phonon description to explain the structural modifications induced with gigaelectronvolt monomers (Dammak *et al.* 1999).

The relaxation of the high deposited energy density generates around the C_{60} ion path strong stress waves leading to structural modifications. At a low temperature (liquid N_2) the remaining displacements are correlated leading to ω-phase formation in the track. At room temperature the remaining lattice displacements are only correlated along $(010)_\alpha$, leading to the $(030)_\omega$ reflection in the electron diffraction pattern. The effect of the irradiation temperature is related to the temperature–pressure structural properties

Acknowledgements

The authors greatly acknowledge the help of J. Ardonceau, S. Guillous and T. Pouthier (Laboratoire des Solides Irradiés, Palaiseau) and S. Della-Negra, J.P. Prestel and G. Magneney (Institute de Physique Nucléaire, Orsay) for modifications of the cryostat and for their help during the irradiation.

References

Dammak, H., Barbu, A., Dunlop, A., Lesueur, D., and Lorenzelli, N., 1993, *Phil. Mag. Lett.*, **67**, 253.

Dammak, H., Dunlop, A., and Lesueur, D., 1996, *Nucl. Instrum. Meth.* B, **107**, 204; 1999, *Phil. Mag.* A, **79**, 147.

Dammak, H., Dunlop, A., Lesueur, D., Brunelle, A., Della-Negra, S., and Le Beyec, Y., 1995, *Phys. Rev. Lett.*, **74**, 1135.

Dunlop, A., Jaskierowicz, G., Jensen, J., and Della-Negra, S., 1997, *Nucl. Instrum. Meth.* B, **132**, 93.

Dunlop, A., Legrand, P., Lesueur, D., Lorenzelli, N., Morillo, J., Barbu, A., and Bouffard S., 1991, *Europhys. Lett.*, **15**, 765.

Duvall, G. E., and Graham, R. A., 1977, *Rev. mod. Phys.*, **49**, 523.

HENRY, J., BARBU, A., LERIDON, B., LESUEUR, D., and DUNLOP, A., 1992, *Nucl. Instrum. Meth.* B, **67**, 390.
KUSTAR, A. R., and GERMAN, V. N., 1979, *Proc. Phys. pulsed pressures,* **44**, 166.
LAVRENTIEV, V., HAMMERL, C., RENNER, B., ZEITLER, M., RAUSCHENBACH, B., GAPONENKO, N., LONIN, YU., and PISANENKO, A., 1999, *Surf. Coatings Technol.,* **114**, 143.
RABINKIN, A., TALIANKER, M., and BOTSTEIN, O., 1981, *Acta metall.,* **29**, 691.
SIKKA, S. K., VOHRA, Y. K., and CHIDAMBARAM, R., 1982, *Prog. Mater. Sci.,* **27**, 245.
ZIL'BERSHTEYN, V. A., NOSOVA, G. I., and ESTRIN E. I., 1973, *Fiz. Metall. Metalloved.,* **35**, 584.

ELSEVIER

Nuclear Instruments and Methods in Physics Research B 132 (1997) 93–108

NIM B
Beam Interactions with Materials & Atoms

Track separation due to dissociation of MeV C_{60} inside a solid [1]

A. Dunlop [a,*], G. Jaskierowicz [a], J. Jensen [a,b], S. Della-Negra [c]

[a] *Laboratoire des Solides Irradiés, CEA/Ecole Polytechnique, 91128 Palaiseau, France*
[b] *Physics Department, Odense University, 5230 Odense M, Denmark*
[c] *Institut de Physique Nucleaire, CNRS-IN2P3, 91406 Orsay, France*

Received 16 April 1997

Abstract

Samples of yttrium iron garnet were irradiated at 300 K with 10–40 MeV Au_4 and C_{60} ions at normal and grazing incidences. The samples were then observed in a transmission electron microscope. It is seen that the cluster ions create large size amorphous continuous tracks and that strong sputtering occurs. Irradiations at grazing incidence allow direct observations of the track shape evolution as the projectiles slow down in the target. For the first time it was possible to visualize the dissociation of C_{60} ions inside a solid. The stochastic nature of this separation process results in tracks of different shapes and lengths. The tracks generated in the target keep a constant diameter during the correlated slowing-down of the C_{60} projectile constituents during travelled distances $L_{\mathrm{const}} \approx 100$ nm, although the area on which the constituents are spread increases by almost two orders of magnitude between the target entrance and the depth L_{const}. © 1997 Elsevier Science B.V.

PACS: 61.80; 6170; 3450H
Keywords: Latent tracks; Electronic energy deposition; Fullerene; Cluster irradiation; Electron microscopy; Cluster dissociation

1. Introduction

Interactions of high energetic particles with solids depend on the nature and energy of the projectile and on the properties of the target. The slowing-down of energetic particles in matter occurs through inelastic processes and elastic collisions with the target nuclei. The former process dominates the slowing-down in the high-energy range ($v \gg v_0$, where v_0 is the Bohr velocity), whereas nuclear processes are overwhelming in the low-energy range. The interaction of *fast molecules* with solids has been studied experimentally and theoretically since the early 1970s [1–5]. Using molecules or clusters as projectiles is a unique way to produce simultaneous impacts of several atoms in a very small area. The energy density deposited by electronic processes can therefore be very high. A variety of experiments has been performed with

* Corresponding author. Tel.: 33 01 69 33 4494; fax 33 01 69 33 3022; e-mail: annie.dunlop@polytechnique.fr.

[1] Irradiations were performed on the tandem accelerator, IPN Orsay (France).

PII S0168-583X(97)00390-X

molecular/cluster projectiles and several aspects have been studied: the secondary emission of ions [6–9] or electrons [10,11], the creation of defects [12] including tracks [13] and the energy loss mechanisms [1,2,4,14–16].

When very energetic ($v \geqslant v_0$) molecular ions hit a surface, they break up into single ions or smaller assemblies of ions. The interaction between the cluster ion and the solid can be separated into three effects.

1. The penetration through the first atomic layers during which the projectile constituents lose electrons.
2. The separation process with:
   - the Coulomb repulsion between the charged fragments, which is screened to a certain degree by the target electrons, and which depends on the energy of the projectile;
   - the multiple scattering due to the elastic collision process: it increases when the projectile velocity decreases (changing the incident velocity or during the slowing-down inside the target).
3. The dynamic response of the medium with the fluctuation of the electron density in the track and induced wake forces acting on the projectile constituents.

Both processes described in step Eq. (2) induce a separation of the constituents of the clusters. For a recent survey of trajectory correlations the reader is referred to [17]. The dissociation of fast molecules and clusters, due to the interaction with solids, has mainly been experimentally studied by collecting the fragments which *exit* from thin foils of various thicknesses [3,5,12,18,19].

Track generation as a result of the passage of energetic single particles through materials is a well known phenomenon which has been studied extensively for more than four decades [20]. The objective of the present work is to observe in a well chosen target the modifications of the shapes of the tracks when cluster ions slow down. The target sensitivity to electronic excitations is the important parameter that will possibly allow the visualization of the molecular dissociation. Insulating targets are the best candidates, as they have much lower energy deposition thresholds for track registration than metallic targets [21]. Such experiments should allow: (i) the registration *inside* a solid of the consequences of the deviations of the trajectories of some individual projectile constituents with respect to the initial cluster ion direction or of the molecular projectile dissociation into smaller clusters and (ii) the determination of how long in space and time the constituents of the "molecule" stay close together to give collective or correlation effects.

2. Experimental

As target material we have chosen yttrium iron garnet $Y_3Fe_5O_{12}$, or YIG, a magnetic insulator in which previous studies using monoatomic heavy projectiles have shown that sufficiently high electronic energy deposition can result in track generation along the projectile path [22]. Considering the linear rate of energy deposition in electronic processes $(dE/dx)_e$, it was shown that tracks are induced above a threshold which depends on the projectile velocity and lies in the range $(dE/dx)_e^t \approx 3$ to 4.5 keV/nm [22,23], and that increasing $(dE/dx)_e$ above this threshold, (i) the structure of the tracks evolves from aligned droplets to continuously damaged amorphous cylinders [22] and (ii) the track diameter monotonically increases and seems to saturate at a diameter of ≈13 nm above $(dE/dx)_e \approx 40$ keV/nm.

The projectiles chosen in our study are energetic Au_4 and C_{60} ions delivered by the tandem accelerator at the IPN Orsay. A detailed description of the acceleration process of C_{60} beams can be found in [24,25]. Molecular C_{60}^- ions produced in a sputter ion source are accelerated in the first section of the tandem accelerator. At the positive high voltage terminal in the centre of the accelerator (4–12 MV), the C_{60}^- ions collide with N_2 molecules in a stripper cell and multiply charged C_{60}^{n+} (with $n \leqslant 4$) are formed [24]. At the exit of the tandem accelerator a set of different cluster ion beams is present which in most cases can be identified by time of flight (TOF) measurements combined with a magnetic deflector at a small angle (1.5°). In certain cases the magnetic field in combination with a TOF measurement is not sufficient, special fragment ions produced in the gas collision cell can be accelerated with the same magnetic and electrostatic rigidities. A good example is given by C_{60}^{3+} and C_{20}^{+} produced in the stripper channel from C_{60}^{-} ions introduced into the tandem accelerator. These ions have exactly the same TOF and the same magnetic rigidity, so that only energy measurements with a silicon detector allow us to distinguish the two components. This kind of coincidence measurement between energy and TOF of ions has been described in [26]. Fig. 1 presents the energy spectra of different fullerene ions after magnetic deflection and TOF coincidence with the response of a silicon detector. Fig. 1(a) and (b) show clearly one peak corresponding to C_{60}^{+} at 20.2 MeV and to C_{60}^{2+} at 30.2 MeV respectively. Fig. 1(c) presents the energy spectrum in coincidence with the TOF of C_{60}^{3+} at 40.2 MeV. We see clearly the energy peak corresponding to C_{60}^{3+}

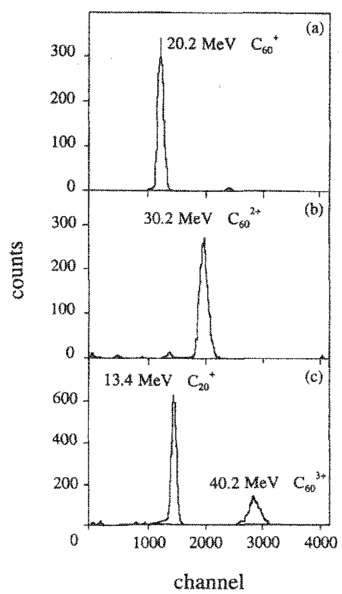

Fig. 1. Energy spectra recorded in coincidence with the arrival time of fullerene ions (C_{60}^{+}, C_{60}^{2+}, C_{60}^{3+}) produced with the tandem accelerator. The terminal voltage of the tandem accelerator is 10 MV and the C_{60}^{-} ion beam is pulsed before the entrance of the accelerator. The TOF spectra of high energy fullerene beams have been obtained after magnetic deflection at 1.5° and measured with a silicon detector. (a), (b) the energy spectra recorded in coincidence with the TOF of C_{60}^{+} and C_{60}^{2+} show only one energy peak. The energies are 20.2 and 30.2 MeV respectively. (c) the energy spectrum presents two peaks corresponding to C_{60}^{3+} at 40.2 MeV and C_{20}^{+} at 13.4 MeV.

and a second peak at low energy attributable to C_{20}^{+} at 13.4 MeV. The assignments are in agreement with the energy calibration of the detector and the correction for pulse height defect observed with this kind of cluster beams [15].

Estimating the rate of electronic energy deposition of such projectiles is still an open question. The few available experimental results [15,16] surprisingly show that the energy loss per carbon is that of an individual carbon of the same velocity within the experimental uncertainty, so that the energy loss of C_{60} is estimated as the sum of the energy loss of 60 individual carbon atoms. Comparing 40.2 MeV C_{60}^{3+} and 13.4 MeV C_{20}^{+} projectiles: (i) their velocity is the same, their calculated projected range is 740 nm, but (ii) the number of constituents differ, leading in a YIG target respectively to $(dE/dx)_e$ values of 78 and 26 keV/nm (the calculation is performed using the TRIM 90 code [27], which does not take into account collective effects in connection with the penetration of *molecules*).

The targets consist of 3 mm diameter discs cut out of bulk polycrystalline $Y_3Fe_5O_{12}$. The starting material is of good crystalline quality (porosity $\ll$ 1%, average grain size $\approx$10 μm) and was synthesized by the ceramic method starting from very high purity Y_2O_3 and Fe_2O_3 using a very long firing time (2 weeks) at 1370°C. Before irradiation they were prepared for transmission electron microscopy observations by which regions of thickness smaller than 100 nm can be imaged. The pellets were cut to thicknesses of 200 μm, polished and ion milled in order to get a central hole surrounded by thin regions. The targets were irradiated at 300 K at normal and grazing incidence ($\approx$80° of normal incidence) up to fluences of a few 10^9 molecules/cm^2 in order to avoid any spatial overlap of tracks. The electron microscopy observations of the samples irradiated at normal incidence give information on the damage induced at the beginning of the slowing-down processes. The samples irradiated at grazing incidence have the major advantage that the projectiles are stopped inside the target in regions where the thicknesses of which are perfectly suitable for electron microscopy observations. The samples were observed with a Philips CM30 transmission electron microscope. Two types of images will be

Table 1
Characteristics of the various irradiations with cluster ions: incident energies, linear rates of energy deposition by the clusters in electronic processes and atomic collisions at these impinging energies, mean projected range in YIG targets and mean track diameters D_{const} (with standard deviations) measured near the entrance surface after 300 K irradiations at normal incidence

Projectile	Incident energy (MeV)	$(dE/dx)_e$ (keV/nm)	$(dE/dx)_n$ (keV/nm)	Projected range (nm)	D_{const} (nm)
Au_4^+	20.2	17.6	13.5	631	8.4 ± 0.4
C_{20}^+	13.4	26.1	0.44	740	11.4 ± 0.9
C_{60}^+	16.2	47.4	2.5	380	16.9 ± 0.5
C_{60}^+	20.2	54.1	2.2	451	18.9 ± 0.8
C_{60}^{2+}	30.2	67.0	1.6	605	20.2 ± 0.8
C_{60}^{3+}	40.2	78.3	1.3	740	21.4 ± 1.2

presented: (i) bright field images performed under conditions such that no crystal planes are in Bragg conditions and (ii) dark field images obtained by using the electrons diffracted from amorphous material, i.e. by placing the objective aperture on the diffuse halo of the diffraction patterns.

3. Results

3.1. Irradiations at normal incidence

Table 1 presents a few parameters characteristic of various irradiations that were performed at 300 K and at normal incidence on YIG targets. The projected ranges of all the projectiles are approximately distributed within 400–700 nm. For the carbon clusters, the linear rate of energy deposition in electronic processes $(dE/dx)_e$ is 20–60 times higher than that in nuclear collisions $(dE/dx)_n$. In the particular case of Au_4 ions, the relative importance of nuclear elastic collisions is much higher. The last column of Table 1 gives the mean track diameters D_{const} (and their standard deviations) deduced from the observations of a large number of impacts (50–100 for each type of projectile).

Fig. 2 is a bright field image of a YIG sample simultaneously irradiated at 300 K with 40.2 MeV C_{60}^{3+} and with 13.4 MeV C_{20}^+ ions at normal incidence. The photograph shows two tracks seen from above at a very high magnification. The picture, as well as the electron diffraction pattern (see below) clearly show that amorphization occurred inside the tracks, in the vicinity of the projectile trajectories. Moreover, using such pictures, it is easy to precisely determine the radii of the tracks (≈19 nm for the C_{60}^{3+} track and 11 nm for the C_{20}^+ track in this particular case).[2]

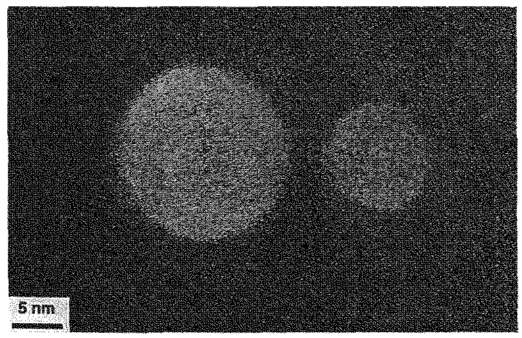

Fig. 2. High resolution transmission electron micrograph of a YIG sample simultaneously irradiated with 40.2 MeV C_{60}^{3+} and 13.4 MeV C_{20}^+ at normal incidence. The incident beam direction is normal to the plane of the image. The matter located inside the two tracks, corresponding to the two types of projectiles, consists of amorphous material.

All the available experimental results concerning the evolution of the track diameter with the amount of electronic energy deposition $(dE/dx)_e$ after monoatomic [22,28] or cluster ions irradia-

[2] The density of C_{20}^+ tracks which are observed is always much smaller than the impinging C_{20}^+ fluence, whereas there is a good agreement between these two parameters concerning C_{60}^{3+} projectiles. The C_{20}^+ ions result from collisions of C_{60} with N_2 molecules in the gas cell, and subsequent fragmentation with a wide internal energy spread. This might well give birth to C_{20} isomers of various shapes, the compact shape of C_{20} being perhaps the only one which leaves a cylindrical track in the YIG target. This hypothesis will be checked in future experiments.

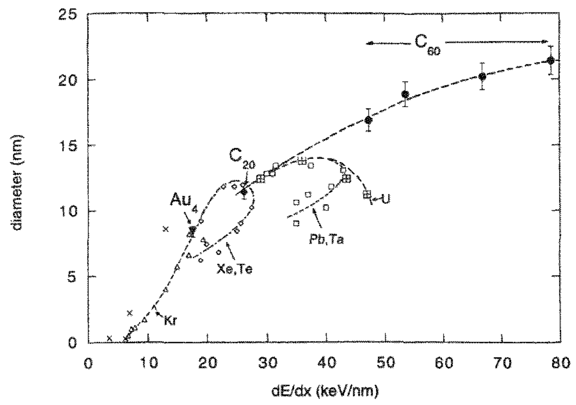

Fig. 3. Graph showing the track diameter in YIG targets as a function of the linear rate of energy deposition in electronic excitation after room temperature irradiations with GeV monoatomic ions [22,28]: (×), Ar, F, S… ; (△), Kr; (◇), Xe, Te; (□), Pb, Ta; (⊞), U; 13–40 MeV cluster ions: (▼) Au_4, (◆) C_{20}, (●) C_{60}. All the dotted lines are drawn to guide the eye.

tions of YIG are reported in Fig. 3. The diameters corresponding to cluster irradiations were all determined from electron microscopy observations of the continuously damaged cylinders, whereas in the case of monoatomic projectiles, the diameters which are reported are "effective" diameters deduced from damage cross-section measurements [22]. More precisely, these effective diameters correspond to those observed in the electron microscope when the rate of energy deposition is sufficiently high to induce continuous tracks, but when the generated tracks have a discontinuous structure, they are the *calculated* diameters of "continuously damaged cylinders" in which the amorphous phase of the discontinuous defects is artificially concentrated.

The points relative to similar types of projectiles (neighbouring atomic masses, carbon clusters,…) are linked by dotted lines, in order to allow an easy quick look at the results. *For a given type of projectile* (see typically the numerous points for Pb or Xe), when its *energy* increases, the diameter of the track generated in the target increases, reaches a maximum value (*at most* ≈ 13 nm after irradiation with the heaviest available *monoatomic* ion: U), and then decreases again when velocity increases beyond the stopping power maximum: this effect is often called the "velocity effect" in the literature, indicating that for the same linear rate of energy deposition $(dE/dx)_e$, slow projectiles induce larger diameter tracks than swift projectiles.

Using carbon clusters it is possible to explore $(dE/dx)_e$ values that lie far above those which are accessible with monoatomic projectiles: the maximum $(dE/dx)_e$ that one could reach in YIG irradiated with C_{60} ions is 94 keV/nm.

In the low $(dE/dx)_e$ region, the track diameters observed at the same $(dE/dx)_e$ after irradiation with monoatomic projectiles and carbon clusters are very similar although the velocities are quite different. For example, at the arrow position around $(dE/dx)_e = 26$ keV/nm, the Xe velocity is $\beta = v/c = 0.055$, whereas C_{20} is much slower ($\beta = 0.011$).

The contribution of elastic collisions to the damage induced by the carbon cluster projectiles has been estimated from the TRIM 90 code, using a displacement threshold energy of 25 eV for Y, Fe and O in YIG, as the experimental determination of the displacement threshold energy of each constituent of YIG has not been done to our knowledge. In the first 100 nm of the path of a 13.4 MeV C_{20}^+ ion in YIG, the calculated number of displacements resulting from nuclear collisions is almost constant and approximately 8 displacements/nm path. The maximum nuclear damage at the target entrance is obtained during irradiations with 16.2 MeV C_{60}^+ and estimated to 30 displacements/nm path, which cannot account for the observed damage [13].

3.2. Irradiations at grazing incidence

Figs. 4 and 5 show bright field and dark field images of two typical regions in a sample simultaneously irradiated at 300 K with 40.2 MeV C_{60}^{3+} and 13.4 MeV C_{20}^+ beams at grazing incidence up to a total fluence of a few 10^9 projectiles/cm^2. Two types of latent tracks induced by both types of projectiles are clearly seen on the bright field images (Figs. 4(a) and 5(a)).

After C_{60}^{3+} irradiations, three features are observed.

(i) A great number of tracks have a "carrot-like" shape, i.e. their average diameter decreases as the projectiles slow down.

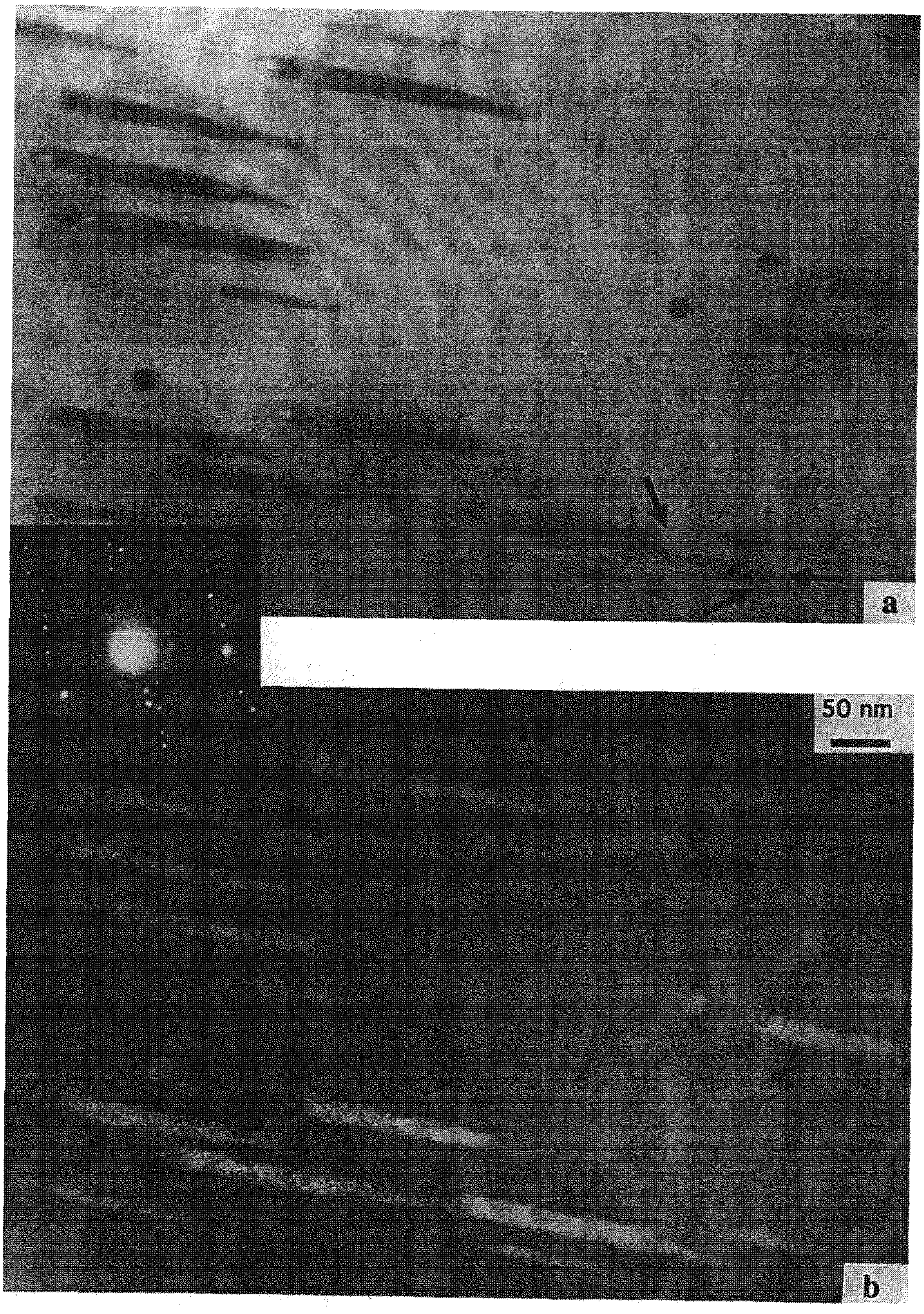

Fig. 4. Transmission electron micrographs of YIG irradiated at 300 K with 40.2 MeV C_{60}^{3+} and 13.4 MeV C_{20}^{+} at grazing incidence. (a) Bright field image. A track separating into three branches is pointed out with the arrows. (b) Dark field image obtained by using the electrons diffracted from amorphous material (diffuse halo of the diffraction pattern).

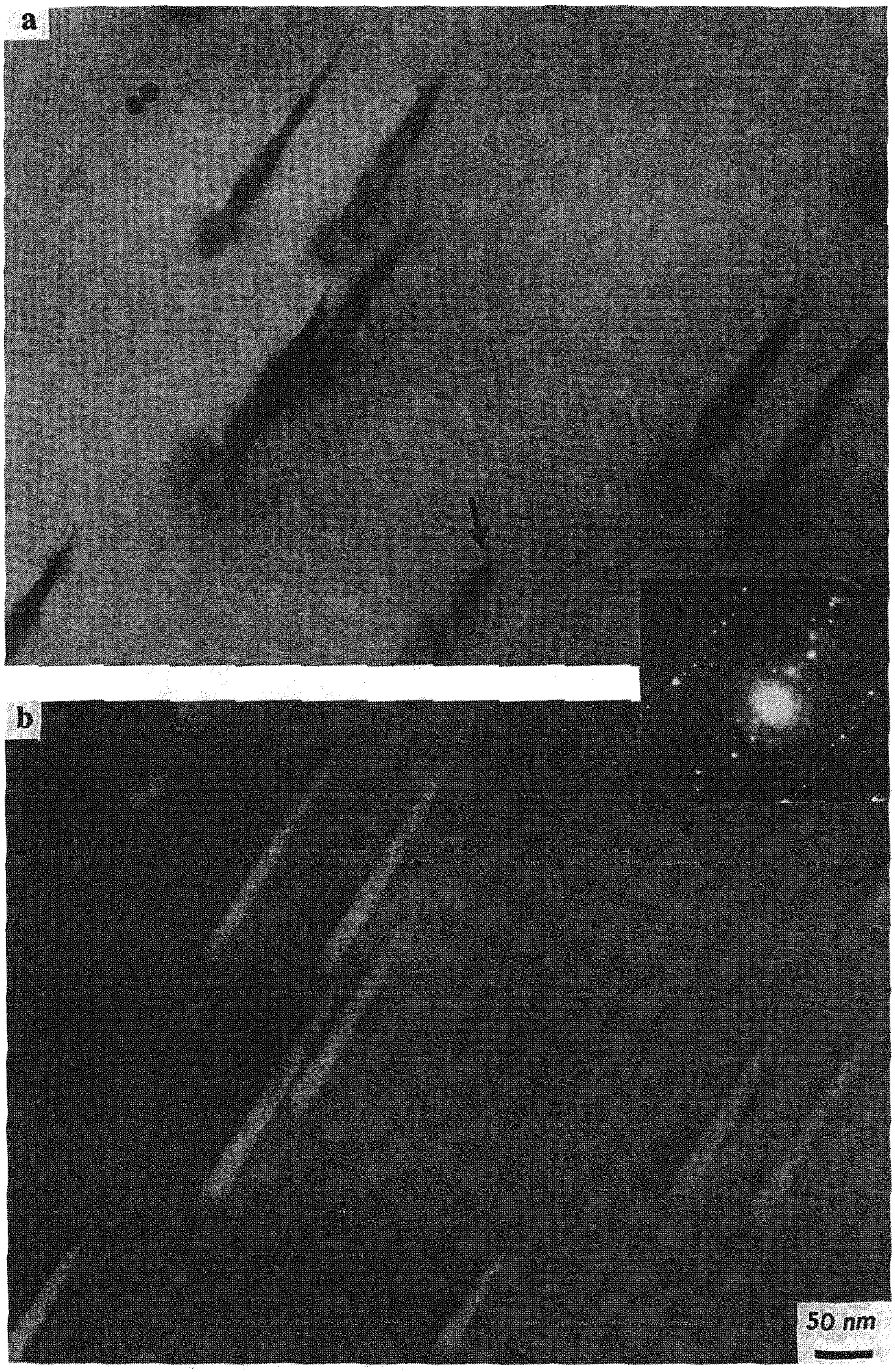

Fig. 5. Transmission electron micrographs of YIG irradiated at 300 K with 40.2 MeV C_{60}^{3+} and 13.4 MeV C_{20}^{+} at grazing incidence. (a) Bright field image. A short track ending abruptly is pointed out with an arrow. (b) Dark field image obtained by using the electrons diffracted from amorphous material (diffuse halo of the diffraction pattern).

(ii) The C_{60}^{3+} tracks often separate into two branches or even three (see Figs. 4(a) and 6(b)). This is an indication of the dissociation of the cluster of ions into smaller size groups: it has to be emphasized that the small groups must consist of sufficient numbers of neighboring constituents, which stay close to each other in order to interact as a unique projectile entity, and thus to deposit sufficient energy in the target to create tracks.

(iii) Sometimes the tracks stop very abruptly (see for example the arrow in Fig. 5(a)): no smaller diameter tracks being generated, this indicates that in this case the group of fragments explodes into very small entities which are unable to create tracks, most probably leading to a widely spread "shower" of almost individual carbon ions.

In the case of C_{20}^{+} irradiations:

(i) The 'carrot-like' shape is often observed.

(ii) The separation into branches is more rarely observed than for C_{60}^{3+}, which is easily explained by the difficulty to overcome the track registration threshold starting from a smaller size cluster, each constituent having the same initial velocity.

Fig. 6 shows magnifications of some tracks. The arrows indicate two interesting features: the *apparent* increase of the track diameter when the cluster breaks up into three large groups of constituents, the existence of very long tracks (≈320 nm, i.e. almost half the projected range), indicating that sometimes a large number of constituents keep a good spatial correlation deeply inside the target.

The observed changes in the morphology of C_{60}^{3+} tracks (decrease of the diameter, separation into branches) are often associated with a shift of the apparent position of the centre of mass of the *remaining* fragments (Fig. 6(a)), but not with a significant angular deviation. Such changes also occur at similar depths (⩾100 nm) on the C_{20}^{+} tracks, of much smaller diameters.

Some statistical information deduced from measurements on a few hundred tracks in three types of irradiations at grazing incidence are reported in Table 2: length L_{const} on which the track diameter stays almost constant, total track length L_{tot} and other quantities that will be used later in the discussion. Histograms for 40.2 MeV C_{60}^{3+}

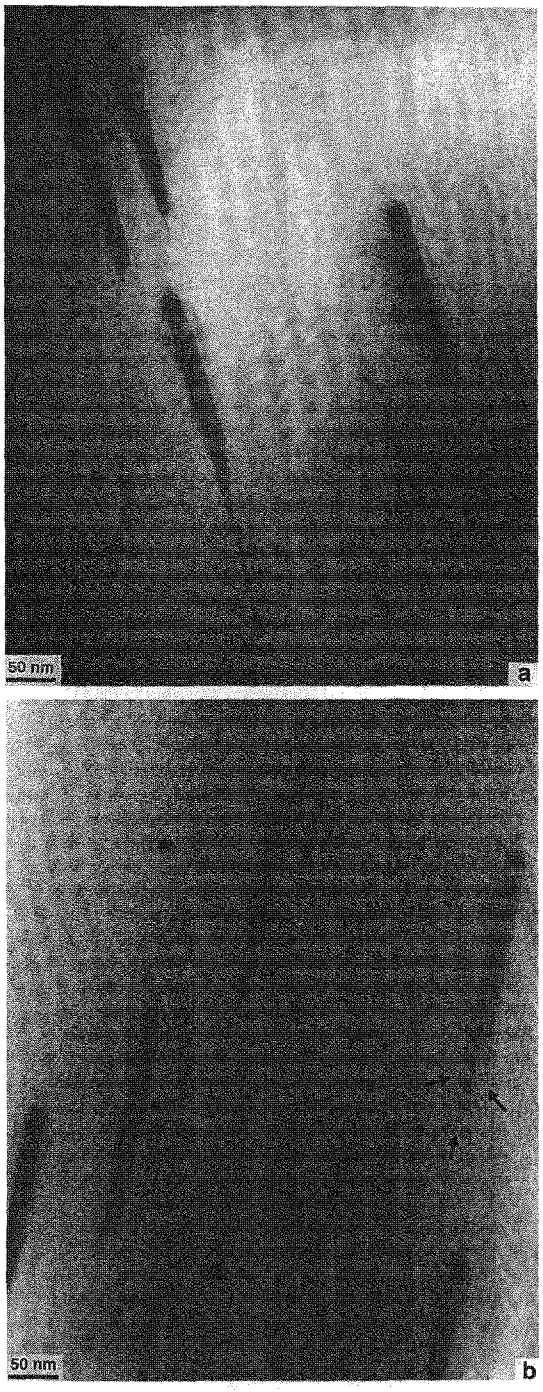

Fig. 6. Bright field images of track induced in YIG irradiated at 300 K with 40.2 MeV C_{60}^{3+} at grazing incidence. The arrows point out two interesting features: (a) an extremely long track in which a large number of ions keep a good spatial correlation; (b) a track which increases in diameter before separating into three branches.

Table 2
Statistical description of the tracks induced in YIG irradiated at 300 K with energetic cluster ions: – D_{const}: observed track diameter near the entrance, – L_{const}: length on which the track diameter stays almost constant, with standard deviation, – L_{tot}: total length on which tracks are registered in the samples, – $R_{\mathrm{str.}}(\sigma)$: lateral straggling radius (dispersion on $R_{\mathrm{str.}}$) estimated from TRIM at a depth L_{const}, – $\mathrm{d}E/\mathrm{d}x_{\mathrm{e,o}}$: linear rate of energy deposition in electronic processes per cluster constituent at the target entrance, – $\mathrm{d}E/\mathrm{d}x_{\mathrm{e},L\mathrm{const}}$: same as above, at a penetration depth L_{const}, – D_{corr}: mean distance between two carbon atoms as deduced from eq. (3) in text

Projectile	Incident energy (MeV)	D_{const} (nm)	$4(\mathrm{d}E/\mathrm{d}x)_{\mathrm{e,o}}/\pi D^2_{\mathrm{const}}$ (eV/nm^3)	L_{const} (nm)	L_{tot} (nm)	R_{str} (σ) (nm)	$(\mathrm{d}E/\mathrm{d}x)_{\mathrm{e,o}}$ per constituent (eV/nm)	$(\mathrm{d}E/\mathrm{d}x)_{\mathrm{e},L_{\mathrm{const}}}$ per constituent (eV/nm)	D_{corr} (nm)
Au_4^+	20.2	8.4	317						
C_{20}^+	13.4	11.4	256	94 ± 21	146 ± 24	3.5 (11)	1305	1140	2.77
C_{60}^+	16.2	16.9	211				789		
C_{60}^+	20.2	18.9	192	79 ± 14	125 ± 18	5.5 (19.5)	902	760	2.51
C_{60}^{2+}	30.2	20.2	209				1118		
C_{60}^{3+}	40.2	21.4	217	118 ± 21	227 ± 32	5 (16)	1305	1110	2.28

and 13.4 MeV C_{20}^+ tracks in YIG are shown in Fig. 7. The mean values reported in Table 2 are extracted from the histograms. At the target entrance the C_{60}^{3+} tracks have an average diameter of 21.4 nm, whereas C_{20}^+ tracks have an average diameter of 11.4 nm. The track diameters stay almost constant during an average travelled distance of 118 nm for C_{60}^{3+} and 94 nm for C_{20}^+.

Fig. 8 shows a detailed study of a group of two tracks registered after a grazing incidence irradiation of YIG with 40.2 MeV C_{60}^{3+} ions. Fig. 8(a) shows a particular track separating into two "branches" (the sample is perpendicular to the electron beam in the microscope). In order to show that one really deals with two separated flows of projectiles, the sample was rotated in the electron microscope by ±40° along the track axis (Fig. 8(c) and (d)). The distance between the two branches is indeed reduced by 20%, which corresponds well to the fact that the image is a projection of the tracks after rotation of the sample.

Finally, it has to be noticed that a different contrast is visible at the entrance of the target (Figs. 4–6). Due to the large amount of energy released at the surface, ejection of matter occurs. The material is sputtered from cones which appear as elongated shapes on the photographs due to the grazing incidence of the projectiles. Fig. 9 shows a group of tracks imaged in different focusing conditions in the microscope: focused (9a), underfocused by 1.2 μm (9b), overfocused by 1.9 μm

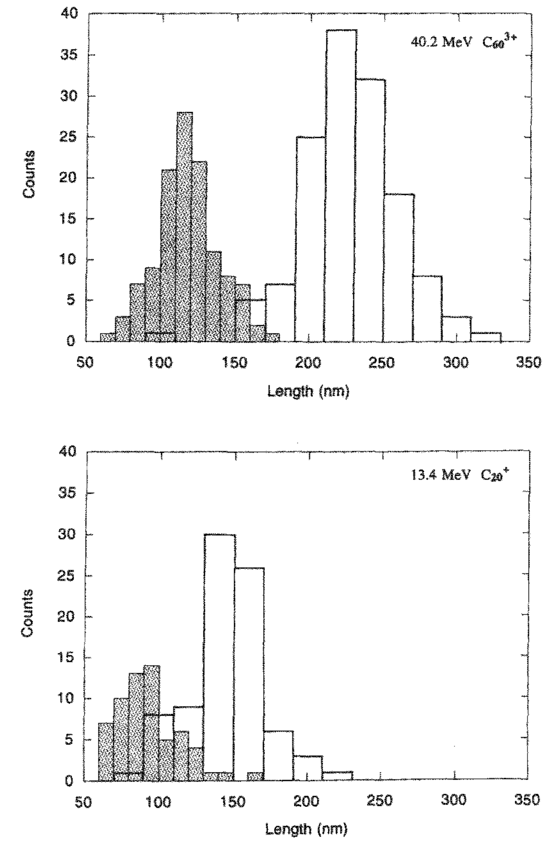

Fig. 7. Histograms giving the repartition of the length on which the track diameter appears to stay almost constant (grey) and of the total length on which the tracks are registered (white) in YIG samples irradiated at 300 K with 40.2 MeV C_{60}^{3+} and 13.4 MeV C_{20}^+ at grazing incidence (see also Table 2).

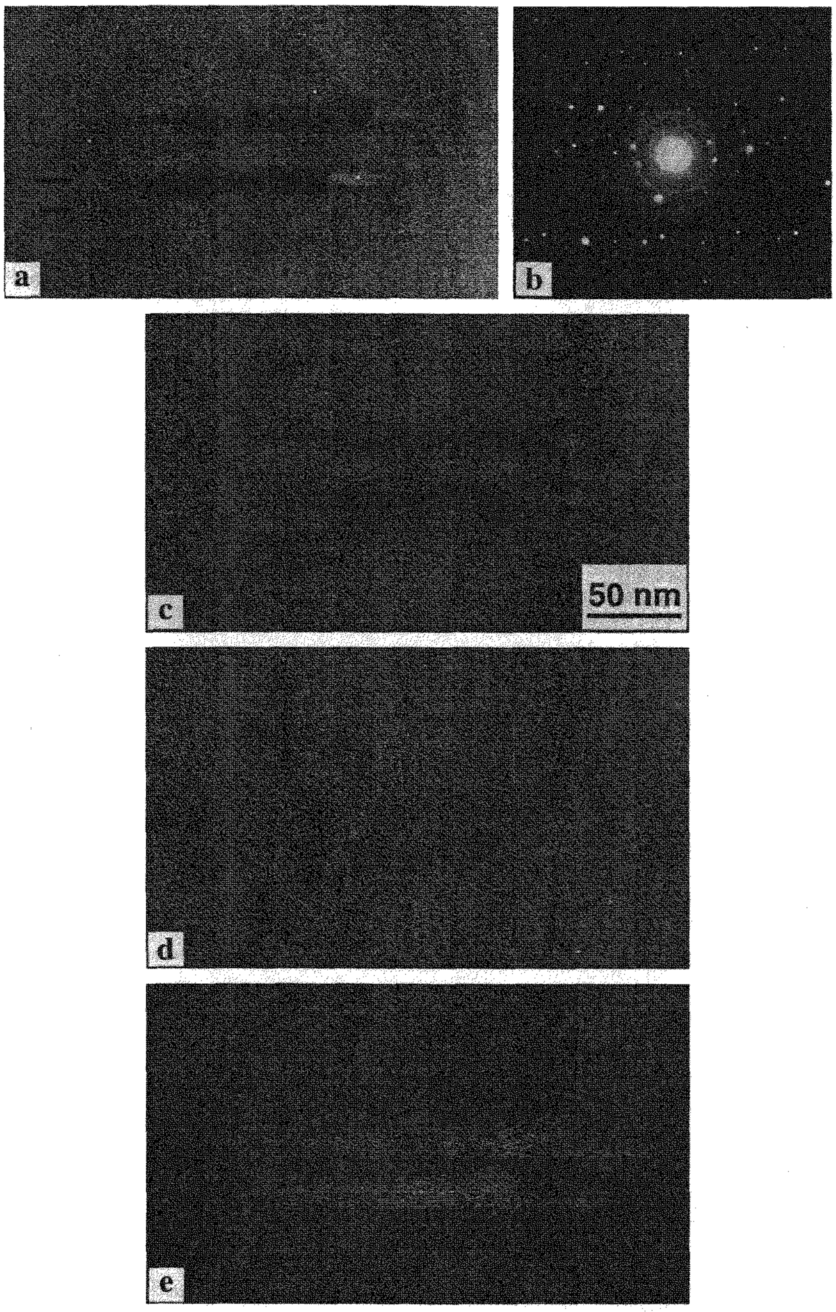

Fig. 8. Electron micrographs of two tracks induced in YIG irradiated at 300 K with 40.2 MeV C_{60}^{3+} at grazing incidence (a), (c) and (d) bright field images in which the sample is respectively normal to the electron beam, tilted by −40° or +40° along the direction of the track axis. (e) dark field image performed in the +40° rotated configuration, using the electrons corresponding to the diffuse halo of the electron diffraction pattern (b).

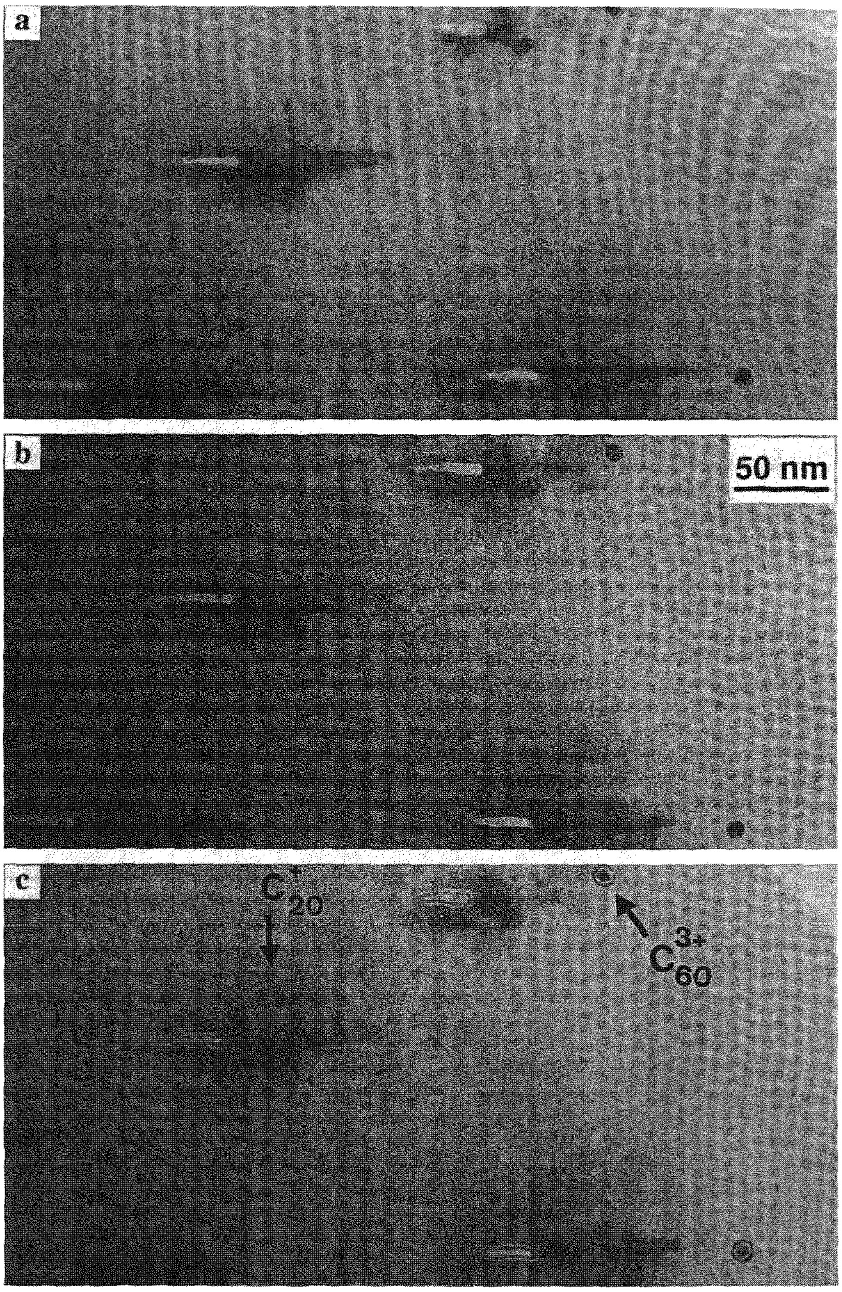

Fig. 9. Bright field images of track induced in YIG irradiated at 300 K with 40.2 MeV C_{60}^{3+} and 13.4 MeV C_{20}^{+} at grazing incidence. Elongated craters and redeposited material resulting from sputtering at the entrance surface of the target are imaged in: (a) focused conditions, (b) underfocused by 1.2 μm, (c) overfocused by 1.9 μm. A strong phase contrast (Fresnel fringes) appears in the regions concerned with sputtering effects.

(9c). The sputtered regions give rise to very strong phase contrast (Fresnel fringes). This sputtering effect is also, in our view, responsible for the dark isolated round spots which come from matter that has been ejected from inside the tracks as large size "clusters" which sometimes fall back on the sample surface. The arrows in Fig. 9 indicate such objects generated by both types of projectiles.

Some matter is also present on top of the sample surface at the entrance of the tracks. A typical example is given in Fig. 8 in which a hillock gives a dark round contrast in Fig. 8(a) when it is seen from above, and appears either below or above the track axis when the sample is rotated (Fig. 8(c) and (d)).

Finally, all dark field images (Figs. 4(b), 5(b) and 8(e)) show that amorphous matter exclusively lies inside (i) the tracks, (ii) the hillocks and (iii) the clusters ejected from the track core. The sputtering effects will be described in more detail elsewhere [29].

4. Discussion

Inside the solid, the track has a constant diameter, and then a variable decrease of diameter (carrot-shape). We assume that:

- the constant diameter is attributed to correlated effects induced by all neighbouring cluster constituents;
- the carrot-shape may have various origins (i) the gradual loss of constituents due to Coulomb repulsion between ionized fragments or (ii) to elastic collisions with the target atoms, (iii) the decreasing energy (and corresponding decrease of the energy deposition rate) of the projectiles. In the energy range that we study here, we can notice (Table 2) that the variation of the energy deposition $(\mathrm{d}E/\mathrm{d}x)_e$ is small, so that this last point should not be of major importance.

In order to account for the experimental observations, we must estimate the scattering of the constituents as a function of the distance travelled by the projectile, both from Coulomb repulsion and from atomic collisions. This will allow us to determine the average distance between two carbon atoms inducing a collective effect. Finally, the response of the target material to different energy densities will be tackled.

4.1. Scattering of the cluster constituents

4.1.1. Scattering due to Coulomb repulsion between the constituents

The fast carbon clusters impinging on a solid target lose their valence electrons in the first atomic layers. At the energies used in this study, the equilibrium charge state of individual carbon atoms is of the order of 2, so that this leads to highly ionized clusters that will gradually increase in diameter leading to a decrease of the deposited energy density.

The ionization cross-section of each carbon constituent is $\sigma_i \approx 10^{-15}$ cm^{-2} [30]. After a travelled distance of 10 Å the mean charge of such a carbon is approximately 80% of the equilibrium charge which is reached after a travelled distance of ≈100 Å. The proximity of the cluster constituents may change the charge state inside the solid. The study of this effect is in progress [31]. It has been shown that the mean charge state is smaller (15% with C_5) than when the atoms independently penetrate into the solid. The use of the atomic equilibrium charge state for qualitative evaluations of the expansion due to Coulomb repulsion will thus maximize the effect.

As soon as the incident cluster is stripped, the positively charged ions begin to separate due to Coulomb forces. This Coulomb interaction between two constituents at a distance r can be written as

$$U(r) = [q_1 q_2 (e^2/r)]\exp(-r/a_s) \tag{1}$$

in which q_1 and q_2 are the charge states of the two ions and the exponential term is the screening due to the target electrons. For slow projectiles, the screening length does not depend on the velocity of the projectile and is always smaller than the internuclear distance for molecules and clusters [32]. At high velocities, the screening length is proportional to the velocity. In our case the velocity of the fast fullerene is just in the intermediate region.

Experimental results concerning irradiations with small molecules [5] indicate that the Coulomb explosion dominates in *very thin* films. At the entrance of the target, it is difficult to completely ignore the Coulomb repulsion: the stripped cluster constituents expand in the first layers and screening appears. The *maximum* expansion of the C_{60} molecule due to the Coulomb repulsion can be approximated in the vacuum, i.e. *without screening* by the expansion of a homogeneous charged spherical surface. This simple assumption and the knowledge of the projectile velocity permit to calculate the radius of the sphere after a given path: for example the sphere radius of C_{60}^{120+} at 40.2 MeV reaches 2 nm after a flight of 100 nm. This value which corresponds to the *maximum* size of the expanding sphere is smaller than the lateral spread due to the multiple scattering processes, as will be shown just below.

4.1.2. Scattering due to elastic collisions

More than 20 years ago, several groups have studied multiple scattering of ions transmitted through thin foils, in the keV to MeV energy range, with many target–projectile combinations: a few experimental results are given in [33–40]. A good agreement has been obtained between theories [41–43] and experiments in amorphous and polycrystalline targets. The differences which were observed for the experiments in crystalline targets (the experimental angular distributions were narrower than the predicted distributions) have been attributed to the target texture causing correlated scattering [37].

Now for heavy cluster ions as projectiles, there is no experimental result concerning the lateral straggling induced by elastic collisions. In our analysis we assume that the cluster ion dissociates due to initial Coulomb repulsion and that the constituents trajectories begin to evolve independently. The lateral distribution due to multiple scattering can then be calculated for independently moving fragment ions.

The depth dependence of the lateral straggling of the carbon into YIG due to multiple scattering has been calculated at different energies as a function of the penetration depth, and the values R_{str} corresponding to L_{const} have been reported in Table 2. If we assume that the lateral straggling follows a gaussian radial distribution, exp $(-r^2/R_{\mathrm{str}}^2)$, then there is a probability of 95% to find all cluster constituents in the area $\pi(2R_{\mathrm{str}})^2$.

An estimation of the maximum average distance D_{corr} between two adjacent carbon inducing additional effects can be calculated. We have assumed that the 60 carbon atoms are distributed in an area of radius equal to $2R_{\mathrm{str}}$. The mean projected distance between two carbon is calculated using the relation

$$D_{\mathrm{corr}}^2 = 4(\pi R_{\mathrm{str}}^2)/n \qquad (2)$$

in which n is the number of constituents of the cluster.

These calculated distances D_{corr} are found almost constant ($\approx$2.5 nm). The dispersion can be explained either by the uncertainties of the calculation (20% uncertainty on the radius is enough to correct the differences) or by the Coulomb repulsion which increases the straggling.

The distance D_{corr} is close to twice the radial range of the δ electrons ($\approx$1 nm, see Section 4.2) and suggests that the loss of correlation of the incident cluster constituents appears when the mean distance between two fragments exceeds the range of the δ electrons. This analysis is in agreement with the simple understanding of the coherent effect in terms of overlapping of δ electron expansion around the constituent trajectories.

Beyond the total correlation length L_{const}, the proximity or overlapping of carbon trajectories does not permit to consider that all the constituents of the C_{60} projectiles are correlated. The transmission electron microscopy images (Fig. 6) show clearly that the distribution of the fragments around the straight path of the projectile centre of mass is not always of cylindrical symmetry or homogeneous within the section of the cylinder, as the carrot-like shapes present either one or a few "carrot" endings which are not always aligned along the impinging projectile axis. The statistical nature of energy loss and scattering processes lead to this complexity of track shapes.

The only simple correlation that can be established is that the travelled distance which is necessary to obtain a correlation loss increases with the number of cluster constituents and with the projectile velocity.

4.2. Energy density considerations

The role of the deposited energy can be extracted from the experimental results obtained with different kinds of clusters (Au_4, C_{20}, C_{60})

and different energies for C_{60} (see Table 1). The first experimental comparison of the diameters of the tracks obtained with cluster beams and atomic ion beams in metals [13] has demonstrated clearly that the linear rate of electronic energy loss is not the relevant parameter governing track formation and that the energy per volume is more relevant.

From the results quoted in Table 2 which are relative to a limited low velocity range, one can extract a simple relation

$$P = [4/(\pi D^2_{\mathrm{const}})](\mathrm{d}E/\mathrm{d}x)_{\mathrm{e,o}} \approx 235\ \mathrm{eV/nm^3}, \qquad (3)$$

which corresponds to an averaged energy of 2.77 eV/atom inside all the track volume.

At the target *entrance*, the mean energy density deposited in the volume of the track is constant in the considered velocity range whatever the number of cluster constituents and the linear rate of electronic energy deposition at the surface $(\mathrm{d}E/\mathrm{d}x)_{\mathrm{e,o}}$. In this formula: (i) the electronic energy loss of the projectile is calculated as the sum of individual carbon ion contributions [15] and (ii) D_{const} is the diameter of the track.

Now let us consider the influence of the deposited energy density in the track. This can be studied comparing energetic monoatomic (GeV Xe to U) and cluster (a few MeV C_{60}) projectiles having the same linear rate of electronic energy deposition in a YIG target, but velocities differing by one order of magnitude. The resulting tracks have very similar diameters (Fig. 3), which could be related to the radial expansion of the energy transferred versus secondary electrons. At low velocities (cluster irradiations), all the secondary electrons produced by the passage of the atomic ion are stopped inside the track (the maximum δ electron energy corresponding to head-on collisions with target atoms is close to 50 eV and corresponds to a range of a few interatomic distances) and all energy provided by the secondary electrons is used to produce the observed damage. With high velocity projectiles (monoatomic GeV beams), the δ electrons have maximum energies of $\approx$10 keV corresponding to ranges ($\approx$1000 nm) which are much larger than the diameter of the track, so that part of the deposited energy does not participate in the track formation.

Apparently, the tracks generated by low velocity atomic projectiles and very low velocity clusters at the same $(\mathrm{d}E/\mathrm{d}x)_{\mathrm{e}}$ have similar diameters. For fullerene ions (0.7 nm diameter) as projectiles the range of δ electrons is less than 1 nm, so that the energy density is initially localized inside a diameter of $\leqslant 3$ nm, whereas the track diameters largely exceed this value (Table 1) in the first nanometer of matter penetration. The initial energy density deposited by the δ electrons is thus not directly related to the track radius, so that the approach developed in Ref. [44] which relates the energy density to the generated track radius (versus the minimum energy density required to break the bond between atoms) cannot explain the experimental results obtained with cluster projectiles. After a travelled distance close to L_{const}, the energy is deposited within an area which is almost two orders of magnitude larger than that defined at the entrance. The *linear rates* of energy deposition by the C_{60} projectiles are similar at the target entrance and at a depth L_{const}; the initial *volumic energy densities* (corresponding to the area on which all the constituents are distributed) are completely different but after lateral spread of the energy they lead to the same final volumic *energy densities* and result in very similar *damage* in the target. Close to the target entrance, the radial expansion of the deposited energy must be of major importance in the process of track formation, whereas at the depth D_{const}, just before correlation decreases, the primary energy deposition is homogeneous and coherent in time in the totality of the track volume. These two extreme ways to deposit energy (primary energy deposition in femtoseconds) finally have the same macroscopic consequences, as the formation of the track in an insulating material needs a duration of the order of picoseconds, which is the time required to reform the atomic bonds.

5. Conclusions

The use of energetic heavy clusters as projectiles allows us to deal with very high and localized initial energy deposits, due to the low velocity of the projectiles. The irradiation at grazing incidence of an insulator (YIG) with C_{60} projectiles gives the possibility to observe the dissociation of these molecules during their slowing-down.

It is seen that some constituents stay close together deeply into the solid giving rise to *constant track diameters* up to $\approx$100 nm penetration depth. The surface on which primary energy deposition takes place varies by almost two orders of magnitude between the target entrance and the region where the track diameter starts decreasing, which shows that in this region all the deposited energy stays uniformly confined inside the track volume.

In some cases, many projectile constituents can stay in close vicinity up to distances of about half the projected range of the projectile. The observations of different branches or of a lateral shift of the centre of mass of the track tail are direct consequences of statistically asymmetric repartitions of the cluster constituents.

Acknowledgements

We would like to express our sincere thanks to Hubert Pascard for the elaboration of the YIG pellets, to Daniel Lesueur for numerous suggestions, to Peter Sigmund for continuing interest in the work and to Dominique Jacquet for a final reading of the manuscript.

References

[1] W. Brandt, A. Ratkowski, R.H. Ritchie, Phys. Rev. Lett. 33 (1974) 2325.
[2] J.W. Tape, W.M. Gibson, J. Remillieux, R. Laubert, H. Wegner, Nucl. Instr. and Meth. 132 (1976) 75.
[3] Z. Vager, D.S. Gemmell, Phys. Rev Lett. 37 (1976) 1352.
[4] M. Steuer, D.S. Gemmell, E. Kanter, E. Johnson, B. Zabransky, Nucl. Instr. and Meth. 194 (1982) 227.
[5] D.S. Gemmell, Nucl. Instr. and Meth. 194 (1982) 255.
[6] J.P. Thomas, R.E. Oladipo, M. Fallavier, Nucl. Instr. and Meth. B 32 (1988) 354.
[7] M. Salehpour, D.L. Fishel, J.E. Hunt, Phys. Rev. B 38 (1988) 12320.
[8] K. Boussofiane-Baudin, A. Brunelle, P. Chaurand, S. Della-Negra, J. Depauw, P. Håkansson, Y. Le Beyec, Nucl. Instr. and Meth. B 88 (1994) 61.
[9] K. Baudin, A. Brunelle, S. Della-Negra, D. Jacquet, P. Håkansson, Y. Le Beyec, M. Pautrat, R.R. Pinho, Ch. Schoppmann, Nucl. Instr. and Meth. B 112 (1996) 59.
[10] H. Rothard, D. Dauvergne, M. Fallavier, K.O. Groeneveld, R. Kirsch, J.C. Poizat, J. Remillieux, J.P. Thomas, Radiat. Eff. Defects in Solids 126 (1992) 373.
[11] A. Billebaud, D. Dauvergne, M. Fallavier, R. Kirsch, J.C. Poizat, J. Remillieux, H. Rothard, J.P. Thomas, Nucl. Instr. and Meth. B 112 (1996) 79.
[12] M. Döbeli, R.M. Ender, U.S. Fisher, M. Suter, H.A. Synal, D. Vetterli, Nucl. Instr. and Meth. B 94 (1994) 388.
[13] H. Dammak, A. Dunlop, D. Lesueur, A. Brunelle, S. Della-Negra, Y. Le Beyec, Phys. Rev. Lett. 74 (1995) 1135.
[14] E. Ray, R. Kirsch, H.H. Mikkelsen, J.C. Poizat, J. Remillieux, Nucl. Instr. and Meth. B 69 (1992) 133.
[15] K. Baudin, A. Brunelle, M. Chabot, S. Della-Negra, J. Depauw, D. Gardès, P. Håkansson, Y. Le Beyec, A. Billebaud, M. Fallavier, J. Remillieux, J.C. Poizat, J.P. Thomas, Nucl. Instr. and Meth. B 94 (1994) 341.
[16] Ch. Tomaschko, D. Brandl, R. Kügler, M. Schurr, H. Voit, Nucl. Instr. and Meth. B 103 (1995) 407.
[17] P. Sigmund, I. Bitensky, J. Jensen, Nucl. Instr. and Meth. B 112 (1996) 1.
[18] Z. Vager, R. Naaman, E.P. Kanter, Science 244 (1989) 426.
[19] O. Heber, D. Kella, D. Zajfman, H. Feldman, D. Majer, Z. Vager, R. Naaman, Nucl. Instr. and Meth. B 79 (1993) 227.
[20] R.L. Fleischer, P.B. Price, R.M. Walker, Nuclear Tracks in Solids, University of California Press, Berkeley, CA, 1975.
[21] A. Barbu, H. Dammak, A. Dunlop, D. Lesueur, Mat. Res. Soc. Bull. 20 (12) (1995) 29.
[22] A. Meftah, F. Brisard, J.M. Costantini, M. Hage-Ali, J.P. Stoquert, F. Studer, M. Toulemonde, Phys. Rev. B 48 (1993) 920.
[23] A. Meftah, M. Hage-Ali, J.P. Stoquert, F. Studer, M. Toulemonde, Radiat. Eff. Defects in Solids 126 (1992) 373.
[24] S. Della-Negra, A. Brunelle, Y. Le Beyec, J.M. Curaudeau, J.P. Mouffon, B. Waast, P. Håkansson, B.U.R. Sundqvist, E.S. Parilis, Nucl. Instr. and Meth. B 74 (1993) 453.
[25] P. Håkansson, S. Della-Negra, J.P. Mouffron, B. Waast, P. Sullivan, Nucl. Instr. and Meth. B 112 (1996) 39.
[26] K. Boussofiane-Baudin, A. Brunelle, P. Chaurand, J. Depauw, S. Della-Negra, P. Håkansson, Y. LeBeyec, Int. J. Mass. Spectrom. Ion Proc. 130 (1994) 73.
[27] J.P. Biersack, L.G. Haggmark, Nucl. Instr. and Meth. 174 (1980) 257; J.F. Ziegler, J.P. Biersack, U. Littmark in Stopping Power and Ranges of Ions in Matter, vol. 1, Pergamon, New York, 1985.
[28] A. Meftah, J.M. Costantini, M. Djebara, N. Khalfaoui, J.P. Stoquert, F. Studert, M. Toulemonde, Nucl. Instr. and Meth. B 122 (1997) 470.
[29] J. Jensen, A. Dunlop, S. Della-Negra, G. Jaskierowicz, (in preparation).
[30] J.A. Kune, W.H. Soon, J. Chem. Phys. 95 (1991) 5738.

[31] A. Brunelle, S. Della-Negra, J. Depauw, D. Jacquet, Y. Le Beyec, M. Pautrat, Ch. Schoppmann, Nucl. Instr. and Meth. B. 125 (1997) 207.
[32] W. Brandt, in: S. Datz, B.R. Appleton, C.D. Moak (Eds.), Third International Conference on Atomic Collisions in Solids, vol. 1, Plenum, New York 1975, p. 261.
[33] H.H. Andersen, J. Bøttiger, Phys. Rev. B 4 (1971) 2105.
[34] S. Schwabe, R. Stolle, Phys. Stat. Sol. B 47 (1971) 111.
[35] F. Bernhard, P. Krygel, R. Manns, G. Schwabe, Radiat. Eff. 13 (1972) 197.
[36] H.H. Andersen, J. Bøttiger, H. Knudsen, Radiat. Eff. 13 (1972) 203.
[37] H.H. Andersen, J. Bøttiger, H. Knudsen, P. Møller Petersen, T. Wohlenberg, Phys. Rev. A 10 (1974) 1568.
[38] G. Sidenius, N. Andersen, Nucl. Instr. and Meth. 128 (1975) 271.
[39] G. Sidenius, N. Andersen, Nucl. Instr. and Meth. 131 (1975) 387.
[40] H. Knudsen, F. Besenbacher, J. Heinemeier, P. Hvelplund, Phys. Rev. A 13 (1976) 2095.
[41] L. Meyer, Phys. Stat. Sol. B 44 (1971) 253.
[42] P. Sigmund, K.B. Winterbon, Nucl. Instr. and Meth. 119 (1974) 541.
[43] A.D. Marwick, P. Sigmund, Nucl. Instr. and Meth. 126 (1975) 317.
[44] T.A. Tombrello, Nucl. Instr. and Meth. B 83 (1993) 508.

ELSEVIER

Nuclear Instruments and Methods in Physics Research B 135 (1998) 295–301

NIM B Beam Interactions with Materials & Atoms

Tracks in YIG induced by MeV C_{60} ions

J. Jensen [a,c], A. Dunlop [a,*], S. Della-Negra [b], H. Pascard [a]

[a] *Laboratoire des Solides Irradiés, CEA/CNRS/Ecole Polytechnique, 91128 Palaiseau, France*
[b] *Institut de Physique Nucléaire, CNRS-IN2P3, 91406 Orsay, France*
[c] *Fysisk Institut, Odense Universitet, 5230 Odense M, Denmark*

Abstract

Samples of yttrium iron garnet ($Y_3Fe_5O_{12}$ or YIG) were irradiated at 300 K with MeV C_{60}-ions at normal and tilted incidence. As observed by transmission electron microscopy, the cluster ions create amorphous and continuous tracks. Craters generated both at the entrance and exit surfaces of the samples are clearly visible at tilted incidence. Moreover, hillocks are seen at the entrance and exit of the tracks. On the sample surface matter ejected from the tracks has been deposited. Some of the tracks induced by high energy C_{60}-ions contain a "bubble-like structure" inside the amorphous part of the tracks, which appears only in very thin zones of the samples and when the projectiles exit from the sample. This is in contrast to the tracks created by smaller cluster ions and by GeV heavy ions for which no structure was seen. © 1998 Elsevier Science B.V.

PACS: 61.80J; 61.80L
Keywords: Cluster irradiation; Electronic energy deposition; Fullerene; Latent tracks; Transmission electron microscopy; Yttrium iron garnet

1. Introduction

The passage of an energetic ion through an insulating material may leave, due to electronic excitations, a latent ion track. This phenomenon has been studied extensively for more than four decades [1] and various techniques have been used to study latent track formation, e.g. transmission electron microscopy (TEM). The intersections of bulk tracks with a surface, have also been widely studied, most recently by Scanning Force Microscopy (SFM), although the imaging process remains controversial (see [2,3] and references therein).

There is now a growing interest in using polyatomic projectiles for particle–solid interaction studies. An interesting feature of using clusters as projectiles is the unique way to produce impacts of several atoms simultaneously in a very small area. The energy density deposited by electronic processes can therefore be very high. As a result, a variety of secondary processes, such as track formation, energy transfer and sputtering, can be more pronounced compared to the situation for atomic impact. Several experiments have already

* Corresponding author. Tel.: 33 01 69 33 44 94; fax: 33 01 69 33 30 22; e-mail: annie.dunlop@polytechnique.fr.

PII S0168-583X(97)00606-X

been performed with clusters as projectiles and a review has recently been given in [4]. Using C_{60}-ions, track formation in metals [5], insulators [6] and semiconductors [7] have been observed. Craters and hillocks have been seen on different insulators [3,8].

Yttrium Iron Garnet ($Y_3Fe_5O_{12}$, or YIG), a radiolysis resistant and amorphisable ferrimagnetic insulator, is especially adapted to study latent ion tracks as the tracks stay stable during TEM observations. Previous studies using monoatomic heavy projectiles have shown that sufficiently high electronic energy deposition can result in track generation along the projectile path [9].

Some results have recently been obtained after MeV C_{60} irradiation of YIG [6]. In this paper we present further results obtained by TEM studies of YIG irradiated with C_{60} ions at different energies and incident angles. The irradiation at different incident angles should allow one to vary the observable travelled length in the electron microscope of the C_{60} constituents.

2. Experimental

Targets, consisting of 3 mm diameter polycrystalline YIG discs [6], were prepared for TEM before irradiation. The disks were cut to a thickness of 200 μm, mechanically polished, dimpled and ion milled in order to get a central hole surrounded by thin regions transparent to the electron beam of a TEM.

Energetic C_{60}-ions delivered by the Orsay tandem accelerator [10] were used to irradiate the YIG samples. The experimental procedure is described in detail elsewhere [6]. A new target chamber was used in this experiment in order to irradiate samples at various incident angles ranging from normal to grazing incidence (≈80° with respect to normal). The samples were irradiated up to fluences of a few 10^9 molecules/cm^2. An irradiation with 0.88 GeV U ions was performed at GANIL, Caen, up to a fluence of 10^{10}/cm^2 and with the beam direction normal to the surface of the target. The fluences were chosen in order to avoid any spatial overlap of tracks. All irradiations were done at room temperature.

The evaluation of the linear rate of electronic energy deposition, $(\mathrm{d}E/\mathrm{d}x)_e$, for C_{60}-ions is still an open question. The few available experimental results [11] show that the energy loss per carbon is, within the experimental uncertainty, that of an individual carbon atom of the same velocity, so that the energy loss of C_{60} is estimated as the sum of the energy losses of 60 individual carbon atoms. For 20 MeV C_{60} projectiles the calculated $(\mathrm{d}E/\mathrm{d}x)_e$ is 54.1 keV/nm and the projected range is 451 nm. The calculation is performed using the TRIM code [12], which does not take into account additional effects that occur in connection with the penetration of molecules. The $(\mathrm{d}E/\mathrm{d}x)_e$ and range of the U ions are calculated to be 46 keV/nm and 27 μm, respectively. These $(\mathrm{d}E/\mathrm{d}x)_e$ values are above the threshold for damage creation, $(\mathrm{d}E/\mathrm{d}x)_e \approx 4.5$ keV/nm, which has been determined using heavy ions [13].

The TEM observations of the samples irradiated at normal incidence give information on the damage induced at the beginning of the slowing-down process. The samples irradiated at grazing incidence have the major advantage that the projectiles are stopped inside the target in regions of a total thickness perfectly suitable for TEM observations. The irradiated samples were observed with a Philips CM30 transmission electron microscope operating at 300 kV.

3. Results and discussion

3.1. Formation of hillocks and isolated islands

Fig. 1 shows bright field images of samples irradiated with 20 MeV C_{60} beams at different angles of incidence with respect to the normal (a) 0°, (b) 40°, (c) 60° and (d) 80°. The observations were done with the electron beam of the TEM normal to the specimen surface. At the entrance and exit side of the tracks black spots are clearly seen.

In Fig. 2(a), the sample has been tilted by ≈40° with respect to the electron beam direction. In Fig. 2(b)–(d) the samples have been tilted by ≈40° around the track axis using a tilt-rotation sample holder. When doing this, the black spots appear to be hillocks. This is clearly demonstrated

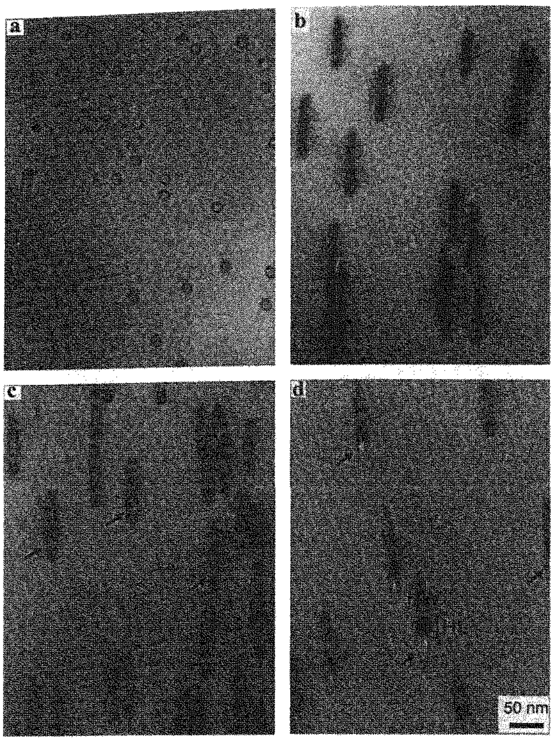

Fig. 1. Bright field images of tracks induced in YIG irradiated at 300 K with 20 MeV C_{60} at different incidence angles. The observations were done with the electron beam of the TEM normal to the surfaces. (a) 0° incidence, (b) 40° incidence, (c) 60° incidence, (d) 80° incidence. The direction of the ion beam is in (a) normal to the picture plane and in the other cases upward. Some examples of craters are indicated by arrows. The meaning of HL and HW is indicated in the text.

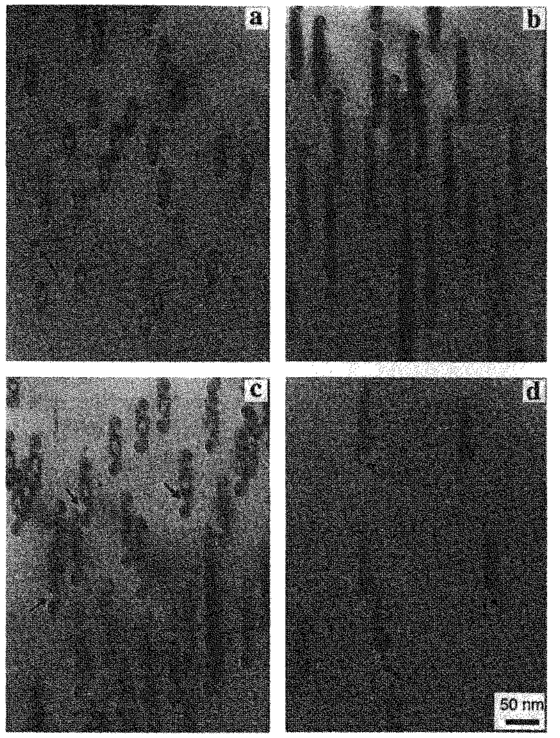

Fig. 2. Bright field images of tracks induced in YIG irradiated at 300 K with 20 MeV C_{60} at different incidence angles. The observations were done after tilting the samples in the microscope. (a) 0° incidence and tilted by 40° with respect to the electron beam direction, (b) 40° incidence and tilted by 42° around the track axis, (c) 60° incidence and tilted by 44° around the track axis, (d) 80° incidence and tilted by 35° around the track axis. The direction of the ion beam is upwards. Some examples of craters are indicated by arrows. In (a) an isolated island is indicated.

in Fig. 3 in which the same region as in Fig. 2(a) is shown when the objective lens of the microscope is underfocused or overfocused. The black spots give rise to phase contrast (Fresnel fringes). As the phase contrast technique is sensitive to the derivative of the total sample thickness, it allows the visualisation of local variations of the sample thickness. The hillocks are lying on different sides of the tracks, at the entrance and exit surfaces. It has been observed that amorphous matter is lying both inside these hillocks and inside the tracks [6].

Fig. 4 corresponds to a sample irradiated with 0.88 GeV U ions at normal incidence. The sample has been tilted in the electron microscope by 40°. Hillocks are also in this case seen at the entrance and exit. The diameters of the entrance and exit hillocks (14.1 nm) are constant whatever the thickness of the region observed by TEM. The track diameter is 13.6 nm.

At normal incidence the hillocks induced by C_{60} appear to be spherical (Figs. 1(a) and 2(a)). For each incident angle a measurement has been made of the width of the entrance hillock parallel, HL, and perpendicular, HW, to the track axis (Fig. 1(d)). The results are shown in Fig. 5. Sometimes there are hillocks missing at the entrance or exit of the tracks, whereas at other times the hillocks are displaced from the entrance or exit of the tracks (Fig. 2(a)).

Some isolated islands are also visible (Figs. 2(a) and 3). They were also shown to be amorphous [6].

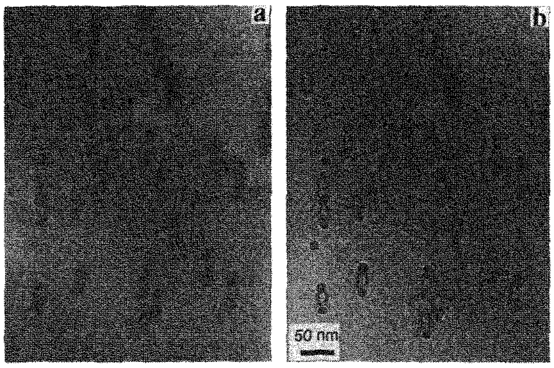

Fig. 3. The same as Fig. 2(a), but imaged under different focusing conditions: (a) with an objective lens overfocused, (b) with an objective lens underfocused. Phase contrast (Fresnel fringes) appears around the entrance and exit spots, and the isolated islands.

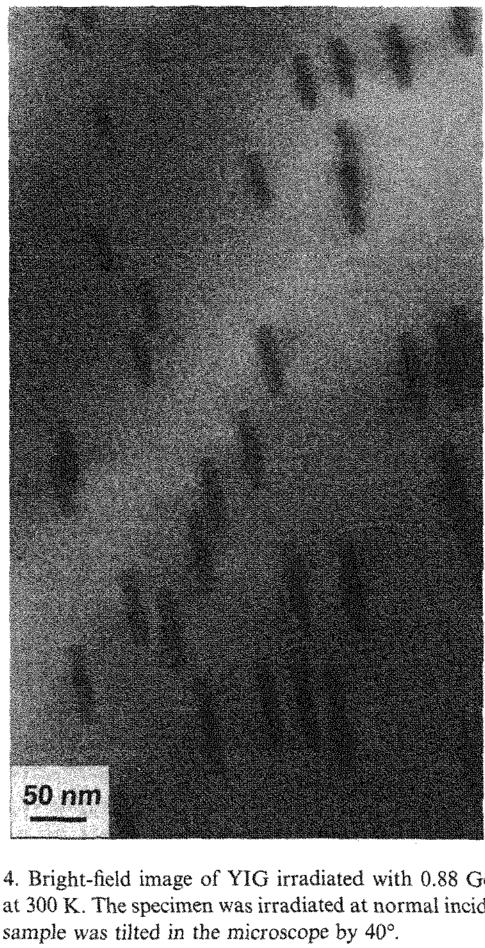

Fig. 4. Bright-field image of YIG irradiated with 0.88 GeV U ions at 300 K. The specimen was irradiated at normal incidence. The sample was tilted in the microscope by 40°.

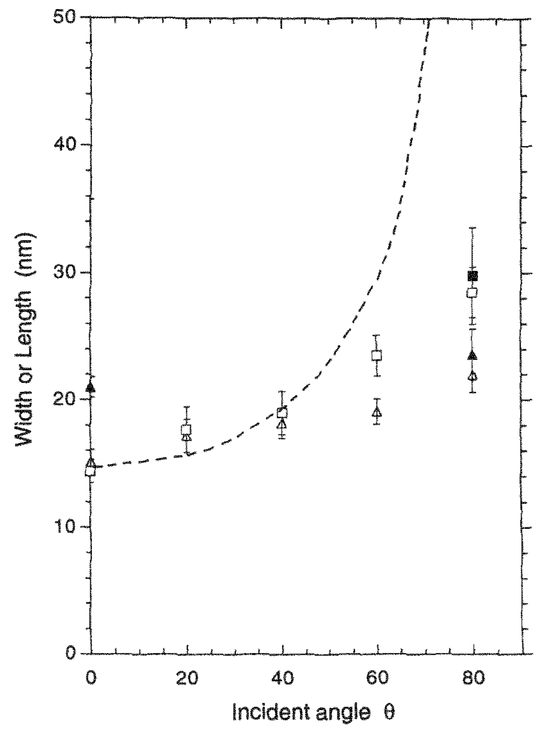

Fig. 5. Influence of the incidence angle θ with respect to the surface normal on the mean values of the entrance hillock dimensions for 20 MeV C_{60}: (□) HL, (△) HW. The values obtained for 40 MeV C_{60} at 0° and 80° incidence is also given, with (■) HL and (▲) HW. The dashed line corresponds to a $1/\cos(\theta)$ relationship for 20 MeV C_{60}.

These isolated islands, which are believed to consist of deposited material, have a spherical shape and are observed at both normal and tilted incidence. A measurement of these islands and hillock diameters has been made after irradiation at normal incidence with C_{60} at different energies (Fig. 6). The diameter of the islands is almost the same as that of the hillocks which is ≈10% smaller than the corresponding track diameter. The diameter of the hillocks and the isolated islands follow the same tendency as the track diameter when increasing the energy. No isolated islands are observed in the sample irradiated with the U beam (Fig. 4).

3.2. Formation of craters

Craters formed at the entrance and exit are often visible. This is especially true for 80° incidence

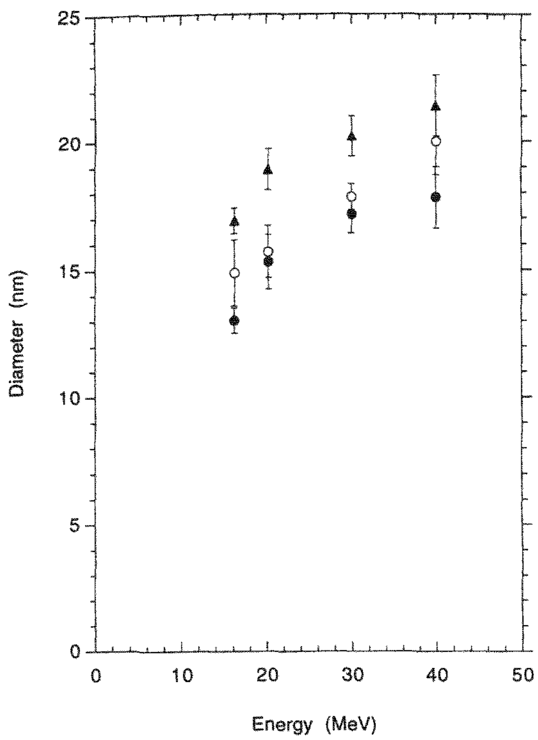

Fig. 6. Influence of the energy of C_{60} ions impinging at normal incidence on the mean hillock diameter: (○) mean hillock diameter, (•) mean diameter of isolated islands, (▲) mean track diameter, taken from [6].

where they are elongated craters, i.e. grooves (Figs. 1(d) and 2(d)). At 40° and 60° incidence, it is also possible to see the entrance and exit craters after tilting the samples around the track axis (Figs. 1(c) and 2(c)). The location of the crater in relation to the hillock seems to change with increasing angle of incidence. At 80° the grooves appear to be in front of the hillock whereas for the smaller angles the craters are behind (Fig. 2).

3.3. Bubble-like structures

In Figs. 1 and 2 some "bubble-like" structure, seen as white contrast, is observed inside the amorphous tracks created by C_{60}-ions. This occurs at all incident angles and has been observed after irradiations with 15–40 MeV C_{60}-ions. The "bubbles" are always located around the track axis and approximately halfway between the track entrance and exit. They are only observed in the very thin parts of the samples and only when the tracks exit from the foil (Figs. 1(c), 2(a) and 2(c)). The structure observed inside the tracks induced by C_{60} has not been observed in the case of MeV Au_4 and smaller size carbon cluster irradiations of YIG [6,14]. Also it has never been observed inside the tracks created by heavy ions, see [9] and Fig. 4.

3.4. Discussion

When an energetic cluster ion hits a surface, the bonds are broken and some of the electrons are stripped off. An ensemble of fragment ions, each with an equilibrium charge, proceeds through the target material in the direction of incidence. The trajectories of the various constituents of the cluster are close to each other, giving rise to a very high density of deposited energy. In addition to this movement, the ions experience a Coulomb repulsion. When the projectile velocities are reduced, multiple scattering becomes increasingly important. Both processes induce a separation of the cluster constituents [15]. In a recent experiment where YIG was irradiated with 20 MeV C_{60} ions [6] it was visualized that the constituents of the molecule keep a spatial correlation for approximately 80 nm and in some cases a few constituents stay close together long enough to create a track for a distance larger than 230 nm. Since the thickness of the samples (<100 nm) is smaller than the range of the clusters (450 nm), $(dE/dx)_e$ can be considered to be almost constant at normal incidence. This is not the case for tilted incidence irradiations, especially at 80°, due to the increased path length.

Hillock formation can be seen as a response to the high deposited energy density at the entrance and the first few nm of the track. The excited matter in the ion track will relax through a radial and axial expansion leading to surface deformation and ejection of matter (see Fig. 1 in [16] and Fig. 5 in [17]). Geometrically, if an ion produces a disturbance on the surface, e.g. crater or deformation, then as the ion angle of incidence θ becomes more grazing, the disturbance would in a simple picture be expected to extend along the surface in the incident direction on a distance proportional to $1/\cos(\theta)$. This variation is indicated for 20 MeV projectiles by a dashed line in Fig. 5. The hillock length (HL), increases only very slowly with increasing θ and the hillock width (HW), appears to stay constant within the experimental uncertainty. This probably results from the fact that the energy density gradient field at the hillock location is of comparable size and directed outwards for all angles of incidence [16,17]. The apparent increase of HL may be a consequence of deformations occurring around the intersection of the tracks with the surface. These deformations will influence the shape of the hillocks observed in the transmission electron microscope. Going from a normal to a surface grazing configuration the deformations would become more pronounced. Especially at grazing incidence there can be a substantial upward push of the matter between surface and ion track giving rise to hillocks. This has been seen after MeV heavy ion [8] and 20 MeV C_{60} [3] irradiations of mica, using SFM.

Hillocks missing at the entrance or exit of the tracks could explain the existence of the isolated islands. Sometimes the matter pushed out is not deposited at the entrance or exit, but further away.

The hillocks at entrance and exit have similar sizes in thin zones of the samples and when the angle of incidence is not too large (Figs. 1(b) and 2(a)). As the travelled length of the C_{60} constituents increases, the exit hillocks get smaller because the deposited energy density decreases due to the separation effects mentioned above and to the decreasing energy of each fragment (Figs. 1(c) and 2(b)). At 80° incidence the occurrence of exit hillocks is rare as the cluster constituents travel a longer distance inside the solid before arriving at the exit surface where spatial correlation is lost (Figs. 1(d) and 2(d)). The variation in exit hillock size is due to the stochastic nature of the separation processes of the cluster constituents. In the case of U ions, Fig. 4, there is no significant change in $(\mathrm{d}E/\mathrm{d}x)_e$ and velocity over the travelled path. The energy density deposited is therefore the same, giving rise to exit hillocks which have the same size as at the entrance.

4. Conclusion

In summary, hillocks are observed with the us of TEM at the entrance and exit of tracks induce in YIG by MeV C_{60} ions. These spherical hillock are believed to be matter pushed out from the io track and deposited at the entrance and exit on th sample surface. The height of these hillocks will b analysed in forthcoming studies. Inside the amor phous tracks a bubble-like structure is observed The fact that this peculiar structure is not seen i tracks created by heavy ions and smaller size clus ters could indicate that the deposited energy den sity has to be higher than a certain threshold t create this bubble-like structure. Further studie will be undertaken in order to explain these fea tures and to look for a possible correlation be tween the bubble formation and the ejection o material from inside the track.

References

[1] R.L. Fleischer, P.B. Price, R.M. Walker, Nuclear Track in Solids, University of California Press, Berkeley, CA 1975.

[2] D.A. Kolesnikov, C.T. Reimann, I.V. Vorobyova, Nucl Instr. and Meth. B 122 (1997) 255.

[3] D.D.N. Barlo Daya, C.T. Reimann, T. Håkansson B.U.R. Sundqvist, A. Brunelle, S. Della-Negra, Y. Le Beyec, Nucl. Instr. and Meth. B 124 (1997) 484.

[4] A. Brunelle, S. Della-Negra, J. Depauw, D. Jacquet, Y. Le Beyec, M. Pautrat, Ch. Schoppmann, Nucl. Instr. and Meth. B 125 (1997) 207.

[5] H. Dammak, A. Dunlop, D. Lesueur, A. Brunelle, S. Della-Negra, Y. Le Beyec, Phys. Rev. Lett. 74 (1995) 1135.

[6] A. Dunlop, G. Jaskierowicz, J. Jensen, S. Della-Negra, Nucl. Instr. and Meth. B 132 (1997) 93.

[7] J. Henry, A. Dunlop, S. Della-Negra, L.T. Chadderton, Radiation Measurements 28 (1997) 71.

[8] D.D.N. Barlo Daya, A. Hallén, J. Eriksson, J. Kopniczky, R. Papaléo, C.T. Reimann, P. Håkansson, B.U.R. Sundqvist, A Brunelle, S Della-Negra, Y Le Beyec, Nucl. Instr. and Meth. B 106 (1995) 38.

[9] A. Meftah, F. Brisard, J.M. Costantini, M. Hage-Ali, J.P. Stoquert, F. Studer, M. Toulemonde, Phys. Rev. B 48 (1993) 920.

[10] S. Della-Negra, A. Brunelle, Y. Le Beyec, J.M. Curaudeau, J.P. Mouffon, B. Waast, P. Håkansson, B.U.R. Sundqvist, E.S. Parilis, Nucl. Instr. and Meth. B 74 (1993) 453.

[11] K. Baudin, A. Brunelle, M. Chabot, S. Della-Negra, J. Depauw, D. Gardès, P. Håkansson, Y. Le Beyec, A.

Billebaud, M. Fallavier, J. Remillieux, J.C. Poizat, J.P. Thomas, Nucl. Instr. and Meth. B 94 (1994) 341.
[12] J.P. Biersack, L.G. Haggmark, Nucl. Instr. and Meth. 174 (1980) 257; J.F. Ziegler, J.P. Biersack, U. Littmark, in: J.F. Ziegler, (Ed.), *The Stopping and Ranges of Ions in Solids*, vol. 1, Pergamon, New York, 1984.
[13] A. Meftah, M. Hage-Ali, J.P. Stoquert, F. Studer, M. Toulemonde, Radiat. Eff. and Defects in Solids 126 (1993) 251.
[14] A. Dunlop, J. Jensen, S. Della-Negra, J. Henry, in preparation.
[15] P. Sigmund, I. Bitensky, J. Jensen, Nucl. Instr. and Meth. B 112 (1996) 1.
[16] R.E. Johnson, B.U.R. Sundqvist, A. Hedin, D. Fenyö, Phys. Rev. B 40 (1989) 49.
[17] J. Kopniczky, C.T. Reimann, A. Hallén, B.U.R. Sundqvist, P. Tengvall, R. Erlandsson, Phys. Rev. B 49 (1994) 625.

ELSEVIER

Nuclear Instruments and Methods in Physics Research B 146 (1998) 412–419

NIM B
Beam Interactions with Materials & Atoms

A comparison between tracks created by high energy mono-atomic and cluster ions in $Y_3Fe_5O_{12}$

J. Jensen [a,d,*], A. Dunlop [a], S. Della-Negra [b], M. Toulemonde [c]

[a] *Laboratoire des Solides Irradiés, CEA/Ecole Polytechnique, 91128 Palaiseau, France*
[b] *Institut de Physique Nucléaire, CNRS-IN2P3, 91406 Orsay, France*
[c] *CIRIL, B.P. 5133, 14040 Caen, France*
[d] *Fysisk Institut, Odense Universitet, Campusvej 55, DK-5230 Odense M, Denmark*

Abstract

Samples of yttrium iron garnet ($Y_3Fe_5O_{12}$ or YIG) were irradiated with Au_4, C_n ($2 \leqslant n \leqslant 20$), C_{60} ions in the MeV energy range. Using transmission electron microscopy (TEM) and Rutherford backscattering spectrometry (RBS), the induced latent tracks are compared with those generated with GeV mono-atomic ions. The cluster ions create amorphous and continuous tracks as in the mono-atomic case. Irradiation at grazing incidence allows to visualise the dissociation of cluster ions inside a solid. Some of the tracks induced by high energy C_{60} ions contain a "bubble-like" structure inside the amorphous part of the tracks, which is in contrast to the tracks induced by smaller cluster and GeV mono-atomic ions for which no structure is seen. The diameters of the tracks induced by MeV cluster ions and by the low velocity mono-atomic ions are seen to follow the same curve as a function of the linear rate of energy deposition $(dE/dx)_e$.

PACS: 61.80J; 61.80L
Keywords: Cluster irradiation; Electronic energy deposition; Latent tracks; Transmission electron microscopy; Yttrium iron garnet

1. Introduction

The slowing down of swift ions penetrating a solid is initially dominated by energy loss to the solids electronic system, $(dE/dx)_e$. Track generation as a result of the passage of such energetic mono-atomic particles through matter is a well-known phenomenon, which has been studied extensively for more than four decades [1]. The existence of an electronic stopping power threshold $(dE/dx)_e^t$ for the creation of latent track and the evolution of the track morphology above this threshold are among the well-established results for dielectric materials, which also have been extended to some metals and metallic alloys. Despite the great number of experimental data, which are now available in the field of $(dE/dx)_e$ induced disorder, the damage mechanism is still an open

* Corresponding author. Fax: +45 66158760; e-mail: jej@dou.dk

0168-583X/98/$ – see front matter
PII: S0168-583X(98)00442-X

question. Various mechanisms have been proposed to explain the conversion between the energy transferred to electrons and the energy responsible for displacements of lattice atoms. Two main models are the thermal spike [2,3] and the Coulomb explosion [4,5] models. Several analysis techniques are used to evidence the radiation induced bulk disorder, e.g. transmission electron microscopy (TEM) and Rutherford backscattering spectrometry (RBS). Within the experimental errors, these different characterisations lead to similar values of the damage cross sections in a given target [6].

The appearance of cluster ion beams in the MeV range provides new ways in the study, and potential applications, of particle–solid interaction [7,8]. Even though the cluster breaks up within the first atomic layers, the projectile constituents deposit their energy simultaneously and their trajectories remain strongly correlated over a distance that depends on the initial energy and number of constituents [9]. The effects of electronic energy deposition using low-Z clusters are interesting, because even for rather light clusters (e.g. C_{10}) with fairly low energies (a few MeV), the electronic stopping power $(dE/dx)_e$ values are comparable to those of GeV heavy ions, while the ion velocity remains quite low (typically around the Bohr velocity). In these conditions the density of deposited electronic energy may reach very large values, while the energy density in elastic collisions remains small. As a result, a variety of secondary processes, such as track formation, energy transfer and sputtering, can be more pronounced compared to the situation of single atomic impact. Several experiments have already been performed with clusters as projectiles and reviews have recently been given in [10]. Using cluster and molecular ions, track formation in insulators [9], semiconductors [11] and even metals [12] has been observed by the use of TEM. The defects induced in insulators along the projectiles trajectories during cluster irradiation have also been studied using other techniques [13,14].

Yttrium Iron Garnet ($Y_3Fe_5O_{12}$, or YIG) is a material on which there has been an extensive study of the damage induced by swift heavy ions using TEM, RBS and other techniques [6,15–18]. It was shown that tracks are induced above a threshold, which depends on the projectile velocity and lies in the range $(dE/dx)_e \approx 4$–5 keV/nm [15,16]. Increasing $(dE/dx)_e$ above this threshold, the structure of the tracks evolves from aligned droplets to continuously damaged amorphous cylinders [18] with a monotonically increasing track diameter, which seems to saturate at a diameter of 13 nm above $(dE/dx)_e \approx 40$ keV/nm. YIG is a radiolysis resistant and amorphisable ferrimagnetic insulator, and is especially adapted to study latent ion tracks as these stay stable during TEM observations. Some results on track creation in YIG by MeV C_{60} irradiation have recently been presented in [9,19].

In this paper we present a comparison between tracks induced in YIG by MeV to GeV monoatomic ions and MeV cluster ions. The tracks are characterised with the help of TEM and RBS.

2. Experimental

Targets consisting of polycrystalline YIG discs, were prepared for TEM before irradiation. They have thus a central hole surrounded by thin regions (thickness ≈100 nm) transparent to the electron beam of a TEM. The preparation methods of the samples are described in [9,19]. Single crystals of YIG deposited on [1 1 1]-$Gd_3Ga_5O_{12}$ were also irradiated and analysed by RBS.

The energetic cluster ions used in our study were delivered by the Orsay tandem accelerator [20]. A detailed description of the experimental procedure is given elsewhere [9,19]. Samples for TEM observations were irradiated at normal and grazing incidence up to fluences of a few 10^9 molecules/cm^2. The fluences were chosen in order to avoid any spatial overlap of tracks. In the case of C_2 ions, TEM samples and single crystals were also irradiated with fluences up to 10^{13} molecules/cm^2. All irradiations were done at room temperature. The main irradiation parameters are listed in Table 1.

The energy losses and ranges of the used projectiles are deduced from the TRIM code [21], which does not take into account additional effects [22] that occur in connection with the penetration

Table 1
Characteristics of the various irradiations with cluster ions. Incident energies, velocities (in units of the Bohr velocity, v_B), linear ra of energy deposition in YIG by the clusters in electronic processes and atomic collisions at these impinging energies, mean project ranges R_p in YIG targets and mean track diameters D (with standard deviation). The diameters were determined by TEM observatio except in the case of C_2 where RBS analysis was used.

Projectile	Incident energy (MeV)	Velocity (v/v_B)	$(dE/dx)_e$ (keV/nm)		$(dE/dx)_n$ (keV/nm)		R_p (nm)	Diameter (nm)
Au_4^+	20.2	1.0	17.6	13.4	13.5	242	631	8.4±0.4
C_2^+	5.2	2.9	4.3	0.1	0.016	220	1700	0.76±0.12
C_2^+	10	4.1	4.4	0.2	0.009	276	2830	0.96±0.1
C_5^+	5.2	1.8	8.0	3.8	0.08	239	953	4.5±0.5
C_5^+	10.2	2.6	10.4	6.2	0.047	199	1470	6.3±0.6
C_5^+	20.2	3.7	11.2	7	0.027	187	2380	6.9±0.3
C_{10}^+	5.2	1.3	11.2	7	0.27	177	605	7.1±0.3
C_{10}^+	10.2	1.8	16.3	12.1	0.16	194	953	8.9±0.5
C_{10}^+	20.2	2.6	21.0	16.8	0.09	218	1470	9.9±0.4
C_{20}^+	13.4	1.5	26.1	21.9	0.44	215	740	11.4±0.9
C_{60}^+	10.2	0.75	35.9	31.7	3.4	154	267	16.2±0.7
C_{60}^+	16.2	0.95	47.4	43.2	2.5	193	380	16.9±0.5
C_{60}^+	20.2	1.1	54.1	49.9	2.2	178	451	18.9±0.8
C_{60}^{2+}	30.2	1.3	67.0	62.8	1.6	196	605	20.2±0.8
C_{60}^{3+}	40.2	1.5	78.3	74.1	1.3	218	740	21.4±1.2

of clusters. The evaluation of the linear rate of electronic energy deposition, $(dE/dx)_e$, for molecular and cluster ions is still an open question. The few available experimental results [23–25] show that the energy loss per carbon is, within the experimental uncertainty, that of an individual carbon atom of the same velocity. It has thus been assumed that the incident energy losses of the cluster projectiles are the sum of the constituents energy loss.

The TEM observations of the samples irradiated at normal incidence give information on the damage induced at the beginning of the slowing-down processes. The samples irradiated at grazing incidence have the major advantage that the projectiles are stopped inside the target in regions of a total thickness perfectly suitable for TEM observations. The irradiated samples were observed with a Philips CM30 transmission electron microscope operating at 300 kV.

The radiation damage of the C_2 irradiated single crystals was analysed by means of Rutherford backscattering under channeling condition (RBS-C). The experiments were performed at the 4 MV Van de Graaff accelerator (Strasbourg) using 2.5 MeV He^+ ions and a backscattering angle of 160°.

Fig. 1 shows a typical RBS-C spectrum of a nor irradiated ("virgin" curve) and an irradiated are ("irradiated" curve) of a YIG crystal in channelin condition along the [1 1 1] direction. Due to th damage induced by the ions, the backscatterin yield increases, but is still below the yield of randomly oriented crystal ("random" curve

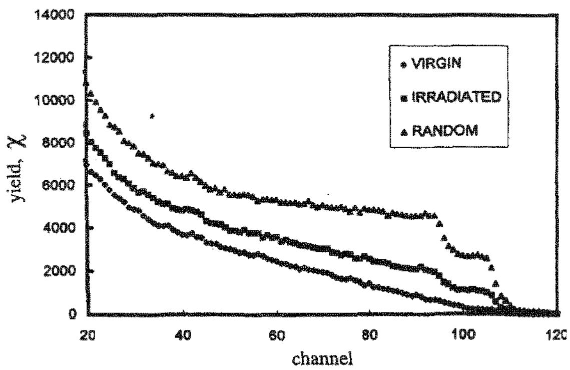

Fig. 1. RBS spectra of backscattered He ions on YIG crystal i channeling conditions, [1 1 1] axis. The lower curve, called vir gin, is a non-irradiated part of the sample. The middle curve called irradiated, is the sample irradiated by 10 MeV C_2 cluster at a fluence of 6×10^{13} molecules/cm². The highest curve, calle random, is the YIG crystal in a random orientation.

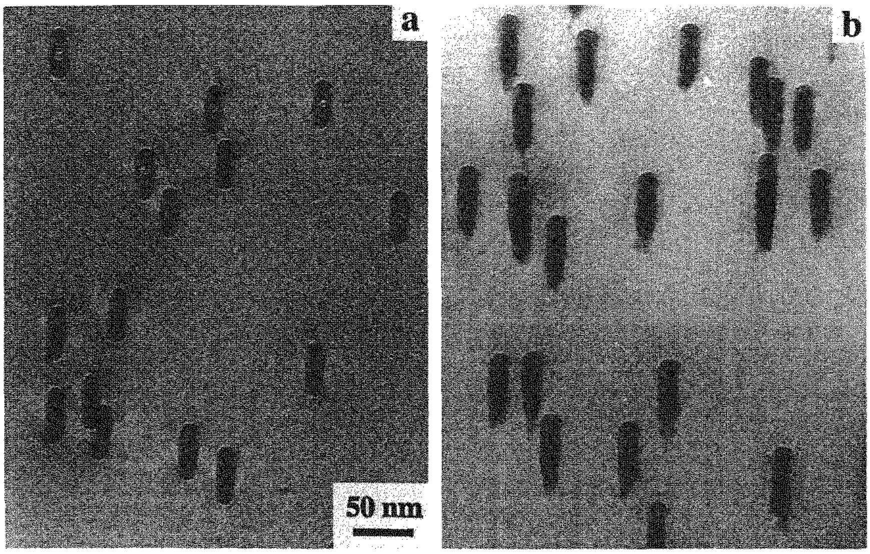

Fig. 2. Bright field images of a sample irradiated with 10 MeV C_{60} at normal incidence. The sample was tilted in the microscope by 30°. (a) is taken near the sample edge and (b) in a thicker region. The direction of the C_{60} beam is downward.

Using the surface approximation, the backscattering yield χ was measured by extrapolating the energy evolution of the yield over the first 150 nm up to the mean energy of the random edge. The damaged fraction F_d of the material is given by $F_d = (\chi_i - \chi_v)/(\chi_r - \chi_v)$, where χ_i and χ_v are the backscattering yield under channeling condition of the irradiated and of the virgin sample, respectively, and χ_r corresponds to the yield of the randomly oriented crystal.

3. Results

Figs. 2–5 shows some typical bright field images obtained from different samples irradiated with some of the projectiles given in Table 1. Continuous zones of extended damage, i.e. tracks are clearly seen in Figs. 2–4. The tracks created by the cluster and the mono-atomic ions can be described as a strongly disordered region and were shown to contain amorphous matter [6,9,15–18].

In Fig. 2(a) some "bubble-like" structure, seen as white contrast, is observed inside the amorphous tracks created by C_{60} ions, as previously reported in Ref. [19] for 20 MeV C_{60}. This has now

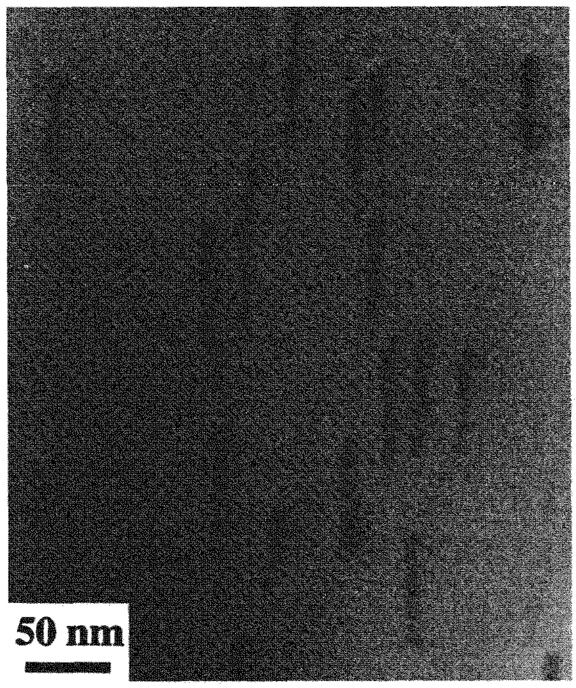

Fig. 3. Bright field images of tracks induced in YIG irradiated with 20 MeV Au_4 ions at normal incidence. The sample was tilted in the microscope by 30°. Beam direction is downward.

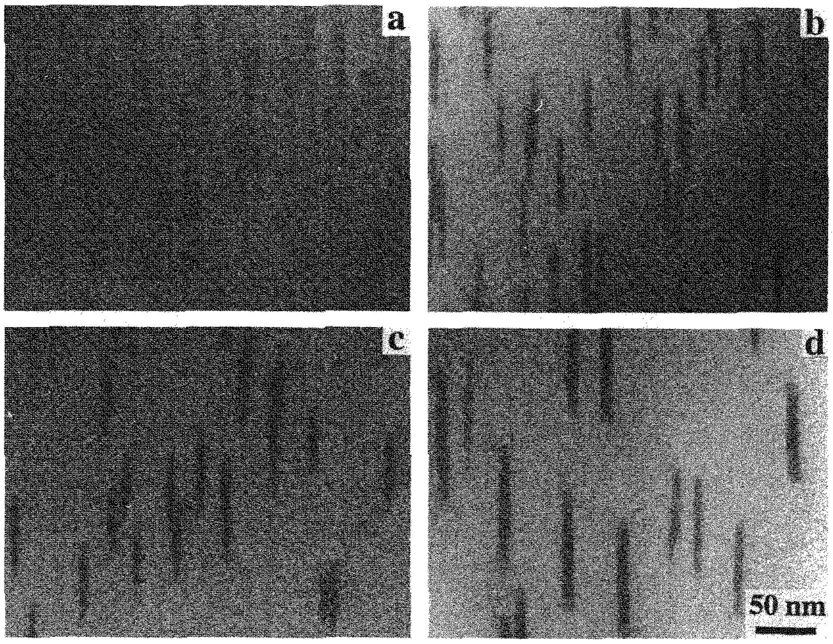

Fig. 4. Bright field images of YIG samples irradiated with (a) 5 MeV C_5; (b) 20 MeV C_5; (c) 5 MeV C_{10} and (d) 20 MeV C_{10} ions. (a was irradiated at 60° incidence and (b)–(d) at normal incidence. The samples were tilted in the microscope by 30° except (a) which wa not tilted.

been observed after all the irradiations with 10–40 MeV C_{60}. By defocusing the objective lens of the microscope, it was seen in Ref. [19] that this structure gave rise to phase contrast (Fresnel fringes) inside the track. As the phase contrast technique is sensitive to local variation in atomic density, the observed structure must have a different density compared to rest of the track. The "bubbles" are always located on the track axis and approximately halfway between the track entrance and exit. They are only observed in the very thin parts of the samples and only when the tracks exit from the target. The transition from an area in the sample where a structure is seen to an area where no structure is observable seems to be very abrupt. This bubble-like structure observed inside the tracks induced by C_{60} is not observed after irradiation with MeV Au_4, (Fig. 3) and the smaller size carbon clusters (Fig. 4) used in our study. Also it has never been observed inside the tracks created by mono-atomic ions [6,15–19].

Black spots are observed at the entrance and exit of the tracks created by cluster ions. This is especially the case for C_{60} ions, (Fig. 2(a)), [9,19 and C_{20} [9] where it is clearly seen. It has also bee observed after irradiation with uranium ions [19 Sometimes the circular contrast is only seen at th entrance of the tracks (Fig. 2(b)). These blac spots were shown to be amorphous [9] and be lieved to be matter pushed out from the track core giving rise to an accumulation of matter, hillocks at the track entrance and exit [19]. Craters hav also been observed after cluster irradiation [19 but mainly after irradiation at oblique incidences

An interesting feature about cluster projectile is the decrease of the track diameter with increas ing penetration depth [9], due to the dissociation o the cluster. An example is shown in Fig. 2(b) fo the case of C_{60} ions, and it can also be seen in Fig 3 for the case of Au_4. The linear rate of energ deposition of each cluster constituent can be con sidered as almost constant along the track portion which are observable in the electron microscop (up to ≈100 nm), so that the decrease in trac diameter can only be due to an efficient latera spread of the cluster constituents. This latera

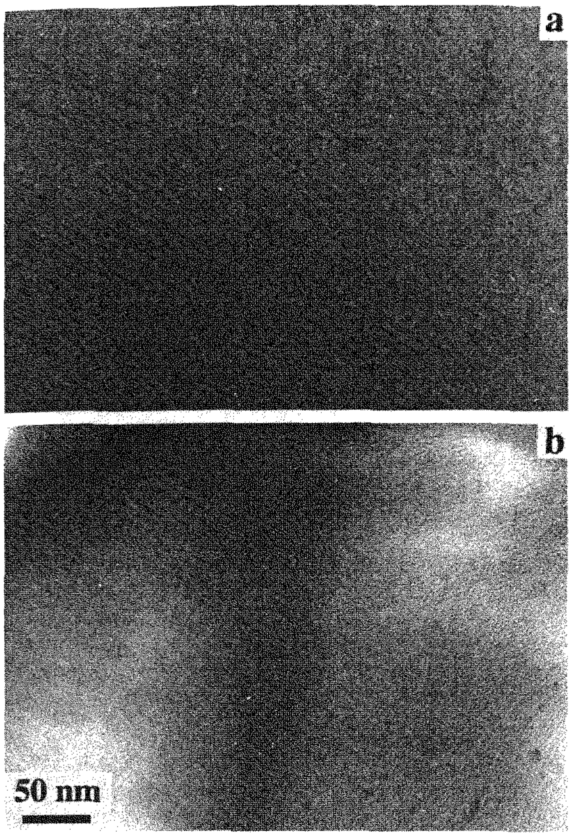

Fig. 5. Bright field images of YIG irradiated with (a) 5 MeV C_2 at 60° incidence and (b) 10 MeV C_2 at 75° incidence. The fluence in (a) was $10^{12}/cm^2$ and in (b) $10^{11}/cm^2$.

spread is caused by Coulomb repulsion between the constituents and multiple scattering with target atoms. As the correlated slowing-down of the constituents is gradually lost, the deposited energy density will at some point fall below the threshold for track creation, after which no damage will be seen in the TEM. In a recent experiment where YIG was irradiated with 40 MeV C_{60} ions [9], it was visualised that the constituents of the molecule keep a spatial correlation for ≈120 nm on average and that in some cases a few constituents stay close together long enough to create a track on a distance larger than 350 nm.

In the case of 5 and 10 MeV C_2 ions (Fig. 5) the tracks are discontinuous and very difficult to see using TEM. The visualisation becomes easier after irradiations at a high fluence as black stripes become visible. 5 and 10 MeV C_2 ions have the same $(dE/dx)_e$, but different velocities (Table 1) located on each side of the stopping maximum. Already in the case of 5 MeV C_5, the tracks are beginning to be diffused and slightly discontinuous (Fig. 4(a)).

The last column of Table 1 gives the mean initial track diameters at the target entrance (and their standard deviations) deduced from the observations of a large number of cluster impacts (30–100 for each type of projectiles). Except for C_2 (see below), all the diameters were determined from TEM observations of the continuously damaged cylinders.

For the C_2 ions an accurate track diameter cannot be obtained with the TEM technique, because of the very discontinuous appearance of the tracks (Fig. 5). By using RBS-C after irradiation of YIG single crystals with 5 and 10 MeV C_2 ions, an "effective" track diameter could be obtained. Assuming that at higher ion fluences Φt, the overlapping of tracks leads to a damage distribution which can be described by $F_d = 1 - \exp(-A_d \Phi t)$, we can deduce the mean cross section A_d of the damage (Fig. 6). If one then assumes that the damage is concentrated within a cylinder, the track radius R can be determined from $A_d = \pi R^2$. For the C_2 clusters a radius of $R = 0.48 \pm 0.05$ nm is deduced at 10 MeV and 0.38 ± 0.06 nm at 5 MeV.

All the available experimental results on track diameter measured after mono-atomic [16,17] and cluster ion irradiations of YIG are shown in Fig. 7

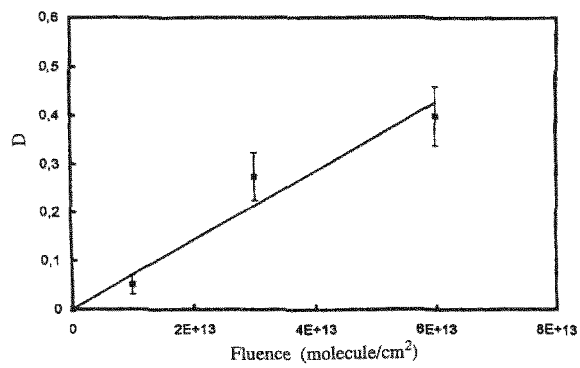

Fig. 6. Fluence evolution of the damage fraction $D = \mathrm{Ln}(1 - F_d)$ measured at the surface of a YIG sample irradiated with 10 MeV C_2.

as a function of the linear rate of electronic energy deposition $(dE/dx)_e$. For all the cluster projectiles, except C_2, the diameters were deduced from TEM observations of continuous tracks. In the case of mono-atomic projectiles and C_2 clusters, the diameters are mainly effective diameters deduced from damage cross section measurements using RBS [16,17]. These effective diameters are similar to those observed in a TEM when $(dE/dx)_e$ is above a certain value (8–10 keV/nm for YIG) where continuous tracks are induced. When the generated tracks have a discontinuous structure, the diameters are calculated as being that of a "continuously damaged cylinders" in which the amorphous phase of the discontinuous defects are artificially located.

4. Discussion and conclusion

As seen from Table 1, the carbon clusters used in this study are mainly slowed down by electronic processes. In the particular case of Au_4 ions, the relative importance of nuclear elastic collisions is much higher, which might explain the rough appearance of the Au_4 tracks. The $(dE/dx)_e$ values are above the threshold for damage creation, $(dE/dx)_e^t \gtrsim 4$ keV/nm, which has been determined using low velocity heavy ions [16]. In the case of cluster ions it is possible to explore $(dE/dx)_e$ values that lie far above those which are accessible with mono-atomic projectiles. The contribution of elastic collisions to the damage induced by the carbon cluster projectiles was shown to be too small to account for the observed track generation [9].

The fact that the same track diameter is obtained after irradiation with C_5 and C_{10} at the same $(dE/dx)_e$ is a first indication of a linear dependence between the track formation parameters and the number of cluster constituents.

The points relative to similar (neighbouring atomic masses) mono-atomic projectiles are connected with lines in Fig. 7 as done in [9]. For a given type of projectile, the track diameter increases with increasing velocity (full lines), reaches a maximum value, and then decreases again when the velocity increases beyond the stopping power

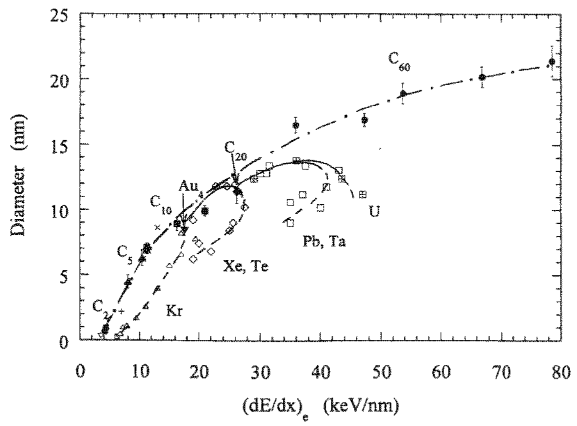

Fig. 7. Graph showing the track diameter in YIG targets as a function of the linear rate of energy deposition in electronic excitation for GeV mono-atomic ions [16,17] and MeV cluster ions. (◪): Ar; (▽): F; (+): S; (×): Cu; (△): Kr; (◇): Xe, Te; (□): Pb, Ta; (⊞): U; (▼): Au_4; (●): C_2; (▲): C_5; (■): C_{10}; (◆): C_{20}; (●): C_{60}. All the lines are drawn to guide the eye. The full and the dashed lines correspond respectively to the low and the high velocity regions for the mono-atomic ions. The dotted–dashed line joins all the points obtained using cluster projectiles (filled symbols).

maximum (dashed lines), giving rise to the "hook-like" curves for the mono-atomic ions. These hook-like curves, relating the track diameters and the linear rate of electronic energy deposition for the atomic ions, demonstrate clearly that there is no simple relation between $(dE/dx)_e$ and the track formation. This effect is often called the "velocity effect" [16], indicating that for the same $(dE/dx)_e$, slow projectiles induce larger diameter tracks than faster projectiles due to differences in the density of deposited energy by low and high velocity ions.

The velocity range of the cluster ions used is on the *low velocity* side of the stopping power maximum. All the points relative to cluster irradiations lie on the dashed–dotted line on Fig. 7. This line coincides very well with a large part of the full line joining all experimental points corresponding to *low velocity* mono-atomic projectiles. This agreement is very good, within the experimental uncertainties, in all the $(dE/dx)_e$ range extending from 4 to 30 keV/nm.

This comparison permits to conclude that there is no difference between the effects induced by the impact of clusters and atomic projectiles at *low* *velocities*. Moreover, it is possible to reach the same $(dE/dx)_e$ using cluster ions in a very low velocity regime. Also there is a confirmation of the $(dE/dx)_e$ threshold of ≈4 keV/nm for track formation in YIG.

The use of cluster projectile allows to concentrate the energy deposition within a small radius around the projectile trajectory, which is generally smaller than the track radius. Thereby one can calculate the energy density leading to the creation of observable tracks. All the results presented in Table 1, follow the relation $\{(dE/dx)_e-(dE/dx)_e^t\}\ 4/\pi D^2=203$ eV /nm^3, in which $(dE/dx)_e^t=4.2$ keV/nm is the threshold for the linear rate of energy deposition in electronic processes and D the track diameter. This relation confirms the role of the energy density distributed in the track as already indicated in Ref. [9].

Acknowledgements

We would like to thank H. Pascard, at the LSI, for the elaboration of the YIG targets and J.J. Grob, at the PHASE laboratory in Strasbourg, for help during the RBS-C measurements.

References

[1] R.L. Fleischer, P.B. Price, R.M. Walker, Nuclear Tracks in Solids, University of California Press, Berkeley, CA, 1975.
[2] L.T. Chadderton, I.M. Torrens, Fission Damage in Crystals, Methuen, Paris, 1969.
[3] M. Toulemonde, C. Dufour, E. Paumier, Phys. Rev. B 46 (1993) 14362.
[4] R.L. Fleischer, P.B. Price, R.M. Walker, J. Appl. Phys. 36 (1965) 3645.
[5] D. Lesueur, A. Dunlop, Radiat. Eff. Def. Solids 126 (1993) 163.
[6] M. Toulemonde, F. Studer, Philos. Mag. 58 (1988) 799.
[7] Y. Le Beyec, Y. Hopillard, H. Bernas (Eds.),. Proc. Int. Workshop on Polyatomic Ion Interaction with Matter, Nucl. Instr. and Meth. B 88 (1994).
[8] J.P. Thomas (Ed.),. Proc. E-MRS Symp. On Cluster Interactions with Matter, Nucl. Instr. and Meth. B 112 (1996).
[9] A. Dunlop, G. Jaskierowicz, J. Jensen, S. Della-Negra, Nucl. Instr. and Meth. B 132 (1997) 93.
[10] A. Brunelle, S. Della-Negra, J. Depauw, D. Jacquet, Y. Le Beyec, M. Pautrat, Ch. Schoppmann, Nucl. Instr. and Meth. B 94 (1997) 207.
[11] J. Henry, A. Dunlop, S. Della-Negra, L.T. Chadderton, Radiat. Measurements 28 (1997) 71.
[12] H. Dammak, A. Dunlop, D. Lesueur, A. Brunelle, S. Della-Negra, Y. Le Beyec, Phys. Rev. Lett. 74 (1995) 1135.
[13] B. Canut, S. Ramos, N. Bonardi, J. Chaumont, H. Bernas, E. Cottereau, Nucl. Instr. and Meth. B 122 (1997) 335.
[14] A. Perez, M. Döbeli, H.A. Synal, Nucl. Instr. and Meth B 91 (1994) 187.
[15] A. Meftah, M. Hage-Ali, J.P. Stoquert, F. Studer, M. Toulemonde, Radiat. Eff. Def. Solids 126 (1992) 373.
[16] A. Meftah, F. Brisard, J.M. Costantini, M. Hage-Ali, J.P. Stoquert, F. Studer, M. Toulemonde, Phys. Rev. B 48 (1993) 920.
[17] A. Meftah, M. Djebara, J.P. Stoquert, F. Studer, M. Toulemonde, Nucl. Instr. and Meth. B 122 (1997) 470.
[18] Ch. Houpert, F. Studer, D. Groult, M. Toulemonde, Nucl. Instr. and Meth. B 39 (1989) 720.
[19] J. Jensen, A. Dunlop, S. Della-Negra, H. Pascard, Nucl. Instr. and Meth. B 135 (1998) 295.
[20] S. Della-Negra, A. Brunelle, Y. Le Beyec, J.M. Curaudeau, J.P. Mouffon, B. Waast, P. Håkansson, B.U.R. Sundqvist, E.S. Parilis, Nucl. Instr. and Meth. B 74 (1993) 453.
[21] J.P. Biersack, L.G. Haggmark, Nucl. Instr. and Meth. 174 (1980) 257; J.F. Ziegler, J.P. Biersack, U. Littmark, in: J.F. Ziegler (Ed.), The Stopping and Ranges of Ions in Solids, vol. 1, Pergamon, New York, 1984.
[22] P. Sigmund, I. Bitensky, J. Jensen, Nucl. Instr. and Meth. B 112 (1996) 1.
[23] K. Baudin, A. Brunelle, M. Chabot, S. Della-Negra, J. Depauw, D. Gardès, P. Håkansson, Y. Le Beyec, A. Billebaud, M. Fallavier, J. Remillieux, J.C. Poizat, J.P. Thomas, Nucl. Instr. and Meth. B 94 (1994) 341.
[24] C. Tomaschko, D. Brandl, R. Kügler, M. Schurr, H. Voit, Nucl. Instr. and Meth. B 103 (1995) 407.
[25] D. Ben-Hamu, A. Baer, H. Feldman, J. Levin, O. Heber, Z. Amitay, Z. Vager, D. Zajfman, Phys. Rev. A 56 (1997) 4786.

ELSEVIER Nuclear Instruments and Methods in Physics Research B 146 (1998) 405–411

NIM B
Beam Interactions
with Materials & Atoms

Craters, bumps and onion structures in MoS_2 irradiated with MeV C_{60} ions ☆

J. Henry [a], A. Dunlop [b,*], S. Della-Negra [c]

[a] *CEA-CEREM, Service de Recherches Métallurgiques Appliquées, 91191 Gif-sur-Yvette, France*
[b] *Laboratoire des Solides Irradiés, Commissariat à l'Energie Atomique/Ecole Polytechnique, 91128 Palaiseau Cedex, France*
[c] *Institut de Physique Nucléaire, CNRS-IN2P3, 91406 Orsay, France*

Abstract

In the scope of a general study of damage creation under high energy deposition by electronic excitation in various types of materials, we present here results relative to irradiations of a lamellar compound with energetic cluster ions. The projectiles are 20–40 MeV C_{60} ions delivered by the tandem accelerator located in Orsay (France). Thin samples suitable for Transmission Electron Microscopy (TEM) are irradiated at 300 K. The damage is characterised by various TEM techniques, in particular Topographical Contrast Imaging. We study the influence of the angle of incidence of the projectiles (varied from normal to grazing incidence) on the morphology of the surface features (craters and bumps). We also characterise the structural modifications occuring in the vicinity of the projectile path. We observe in particular the formation of "onion like structures" either inside the latent tracks or deposited on the surface of the specimens. © 1998 Elsevier Science B.V. All rights reserved.

Keywords: Radiation damage; Electronic excitation; Fullerene; Latent tracks; Transmission electron microscopy; Molybdenite

1. Introduction

This paper is relative to the study of the damage induced in molybdenite submitted to very high electronic excitations. The chosen projectiles are 20 and 40 MeV fullerene ions, which respectively have ranges of 500 and 800 nm in MoS_2. Due to their high masses and slow velocities ($v/c \approx 0.01$), they deposit very high densities of energy ($\geqslant 10$ eV/Å^3) in the target in electronic excitations and ionisations. Samples suitable for Transmission Electron Microscopy (TEM) were irradiated. TEM observations were performed in regions of thicknesses smaller than 100 nm, i.e. in which elastic processes are almost negligible compared to electronic processes.

It has been previously shown that after irradiations at low fluences ($\approx 10^9$ ions/cm^2) cylindrical

☆ The irradiations were performed on the tandem accelerator in Orsay.

* Corresponding author. Fax: +33 01 6933 3022; e-mail: annie.dunlop@polytechnique.fr

PII: S0168-583X(98)00516-3

tracks are generated along the path of C_{60} projectiles [1] and that very strong surface deformations occur at the entrance and exit surfaces [1,2]. They mainly consist in craters located at the track entrance and exit. Protruding matter is generally found in the vicinity of the craters: it consists in either a circular rim or an elongated "flow" in particular directions [2]. In this work, we present preliminary results concerning the *microstructural* transformations induced by the irradiation, both in bulk material and on the sample surface. A more detailed investigation of the different types of tracks created at grazing incidence is under way.

2. Experimental

Prethinned molybdenite targets were irradiated at 300 K with 20–40 MeV C_{60} ions delivered by the tandem accelerator in Orsay. A detailed description of the acceleration process of C_{60} beams is given in [3].

Irradiations were performed: (i) At normal incidence and at high fluences (3×10^{11} ions/cm^2) in order to strongly perturb the targets in the hope of an easier characterisation of the damage. (ii) At grazing incidences (80° respective to the sample normal) and at low fluences ($\approx10^9$ ions/cm^2) in order to avoid any spatial overlap of the damaged regions. The use of grazing incidences and higher energy projectiles (40 MeV) allows an easier observation by TEM of the evolution of the track morphology during the slowing-down of the projectiles.

After irradiation, the specimens were characterised by TEM using in particular the topographical contrast imaging technique, which is described in more details in [4,5,2].

3. Results

3.1. Irradiations at grazing incidence

Fig. 1 presents electron micrographs relative to various samples irradiated with 40.2 MeV C_{60}^{3+} ions. [1] The tracks with a small diameter which a seldom observed (track at the top of Fig. 1(a) f example), are generated by the C_{20} ions, and th will not be considered below. Returning to tl tracks created by 40 MeV C_{60} ions, various typ of tracks *very commonly* observed are presented Fig. 1(a)–(c). The micrographs are obtained in tl bright field mode (without any reflection strong excited). Fig. 1(d) features the same group tracks as shown in Fig. 1(a), imaged using tl topographical contrast technique.

As seen from Fig. 1(a) and (d), elongated cr ters are formed in the projectile impact region. A previously observed in [2], protruding matte elongated in the forward direction, is present in tl vicinity of the crater. In the bulk of the materia the track appears as a cylindrical damaged regio the diameter of which decreases as the projecti proceeds inside the target and looses energy. It h to be mentioned that some diffraction contrast ca be seen in the vicinity of the perturbed track r gion. It is most probably due to local deformatio of the regions surrounding the track.

In Fig. 1(b), the entrance crater and the d fraction contrast surrounding the track region a again visible. Moreover, a circular contrast locat next to the crater is clearly observed. In Fig. 1(some appendices extending outwards from tl track region and located at various depths are see

Fig. 2 presents another group of tracks imag in bright field and topographical contrast cond tions. On track number 1, faint surface deform tions are seen around the crater at the entrance the projectile. A circular contrast is again visible the vicinity of the entrance crater of track numb 2. Fig. 2(b) shows that this object is located on tl surface and has a roughly spherical shape. Son fringes are seen both in the track core and in tl deformed regions of track 1, as well as inside tl

[1] At the target site, energy spectra are recorded in coin dence with the arrival time of fullerene ions. The energy spec recorded in coincidence with the time of flight of C_{60}^{+} and C show only one energy peak (20.2 MeV C_{60}^{+} and 30.2 MeV C_{6}^{2} whereas two peaks are seen when accelerating C_{60}^{3+} [6]. Th correspond to 40.2 MeV C_{60}^{3+} and 13.4 MeV C_{20}^{+} ions, whi cannot be separated. Thus, the experiments performed with t C_{60} ions of highest energy always consist in dual bea irradiations.

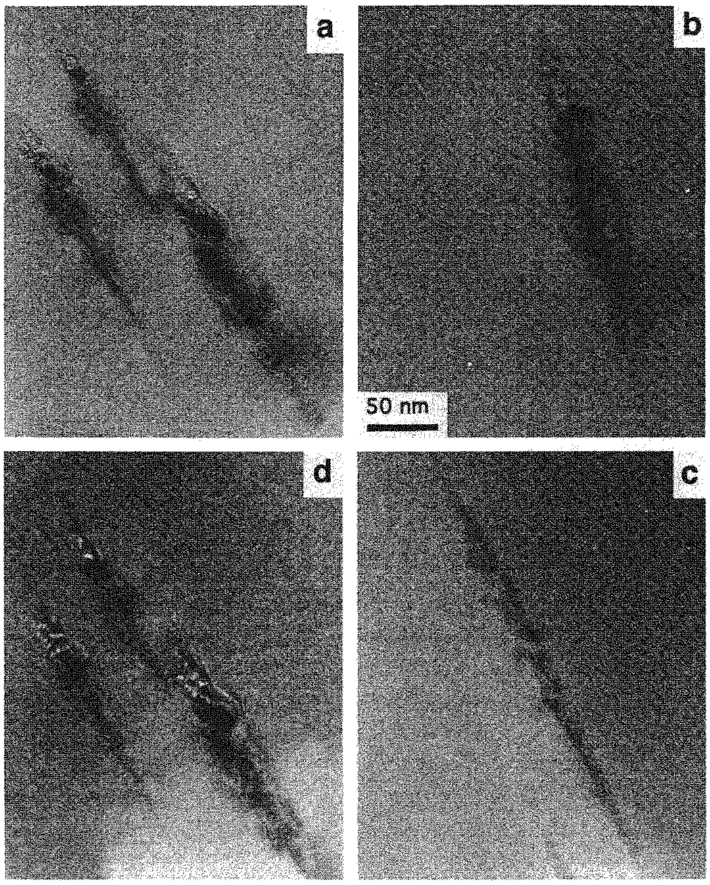

Fig. 1. MoS_2 irradiated at 300 K and at grazing incidence with 40.2 MeV C_{60} ions up to a fluence of 3×10^9 ions/cm^2. (a)–(c) Bright field micrographs taken without any reflection strongly excited, and showing a few typical track shapes which are very commonly observed. (d) Same region as shown in (a), but observed in topographical contrast imaging conditions.

circular feature in track 2. They are studied in more details in Fig. (3). Fig. 3(a) presents a high magnification micrograph, in which one can clearly see inside the tracks numerous small intertwined patches of parallel fringes; the direction of these patches seems randomly oriented. The measured fringe spacing is 0.616 ± 0.003 nm. In the spherical "object", the structure of the fringes is different: a concentric arrangement of fringes is seen. This arrangement is far from perfect and some of the concentric sheets seem to extend inside the track structure (area indicated by the arrow in the micrograph).

Micrograph 3b shows the same group of tracks which have been tilted by 28° in the microscope around an axis approximately parallel to the track direction. Here again many domains containing parallel fringes are present in both tracks; the "object" exhibits an imperfect nested structure. One can also notice that whereas the projected shape of the object is slightly elongated in the forward direction in the untilted case, the shape becomes much more circular after 28° tilt.

3.2. Irradiations at normal incidence and high fluence

Fig. 4 presents the microstructure of the irradiated sample, imaged under topographical con-

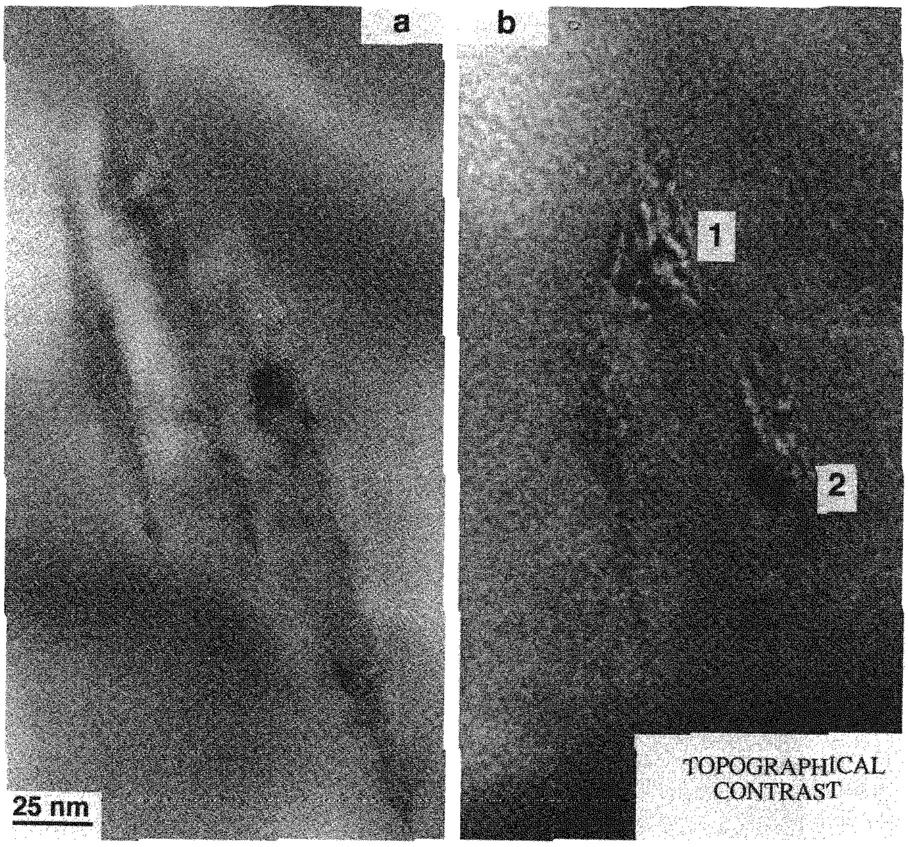

Fig. 2. MoS_2 irradiated at 300 K and at grazing incidence with 40.2 MeV C_{60} ions up to a fluence of 3×10^9 ions/cm^2. The same of tracks are imaged in (a) bright field conditions; (b) topographical contrast imaging conditions.

trast conditions. It consists of a high density of overlapping craters.

Fig. 5 corresponds to a high magnification micrograph of the microstructure. The sample is oriented with the [0001] direction parallel to the electron beam direction. As a result, the three sets of {10.0} planes are imaged in the undamaged regions (U). At the positions of the impacts (I) of the C_{60} projectiles, small domains of parallel fringes can be seen which have the same interplanar distance as in the case of Fig. 3. An object (O) with a nested structure is also present as well as an elongated structure (E). The elongated structure could well correspond to the "lava-flow like" structures described in [2]. Here again the fringe spacing is found equal to 0.616 ± 0.003 nm.

4. Discussion and conclusion

The volume energy density deposited by 2(MeV fullerene ions is very high ($\geqslant$ 100 eV/ato the vicinity of the projectile path). The relaxa of the excited matter which is under stress leac surface deformation as qualitatively describe [2]. At grazing incidence, different types of sur deformation were seen to occur: protruding ma elongated in the forward direction or of rou spherical shape (Figs. 1(d) and 2), as well as " pendices" extending from the track core regio

Another effect of the energy relaxation pro concerns the microstructure of the damaged terial. Before irradiation, the sample consists MoS_2 crystal with the [0001] direction of

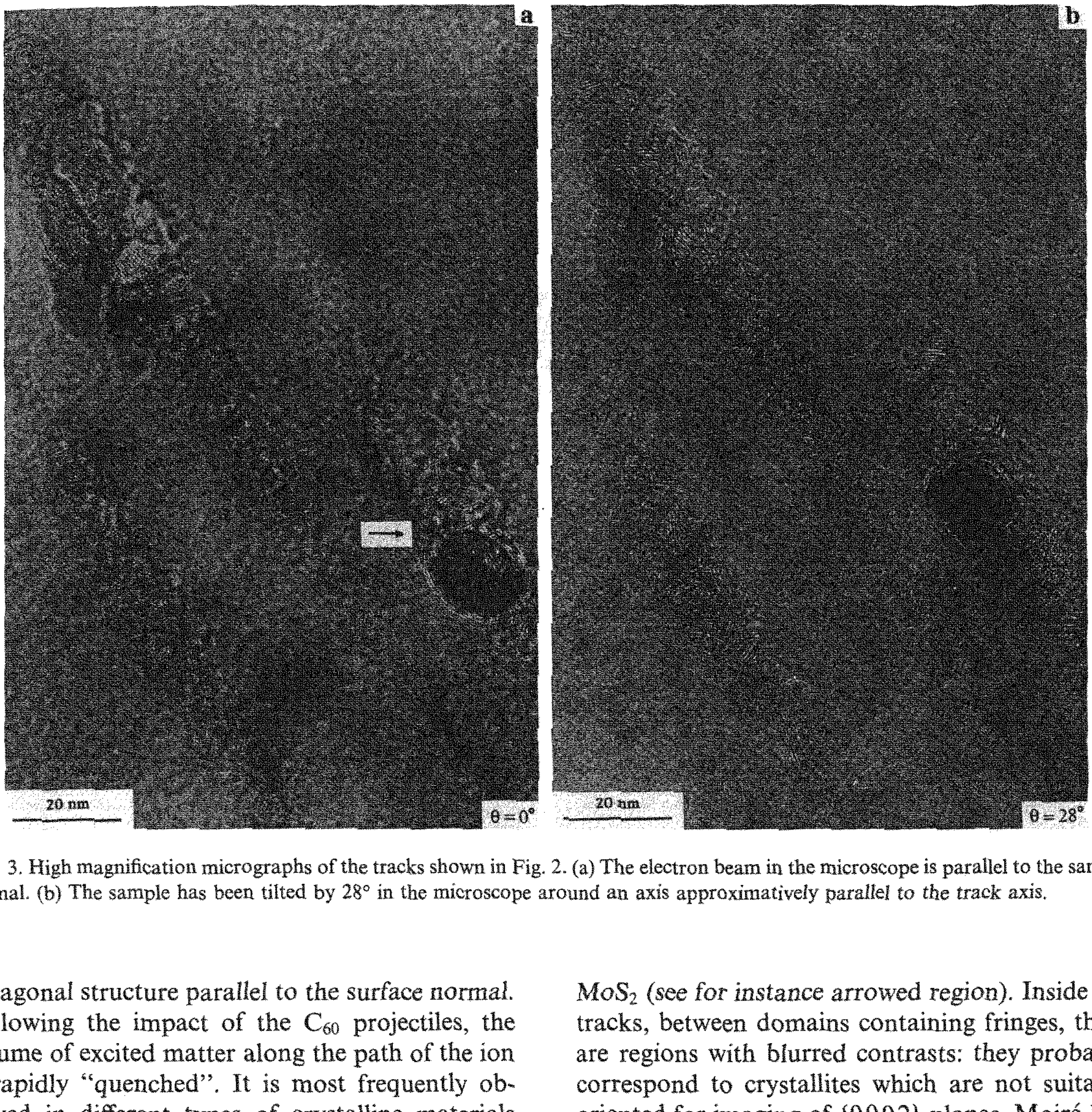

Fig. 3. High magnification micrographs of the tracks shown in Fig. 2. (a) The electron beam in the microscope is parallel to the sample normal. (b) The sample has been tilted by 28° in the microscope around an axis approximatively parallel to the track axis.

hexagonal structure parallel to the surface normal. Following the impact of the C_{60} projectiles, the volume of excited matter along the path of the ion is rapidly "quenched". It is most frequently observed in different types of crystalline materials irradiated with particles which deposit very high amounts of energy in electronic processes, that the damaged matter inside the tracks is in the amorphous state [7,8]. For MoS_2 targets, however, the micrographs in Fig. 3 show that, as a result of the rapid deexcitation process, the microstructure inside the tracks consists of small crystallites which have apparently the same crystallographic structure as the unirradiated matrix: indeed the fringe spacing corresponds to the {0002} interplanar distance (0.6145 nm) of the hexagonal structure of MoS_2 (see for instance arrowed region). Inside the tracks, between domains containing fringes, there are regions with blurred contrasts: they probably correspond to crystallites which are not suitably oriented for imaging of {0002} planes. Moiré-like contrasts can also be seen: they result from the stacking of crystallites with various orientations, present at different depths inside the sample. Moreover, the facts that (i) {0002} planes are imaged both at 0° and 28° tilt angles and that (ii) for a given tilt angle there is no preferential orientation of the fringes, indicate that the crystallites are randomly oriented.

If we now consider the nested objects in Figs. 3 and 5, they are very similar to the fullerene like nested polyhedra which were reported in WS_2 [9]

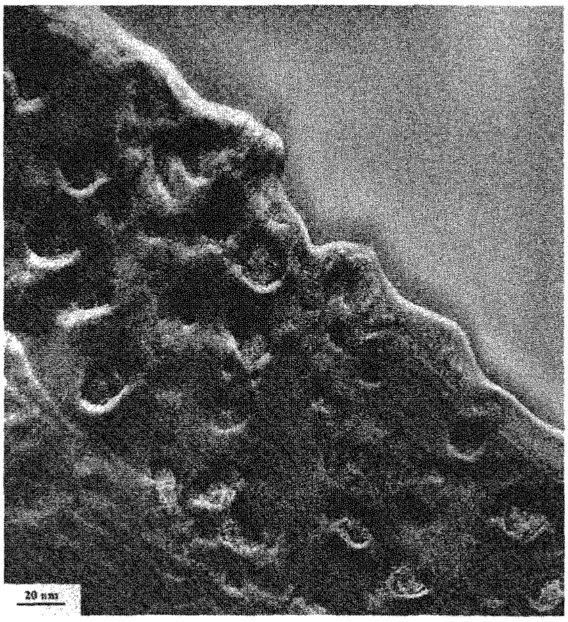

Fig. 4. MoS_2 irradiated at 300 K and at normal incidence with 20.2 MeV C_{60} ions up to a fluence of 3×10^{11} ions/cm^2. The overlapping craters are imaged in topographical imaging conditions.

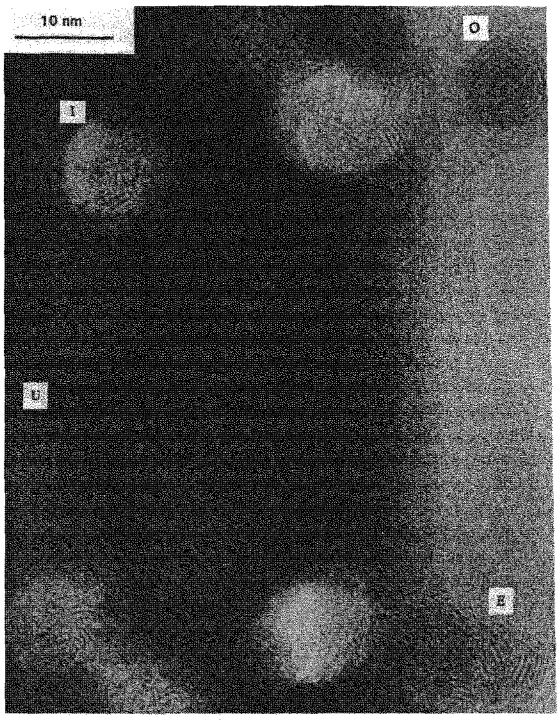

Fig. 5. MoS_2 irradiated at 300 K and at normal incidence wi 20.2 MeV C_{60} ions up to a fluence of 3×10^{11} ions/cm^2. Hi magnification micrograph of a very thin region of the target.

and MoS_2 [10]. This is confirmed by the fact that the nested structure is preserved when the sample is tilted by nearly 30° (Fig. 3(a) and (b)) and by the topographical image of the object (Fig. 2(b)). However the stack of concentric shells shows a lot of disorder: the same phenomenon, although less pronounced, was observed for onion-like structures created in MoS_2 by electron irradiation [11]. Furthermore, as already pointed out in Section 3.1, the outer shells of the nested object seem to extend inside the track: this is perhaps related to the formation mechanism of the structure which could develop during or after the upwards push of excited matter with the outer shells of the nested structure being formed first and extending into the bulk of the track, followed by the formation of the inner shells. This mechanism is different from the icospiral nucleation which leads to snail shaped crystallites by accretion of ever larger shells [12].

Concerning the fact that amorphous matter is not formed inside the tracks, let us mention the work of Hershfinkel et al. [13] who studied the room temperature evolution of an amorphous WS_x film: they observed after 22 months (samp kept at room temperature) the existence of sma nested crystallites in the amorphous matrix, whic is consistent with the suggestion [10] that close fullerene-like polyhedra of MX_2 (M = Mo or W X = S, Se) are an intermediate metastable "phase between the amorphous state and the thermody namically stable phase. In analogy with the for mation of a quasicrystalline phase by a rapi quenching of some molten metallic alloys, Hers hfinkel et al. put forward the hypothesis that, if i were possible to quench the melt of layered-typ materials such as MX_2, nested fullerene-lik structures could well be obtained. In a way, th experimental results presented here are a confir mation of this hypothesis. Furthermore, it woul be interesting to irradiate MoS_2 at low tempera ture (4 K) with 30–40 MeV C_{60} ions to see whethe more severe "quenching" conditions would lead to the formation of amorphous phase inside th tracks.

References

[1] J. Henry, A. Dunlop, S. Della-Negra, L.T. Chadderton, Radiation Measurements 28 (1997) 71.

[2] J. Henry, A. Dunlop, S. Della-Negra, submitted for publication.

[3] S. Della-Negra, A. Brunelle, Y. Le Beyec, J.M. Curaudeau, J.P. Mouffron, B. Waast, P. Hakansson, B.U.R. Sundqvist, E.S. Parilis, Nucl. Instr. and Meth. B 74 (1993) 453.

[4] A.G. Cullis, D.M. Maher, Philos. Mag. 30 (1974) 447.

[5] A.G. Cullis, D.M. Maher, Ultramicroscopy 1 (1975) 97.

[6] H. Dammak, A. Dunlop, D. Lesueur, A. Brunelle, S. Della-Negra, Y. Le Beyec, Phys. Rev. Lett. 74 (1995) 1135.

[7] See for instance the Proceedings of the "Swift Heavy Ions in Matter" Conference, Caen, published in Nucl. Instr. and Meth. B 107 (1996) 181–275.

[8] A. Barbu, A. Dunlop, D. Lesueur, R.S. Averback, Europhys. Lett. 15 (1991) 37.

[9] R. Tenne, L. Margulis, M. Genut, G. Hodes, Nature 360 (1992) 444.

[10] L. Margulis, G. Salitra, R. Tenne, M. Talanker, Nature 365 (1993) 113.

[11] M. José-Yacamán, H. López, P. Santiago, D.H. Galván, I.L. Garzón, A. Reyes, Appl. Phys. Lett. 69 (1996) 1065.

[12] H.W. Kroto, Science 242 (1988) 1139.

[13] M. Hershfinkel, L.A. Gheber, V. Volterra, J.L. Hutchinson, L. Margulis, R. Tenne, J. Am. Chem. Soc. 116 (1994) 1914.

ELSEVIER

Nuclear Instruments and Methods in Physics Research B 146 (1998) 302–308

NIM B
Beam Interactions with Materials & Atoms

Latent track formation in silicon irradiated by 30 MeV fullerenes ☆

A. Dunlop [a,*], G. Jaskierowicz [a], S. Della-Negra [b]

[a] *Laboratoire des Solides Irradiés, Commissariat à l'Energie Atomique/Ecole Polytechnique, 91128 Palaiseau Cedex, France*
[b] *Institut de Physique Nucléaire, CNRS-IN2P3, 91406 Orsay, France*

Abstract

It is now well accepted that electronic excitation and ionisation arising from the slowing-down of swift heavy ions can lead to structural modifications in most targets. It is shown here that new effects take place during irradiations with high energy fullerene beams. Electron microscopy observations were performed at room temperature on prethinned monocrystalline silicon samples after irradiation with 30 MeV fullerene ions. The observed damage is continuous and confined around the projectile paths. The tracks consist of amorphous material as shown by high resolution transmission electron microscopy observations. These tracks recrystallize very rapidly in the electron microscope during the observations in high resolution conditions. Furthermore, a decrease of the track diameter is observed as the cluster ions penetrate deeper inside the target, which is related to an angular scattering of the cluster constituents. At large penetration depths, before disappearing completely, the tracks end as aligned damaged regions of decreasing diameters. Finally, strong sputtering effects occur on the target surfaces, so that craters are generated at the impacts of the projectiles. The fact that amorphous tracks are generated in crystalline silicon following heavy cluster bombardment can be attributed to the strong localization of the deposited energy during the slowing-down process of rather slow projectiles.

Keywords: Radiation damage; Electronic excitation; Fullerene; Latent track; Transmission electorn microscopy; Silicon

1. Introduction

In this paper we present preliminary results concerning damage creation in monocrystalline silicon bombarded with energetic cluster projectiles. We describe here the microstructural changes observed after irradiation with energetic (a few 10 MeV) heavy (mass > 700) cluster ions in order to reach very high levels of energy deposition in electronic processes.

Let us first recall some previous related experimental results:

(i) After monoatomic GeV heavy (Ar to U) ion irradiation of silicon, i.e. exploring linear rates of energy deposition in electronic processes ($S_e = (dE/dx)_e$) in the range 4–28 keV/nm, Levallois et al. [1] conclude from *electrical resistance measurements* that "the observed damage is due only to nuclear collisions".

☆ The irradiations were performed on the tandem accelerator, IPN, Orsay (France).

* Corresponding author. Fax: +33 01 6933 3022; e-mail: annie.dunlop@polytechnique.fr

0168-583X/98/$ – see front matter
PII: S0168-583X(98)00509-6

(ii) After GeV U irradiation, corresponding once again to $S_e = 28$ keV/nm, *DLTS measurements* show that electronic energy deposition is inefficient for defect creation at room temperature in silicon [2]: in particular, no extended defects could be detected. *Transmission electron microscopy* observations [3] are in complete agreement with the above conclusion: no latent track can be imaged in the electron microscope after GeV uranium irradiation.

(iii) To our knowledge, the only observation of tracks in silicon is due to Furuno et al. [4]. These observations are performed in very particular conditions: the targets consist of 5 nm thick evaporated films with a very small grain size of typically 1 nm [5]. In such samples, 207 MeV Au projectiles ($S_e = 17$ keV/nm) produce 7 nm diameter discontinuous tracks, the nature of which has not been determined. The generation of tracks in small grain size very thin films is most probably due to the strong limitations to the spreading of the deposited energy by the close vicinity of the grain boundaries and surfaces. A very similar observation was made more than 30 years ago in thin [6] or discontinuous [7] metallic films in which MeV heavy ions could generate latent tracks, whereas using the same projectiles, no damage was generated in bulk samples.

Due to their high masses and rather low velocities ($v/c \approx 0.01$), the 30 MeV fullerene projectiles deposit very high densities of energy (>10 eV/Å^3) in electronic excitation and ionisation of the target during their slowing-down [8]. These are thus ideal conditions to check whether amorphisation of bulk silicon could result from very strong and localised energy deposition in electronic processes.

2. Experimental

The projected range of 30 MeV C_{60} ions is small (≈ 1 μm) in silicon, so that we irradiated only monocrystalline samples which were prethinned for electron microscopy ($\leqslant 100$ nm) in order to avoid the stopping region of the ions and to stay in a slowing-down regime in which electronic processes are predominant. The energy losses and ranges of the clusters were calculated using the TRIM code [9], supposing that the energy loss per projectile constituent is that of an individual ion of the same velocity. This additive rule is verified by the few experimental measurements of energy losses of various cluster ions [10–12]. At 30 MeV, the linear rates of energy deposition in electronic and elastic processes, respectively, are $(\mathrm{d}E/\mathrm{d}x)_e = 46$ keV/nm and $(\mathrm{d}E/\mathrm{d}x)_n = 0.88$ keV/nm, so that $(\mathrm{d}E/\mathrm{d}x)_e/(\mathrm{d}E/\mathrm{d}x)_n \approx 50$.

The samples were irradiated at 300 K in the tandem accelerator in Orsay [13] up to fluences of a few 10^9 ions/cm^2 in order to avoid any spatial overlap of the damaged regions. Irradiations were performed either at normal or grazing incidences ($\approx 80°$ of normal incidence). The samples were examined with a Philips CM 30 transmission electron microscope operating at 300 kV. The micrographs of the samples irradiated at normal incidence give information on the damage induced at high energies, whereas after grazing incidence irradiations, it is possible to image the evolution of the damage structure during the slowing-down of the projectiles.

3. Results

3.1. Generation of amorphous latent tracks

The main result of this work is that large size continuous latent tracks are observed after 30 MeV C_{60} irradiation of monocrystalline silicon. Fig. 1 is a high resolution electron micrograph of tracks generated in a sample irradiated at normal incidence. The density of observed tracks corresponds to the impinging cluster fluence. In the unirradiated silicon matrix, the {220} type atomic planes are imaged (interplanar distance ≈ 1.9 Å) whereas the track core presents an amorphous structure.

3.2. Stability of the tracks

A very striking feature of the tracks is that their diameter decreases very rapidly during room temperature observation in the electron microscope. This is shown in Fig. 2 in which a group of

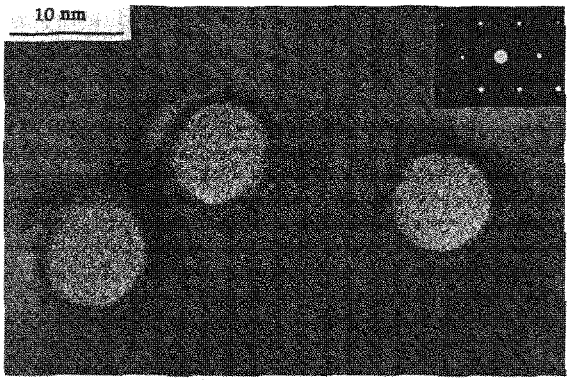

Fig. 1. High resolution transmission electron micrograph of a silicon monocrystal irradiated at 300 K with 30 MeV C_{60} cluster ions. The micrograph is taken from the ⟨1 1 1⟩ direction. {2 2 0} type atomic rows (interplanar distance ≈1.9 Å) are visible in the unperturbed matrix.

two tracks is imaged in high resolution conditions after observation time of 1 to 6 min. The initial diameter of the tracks is found to be close to 10 nm. The tracks recrystallise in epitaxy with the surrounding matrix within a few minutes. After total recrystallisation of the track regions, only some contrasts related to residual strain in the crystalline silicon matrix remain visible.

This recrystallisation effect is also seen when the sample is held at 100 K during the observations in the microscope; moreover this annealing of the defective regions occurs at exactly the same time-scale at 100 and 300 K, which indicates that it is related to the energy deposition and subsequent atomic movements induced by the electron beam, and not only to some local temperature increase under the electron beam. As a matter of fact, the sample temperature increase is certainly very small, due to the limited electron beam intensity that we use during the observations. Let us recall here that "the crystallisation temperature of amorphous silicon depends strongly on the sample purity, thickness, environment" [14], but is found to lie in the range 450–650°C. Moreover if thermal effects were at the origin of the observed track shrinkage, the recrystallisation should occur slower when a cold sample-holder is used.

The straightforward consequence of this observation is that it is almost impossible to determine precisely the initial track diameter from high

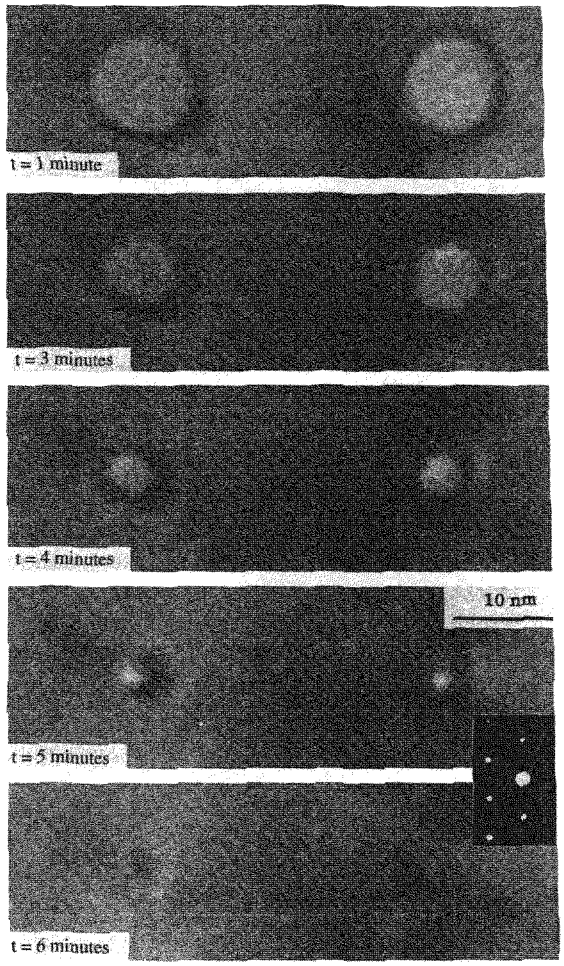

Fig. 2. High resolution transmission electron micrographs of group of two neighbouring tracks generated by 30 MeV C ions impinging at normal incidence in monocrystalline silico The recrystallisation of the track core in epitaxy with the su rounding matrix is obtained within an observation time of a fe minutes in high resolution observation conditions. The micr graphs are once again taken from the ⟨1 1 1⟩ direction.

resolution micrographs (see Section 3.3), as there i necessarily some reduced (but not always neglig ble) time spent for adjustments before startin image registration.

3.3. Evolution of the track shape as the projectile slow down in the target

When energetic cluster ions enter a target an slow down, they break up into single ions o smaller assemblies of ions within the first atomic layers. The projectile constituents stay close together and initially slow down in a correlated manner. But as the penetration depth increases, there is a spatial separation of the constituents of the cluster due to (i) Coulomb repulsion between the charged fragments and (ii) multiple scattering in elastic collision processes.

Fig. 3 is relative to a sample which was irradiated at grazing incidence, so that the projectiles are stopped inside the target in regions the thicknesses of which are perfectly suitable for electron microscopy observations. This process allowing the observation of the track shape evolution as the projectile enters deep in the target was previously used to study the damage induced by C_{60} ions in an insulator: yttrium iron garnet ($Y_3Fe_5O_{12}$ or YIG) [15]. It was shown in YIG that the diameters of the generated amorphous tracks stay constant for distances D of 80–100 nm, according to the incident energy of the fullerene ion, and that when the projectiles enter deeper into the target the track shape changes: the track diameters decrease, the tracks sometimes separate into various branches. This was attributed [15] to the fact that beyond the travelled distance D, there is a partial loss of correlation among all the projectile fragments. At large penetration depths, when the correlated slowing-down of the cluster constituents is partially lost, the deposited energy density falls rapidly and drops below the threshold for track generation, so that no more damage can be imaged by transmission electron microscopy.

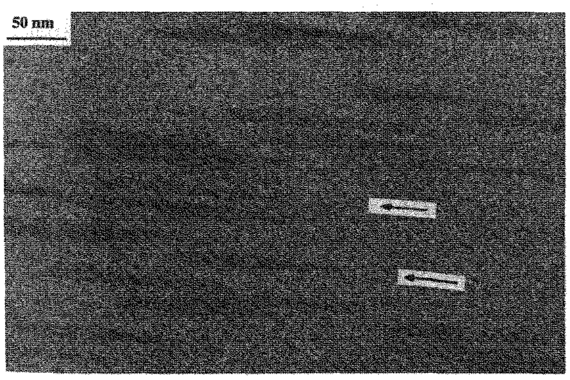

Fig. 3. Bright field electron micrograph of a monocrystalline silicon target irradiated at grazing incidence ($\approx$80° of normal incidence) with 30 MeV C_{60} cluster ions. The micrograph is taken without any reflection strongly excited.

For silicon targets, the following facts are seen in Fig. 3:

- The tracks have an initial diameter of 10 nm at the target entrance. This exact diameter is very difficult to observe on the high magnification micrographs, as track shrinkage usually starts during the adjustments for high resolution observations (see Section 3.2).
- Their diameter stays almost constant during a travelled distance $D \approx 80$ nm.
- Beyond this distance, the track diameter gradually decreases. The tracks very often end by a series of aligned droplets of damaged material (see in particular the tracks indicated by arrows). The diameter of these aligned droplets gradually decreases until no more damage is visible in the electron microscope. Track separation in different branches has not been observed in irradiated silicon.

The above features on track shape evolution are here again direct consequences of the increased separation of the cluster constituents when the projectiles proceed into the target.

3.4. Sputtering at the track entrance and exit

Fig. 4 shows a bright field electron micrograph of a sample which was irradiated at normal incidence with 30 MeV C_{60} ions, and tilted by 30° in the electron microscope. This allows the visualisation of the cylindrical damaged regions through the target thickness. The projectile propagation direction is indicated by the arrow. The target thickness gradually increases going from the top to the bottom of the area are shown in Fig. 4. The amorphous track core appears with a dark contrast.

The micrograph was taken in phase contrast imaging conditions, i.e. after slightly defocusing the objective lens of the microscope. This allows the visualisation of local thickness variations in the sample. In the very thin target regions (top of Fig. 4), a white circular contrast appears at the track entrance, and another circular contrast is visible on the exit surface of the projectile. In the lower

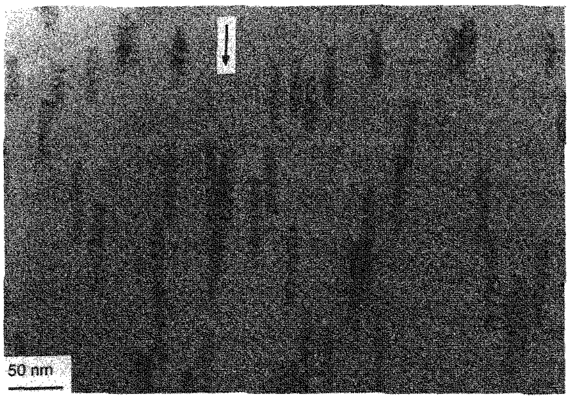

Fig. 4. Bright field electron micrograph of a monocrystalline silicon target irradiated at normal incidence with 30 MeV C_{60} cluster ions. The sample was tilted by 30° in the electron microscope. Phase contrast imaging in slightly defocused conditions.

part of the micrograph, the target gets thicker, so that the track diameters start decreasing due to the loss of correlation of the projectile constituents: circular contrasts appear only at the track entrance. These contrasts are associated to missing matter due to strong sputtering at the target surface. Fig. 5 features a very thin region of a sample which was irradiated at grazing incidence. Sputtering creates now elongated craters at the projectile impact on the target: these craters are almost invisible in focused conditions (Figs. 3 and 5(a)), but are well imaged using the phase contrast technique.

4. Discussion and conclusion

As recalled in the introduction, numerous irradiations of silicon targets under high electronic energy deposition, showed that the observed damage was solely due to elastic collisions and that latent tracks along the paths of *very energetic monoatomic ions* were never observable up to the higher linear rates of energy deposition available with such projectiles ($S_e = 28$ keV/nm).

Monocrystalline silicon targets were recently irradiated with small size carbon clusters (C_1–C_8) at energies of 0.8 MeV per carbon [16]. The damage induced in the vicinity of the sample sur-

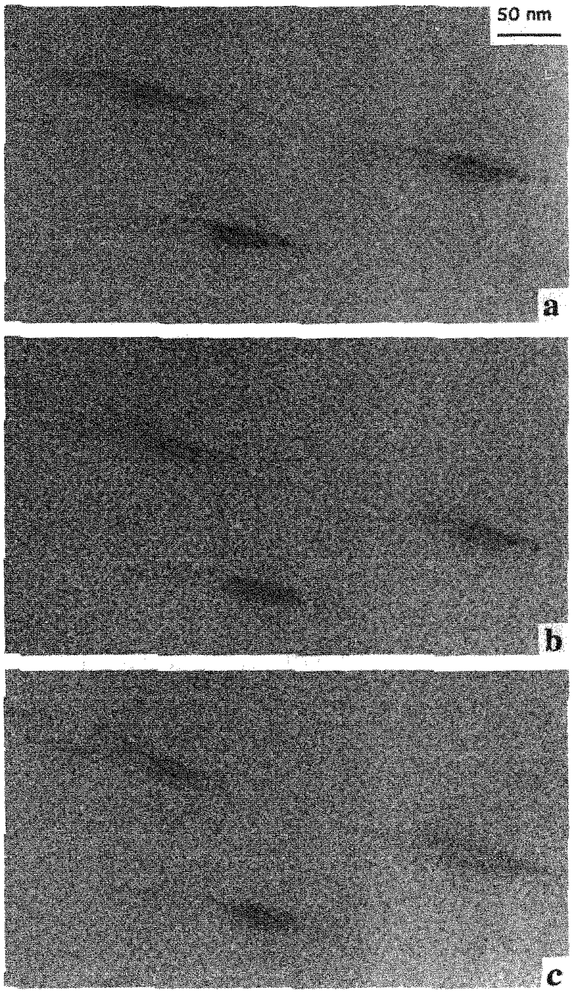

Fig. 5. Transmission electron micrographs of a monocrystalline silicon target irradiated at grazing incidence (≈80° of normal incidence) with 30 MeV C_{60} cluster ions. (a) bright field imaging in focused conditions, (b) and (c): phase contrast imaging respectively in underfocused and overfocused conditions.

face (i.e. in regions in which electronic energy deposition overwhelms elastic collision processes) was studied by Channeling Rutherford Backscattering Spectrometry. The main conclusion is that, at constant cluster velocities, when increasing the size of the clusters, i.e. increasing the amount of energy deposition in electronic processes ($S_e = 1$ to 8 keV/nm), the ratio of the defect concentration produced per cluster constituent to that produced by single carbon atoms starts decreasing (up to four constituents, i.e. to $S_e = 4$ keV/nm) and then

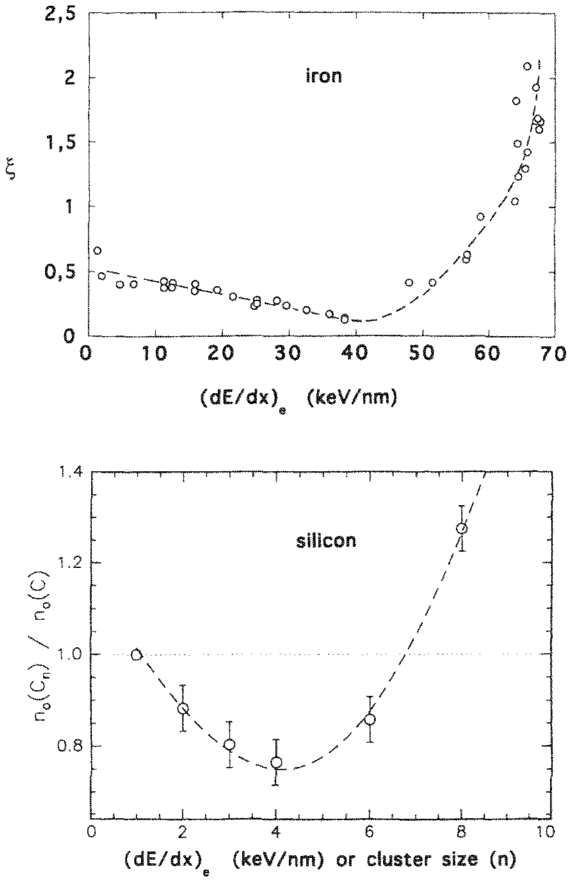

Fig. 6. Top: Evolution of the damage production efficiency ξ (defined in the text) as a function of the linear rate of energy deposition in electronic processes in an iron target irradiated with O to U GeV projectiles (from [17]). Bottom: Evolution of the defect production per cluster constituent as a function of the number n of constituents (or as the function or the linear rate of energy deposition in electronic processes) in a silicon target irradiated with C_n ($n = 1$–8) carbon clusters at constant velocities (0.8 MeV per carbon). Results taken from [16].

significantly increases (Fig. 6). These results are very similar to those previously obtained in a pure metal irradiated with energetic monoatomic heavy ions [17]. Fig. 6 features the evolution of the damage production efficiency ξ (defined as the ratio of the measured damaging cross-section to the calculated damaging cross-section due to elastic collisions) deduced from in situ electrical resistance measurements during low temperature irradiations of iron. Here again, it is observed that when the linear rate of energy deposition in electronic processes increases, there is a gradual evolution from a first regime (up to $S_e = 40$ keV/nm) in which the main effect of electronic energy deposition is to anneal part of the defects induced by elastic collisions to a second one ($S_e > 40$ keV/nm) in which part of the energy deposited in the target electronic system is converted into atomic displacements. It was shown in this particular case [17] that up to $S_e = 70$ keV/nm, using monoatomic projectiles, electronic processes were only able to create *isolated point defects*, so that "latent tracks" could not be seen by transmission electron microscopy.

Although it might appear a little surprising at first glance, a pure metal, iron, and a semi-conductor, silicon, thus seem to behave similarly under high electronic energy deposition, although the values of S_e at which the transition from the regime of defect annealing to that of isolated defect generation occurs noticeably differ. *The results presented at this conference confirm this analogy, when the range of electronic energy deposition is extended to much higher values* by using heavy energetic cluster ions.

We saw in this paper that after irradiation with 30 MeV C_{60} ions, at $S_e = 46$ keV/nm, 10 nm diameter amorphous tracks are induced in silicon. When iron is bombarded with energetic C_{60} ions, damage located in the vicinity of the projectile path is indeed visible by transmission electron microscopy as shown by Dammak [18]. In the 50–90 keV/nm S_e range, dislocation loops and strain fields are visible in the vicinity of the projectile path.

References

[1] M. Levallois, P. Bogdanski, M. Toulemonde, Nucl. Instr. and Meth. B 63 (1992) 14.

[2] P. Mary, P. Bogdanski, M. Toulemonde, R. Spohr, J. Vetter, Nucl. Instr. and Meth. B 62 (1992) 391.

[3] R. Leguay, thesis, CEA report, CEA-R-5687 (1995), published by the Centre d'Etudes de Saclay, 91191 Gif-sur-Yvette, France.

[4] S. Furuno, H. Otsu, K. Hojou, K. Izui, Nucl. Instr. and Meth. B 107 (1996) 223.

[5] K. Izui, J. Phys. Soc. of Japan 20 (1965) 915.

[6] T.S. Noggle, J.O. Stiegler, J. Appl. Phys. 33 (1962) 1726.

[7] K.L. Merkle, Phys. Rev. Lett. 9 (1962) 150.

[8] H. Dammak, A. Dunlop, D. Lesueur, A. Brunelle, S. Della-Negra, Y. Le Beyec, Phys. Rev. Lett. 74 (1995) 1135.

[9] J.P. Biersack, L.G. Haggmark, Nucl. Instr. and Meth. 174 (1980) 257.

[10] K. Baudin, A. Brunelle, M. Chabot, S. Della-Negra, J. Depauw, D. Gardes, P. Hakansson, Y. Le Beyec, A. Billebaud, M. Fallavier, J. Remillieux, J.C. Poizat, J.P. Thomas, Nucl. Instr. and Meth. B 94 (1994) 341.

[11] C. Tomaschko, D. Brandl, R. Krüger, M. Schurr, H. Voit, Nucl. Instr. and Meth. B 103 (1995) 407.

[12] D. Ben-Hamu, A. Baer, H. Feldman, J. Levin, O. Heber, Z. Amitay, Z. Vager, D. Zajfman, Phys. Rev. A 56 (1997) 4786.

[13] S. Della-Negra, A. Brunelle, Y. Le Beyec, J.M. Curaudeau, J.P. Mouffron, B. Waast, P. Hakansson, B.U.R. Sundqvist, E.S. Parils, Nucl. Instr. and Meth. B 74 (1993) 453.

[14] M.H. Brodsky, R.S. Title, K. Weiser, G.D. Pettit, Phys. Rev. B 1 (1970) 2632.

[15] A. Dunlop, G. Jaskierowicz, J. Jensen, S. Della-Negra, Nucl. Instr. and Meth. B 132 (1997) 93.

[16] M. Döbeli, F. Ames, R.M. Ender, M. Suter, H.A. Synal, D. Vetterli, Nucl. Instr. and Meth. B 106 (1996) 43.

[17] A. Dunlop, D. Lesueur, P. Legrand, H. Dammak, J. Dural, Nucl. Instr. and Meth. B 90 (1994) 330.

[18] H. Dammak, A. Dunlop, these Proceedings (SHIM-98), Nucl. Instr. and Meth. B 146 (1998) 285.